Vol.10, no.2, 2026 eISSN 2587-8999
PEER-REVIEWED SCIENTIFIC AND THEORETICAL JOURNAL

Computational Mathematics and Information Technologies

Computational Mathematics

Mathematical Modelling

Information Technologies

www.cmit-journal.ru
DOI 10.23947/2587-8999

Computational Mathematics and Information Technologies

Peer-reviewed scientific and theoretical journal

eISSN 2587–8999

Published since 2017

Periodicity — 4 issues per year

DOI: 10.23947/2587–8999

Founder and Publisher — Don State Technical University (DSTU), Rostov-on-Don, Russian Federation

The journal "Computational Mathematics and Information Technologies" publishes reviews, original articles and short reports on mathematical modeling, numerical methods and information technologies for solving complex and topical problems of science and modern technology. Research areas include continuum mechanics, fluid dynamics, Earth sciences, chemistry, biology, image processing and pattern recognition, parallel computing theory and its applications, big database and artificial intelligence technologies, etc.

The journal "Computational Mathematics and Information Technologies" accepts scientific and review articles for publication in accordance with the sections:

1. Computational Mathematics
2. Mathematical Modelling
3. Information Technologies

Registration:	Mass media registration certificate ЭЛ № ФС 77–66529 dated July 21, 2016 issued by the Federal Service for Supervision of Communications, Information Technology and Mass Media
Indexing and Archiving:	RISC, Crossref, Cyberleninka
Website:	https://cmit-journal.ru
Address of the Editorial Office:	1, Gagarin sq., Rostov-on-Don, 344003, Russian Federation
E-mail:	CMIT-EJ@yandex.ru
Telephone:	+7 (863) 273–85–14
Date of publication No. 2, 2026:	30.06.2026

Computational Mathematics and Information Technologies

Рецензируемый научно-теоретический журнал

eISSN 2587–8999

Издается с 2017 года

Периодичность — 4 выпуска в год

DOI: 10.23947/2587–8999

Учредитель и издатель — Федеральное государственное бюджетное образовательное учреждение высшего образования «Донской государственный технический университет» (ДГТУ), г. Ростов-на-Дону, Российская Федерация

Журнал «Computational Mathematics and Information Technologies» публикует обзоры, оригинальные статьи и краткие сообщения, посвященные математическому моделированию, численным методам и информационным технологиям для решения сложных и актуальных проблем науки и современной технологии. Область применения исследований — это механика сплошных сред, гидроаэродинамика, науки о Земле, химия, биология, обработка изображений и распознавание образов, теория параллельных вычислений и ее приложения, технологии больших баз данных и искусственного интеллекта и т. д.

Журнал «Computational Mathematics and Information Technologies» принимает к публикации научные и обзорные статьи в соответствии с разделами:

1. Вычислительная математика
2. Математическое моделирование
3. Информационные технологии

Регистрация:	Свидетельство о регистрации средства массовой информации ЭЛ № ФС 77 – 66529 от 21 июля 2016 г., выдано Федеральной службой по надзору в сфере связи, информационных технологий и массовых коммуникаций
Индексация и архивация:	РИНЦ, CrossRef, CyberLeninka
Сайт:	https://cmit-journal.ru
Адрес редакции:	344003, Российская Федерация, г. Ростов-на-Дону, пл. Гагарина, 1
E-mail:	CMIT-EJ@yandex.ru
Телефон:	+7 (863) 273–85–14
Дата выхода № 2, 2026 в свет:	30.06.2026

Contents

Содержание

COMPUTATIONAL MATHEMATICS
ВЫЧИСЛИТЕЛЬНАЯ МАТЕМАТИКА

UDC 519.6

Original Empirical Research

https://doi.org/10.23947/2587-8999-2026-10-2-7-16

Integral Kernel Degeneration Method for Solving the Fredholm Integral Equation

Natalya K. Volosova[1], Konstantin A. Volosov[2], Aleksandra K. Volosova[2], Mikhail I. Karlov[3], Dmitriy F. Pastukhov[4], Yuriy F. Pastukhov[4]

[1] Bauman Moscow State Technical University, Moscow, Russian Federation
[2] Russian University of Transport, Moscow, Russian Federation
[3] Moscow Institute of Physics and Technology (National Research University), Dolgoprudny, Russian Federation
[4] Euphrosyne Polotskaya State University of Polotsk, Novopolotsk, Republic of Belarus
✉ dmitrij.pastuhov@mail.ru

Abstract

Introduction. A modified degenerate kernel method for solving Fredholm integral equations of the second kind is proposed for the first time. The main idea is to expand the integral kernel into a Taylor series with respect to a single variable x, rather than with respect to two variables x and s, as in the classical method.

Materials and Methods. The kernel expansion is performed at the midpoint of the integration interval, which reduces the absolute values of the elements of matrix C, as well as enlarges the nonsingularity region of the matrix $I–\lambda C$. A system of power basis functions is employed on the integration interval. Three theorems establishing sufficient conditions for the correctness of the proposed algorithm based on the degenerate kernel method are obtained. A definition of the factorial Chebyshev norm of a vector-valued function is introduced. The factorial norm for the system of partial derivatives of the integral kernel with respect to the variable x, together with the parameter λ, is included in the inequality of the third theorem, which provides a sufficient condition for the correctness of the algorithm. The inverse matrix arising in the numerical solution was computed using the IMSL library within a finite number of elementary operations.

Results. The proposed numerical algorithm was tested on three Fredholm integral equations with kernels exhibiting exponential growth or periodic sign changes. The numerical solutions coincide with the exact solutions to 15 significant digits in the uniform metric.

Discussion. A modified algorithm for the numerical solution of Fredholm equations of the second kind with double precision is proposed. The solution is represented as the sum of $n+1$ power-type terms vanishing at the midpoint of the interval $[a, b]$ and the right-hand side function of the Fredholm equation.

Conclusion. The degenerate kernel method is of interest for both functional analysis and numerical methods. The integral kernel must possess sufficient smoothness with respect to the variable x.

Keywords: Fredgolm equations, numerical methods, integral equations, matrix method

For Citation. Volosova N.K., Volosov K.A., Volosova A.K., Karlov M.I., Pastukhov D.F., Pastukhov Yu.F. Integral kernel degeneration method for solving the Fredholm integral equation. *Computation Mathematics and Information Technologies*. 2026;10(2):7–16. https://doi.org/10.23947/2587-8999-2026-10-2-7-16

Оригинальное эмпирическое исследование

Метод вырождения интегрального ядра для решения интегрального уравнения Фредгольма

Н.К. Волосова[1], К.А. Волосов[2], А.К. Волосова[2], М.И. Карлов[3], Д.Ф. Пастухов[4] ✉, Ю.Ф. Пастухов[4]

[1] Московский государственный технический университет им. Н.Э. Баумана, г. Москва, Российская Федерация

[2] Российский университет транспорта, г. Москва, Российская Федерация

[3] Московский физико-технический институт (национальный исследовательский университет), г. Долгопрудный, Российская Федерация

[4] Полоцкий государственный университет им. Евфросинии Полоцкой, г. Новополоцк, Республика Беларусь

✉ dmitrij.pastuhov@mail.ru

Аннотация

Введение. Впервые предложен модифицированный метод вырождения интегрального ядра для решения интегральных уравнений Фредгольма второго рода. Идея заключается в том, чтобы интегральное ядро разложить в ряд Тейлора по одной переменной x, а не по двум переменным x, s как в классическом методе.

Материалы и методы. Разложение ядра в ряд проводится в средней точке отрезка интегрирования, что уменьшает модули элементов матрицы C, а также область невырожденности для матрицы $I–\lambda C$. Используется система степенных базисных функций на отрезке интегрирования. Получены три теоремы для достаточных условий корректности предложенного алгоритма методом вырождения интегрального ядра. Введено определение факториальной нормы Чебышева вектор-функции. Факториальная норма для системы частных производных интегрального ядра по переменной x и параметр λ входят в неравенство третьей теоремы — достаточное условие корректности алгоритма. Обратная матрица для решения уравнения Пуассона за конечное число элементарных операций вычислялась библиотекой Msimsl.

Результаты исследования. Предложенный в работе численный алгоритм протестирован на трех интегральных уравнениях Фредгольма с ядрами с экспоненциальным ростом или с периодическим изменением знака ядра. Численные решения совпадают с точными решениями в 15 значащих знаках в равномерной метрике.

Обсуждение. Предложен модифицированный алгоритм численного решения уравнения Фредгольма второго рода с двойной точностью. Решение представимо в виде суммы n+1 слагаемого степенного вида с нулем в середине отрезка $[a, b]$ и функции — правой части уравнения Фредгольма.

Заключение. Метод вырождения интегрального ядра представляет интерес для функционального анализа и численных методов. Ядро интегрального уравнения должно быть достаточно гладким по переменной x.

Ключевые слова: уравнения Фредгольма, численные методы, интегральные уравнения, матричный метод

Для цитирования. Волосова Н.К., Волосов К.А., Волосова А.К., Карлов М.И., Пастухов Д.Ф., Пастухов Ю.Ф. Метод вырождения интегрального ядра для решения интегрального уравнения Фредгольма. *Computational Mathematics and Information Technologies*. 2026;10(2):7–16. https://doi.org/10.23947/2587-8999-2026-10-2-7-16

Introduction. Methods for solving Fredholm and Volterra integral equations are described in detail in [1]. These include direct [1, p. 135] and projection [1, p. 139] methods. In [2], generalized splines are used to solve Fredholm integral equations. In [3, 4], a subdomain selection method based on Kantorovich polynomials is proposed for solving Fredholm integral equations of the second kind, and a special version of the collocation method based on Bernstein polynomials is considered for solving Fredholm equations of the second kind. A collocation method for solving a Volterra integral equation of the second kind using Chebyshev and Legendre polynomials was applied in [5]. In [6], a system of integral equations is solved by a collocation method with nodes given by Chebyshev polynomials of the first and second kinds. In [7], a method is proposed for solving a system of nonlinear convolution-type integral equations with a monotone convex nonlinearity. In [8], a generalized Petrov-Galerkin method is proposed for solving a system of linear Fredholm integral equations of the second kind. In [9], a tabular double-precision solution of an integral equation is obtained by replacing the integral with a quadrature formula having twelfth-order accuracy.

In this paper, a modified degenerate-kernel method is proposed for solving a Fredholm integral equation of the second kind using a basis system of power functions, and a functional form of the solution is obtained. In the three examples considered, twenty basis functions and thirty integration subintervals in the quadrature formulas are sufficient to achieve double precision. The algorithm was tested on examples with exponential variation of the integral kernel or with periodic sign changes of the kernel. Three theorems are proved, giving sufficient conditions for the existence and uniqueness of the numerical solution of problem (1) by algorithm (2)–(7).

Materials and Methods

Problem Statement. Consider the Fredholm integral equation of the second kind [1, p. 135]:

$$y(x)-\lambda\int_a^b K(x,s)y(s)ds=f(x),\ (x,s)\in[a,b]\times[a,b]. \tag{1}$$

In equation (1), the parameter λ, the integral kernel $K(x,s)\in L_2[a,b]\times[a,b]$, and the right-hand side (the function $f(x)$) are given. The unknown function must be square-integrable on the interval $[a, b]$, $y(x)\in L_2[a,b]$. Let the partial derivatives of the kernel with respect to x be continuous on the square $K_x^{(i)}(x,s)\in C[a,b]\times[a,b], i=\overline{0,n}$.

A direct method for solving integral equation (1) by the degenerate-kernel method [1, p. 135] is known; it consists in expanding the integral kernel in a series with respect to the variables x, s (for example, as in Problem 29.11 [1, p. 138]). Equation (1) is then solved by replacing the kernel. In the classical method, two systems of linearly independent basis functions are required $\{A_i(x)\}_{i=1}^n, \{B_i(x)\}_{i=1}^n$. The solution is expanded with respect to one of the systems, and the kernel is represented as a sum of pairwise products of functions, one from each system [1, p. 138]. To obtain a polynomial in two variables from an integral kernel $K(x, s)$ of arbitrary form, the kernel must be expanded in a Taylor series with respect to the variables x, s. This is the idea underlying the traditional approach to solving equation (1) by replacing the integral kernel.

We modify the known method. In this case, one system of linearly independent functions $\{A_i(x)\}_{i=0}^n, x\in[a,b]$ is sufficient. We consider the symmetric variable $y\left|_{-\frac{b-a}{2}}^{\frac{b-a}{2}}\right. = x\left|_a^b\right. - \frac{a+b}{2}, c=\frac{a+b}{2}, h=\frac{b-a}{2}$ with respect to the midpoint of the interval $c=\frac{a+b}{2}, y\in[-h,h]$ and the system of linearly independent power functions $\{A_i(y)=y^i\}_{i=0}^n, y\in\left[-\frac{b-a}{2},\frac{b-a}{2}\right]$.

The idea of the modified degenerate-kernel method is to expand the kernel $K(x, s)$ with respect to the first variable x at the center of the interval $c=\frac{a+b}{2}, x=c+y, dx=dy$:

$$K(x,s)=K(c+y,s)=\sum_{i=0}^n K_x^{(i)}(c,s)\frac{y^i}{i!}+O\left(y^{n+1}\right), K_n(x,s)=\sum_{j=0}^n K_x^{(i)}(c,s)\frac{y^i}{i!}. \tag{2}$$

In formula (2), denote $K_x^{(i)}(c,s)=q_i(s),\ i=\overline{0,n}, s\in[a,b]$. Expand the solution $y(x)$ on the interval $[a, b]$ as the sum

$$y(x)=f(x)+\lambda\sum_{i=0}^n A_i(y)D_i. \tag{3}$$

In formula (3), $D_i, i=\overline{0,n}$ is called the vector of coefficients in the expansion of the solution in the basis functions $\{A_i(y)=y^i\}_{i=0}^n$.

Substituting expansions (2) and (3) into Fredholm integral equation of the second kind (1), we obtain:

$$\begin{gathered}
y(x)-\lambda\int_a^b K(x,s)y(s)ds=f(x), A_i(y)=y^i \Leftrightarrow f(x)+\lambda\sum_{i=0}^n y^i D_i-\lambda\int_a^b\sum_{i=0}^n q_i(s)\frac{y^i}{i!}\left(f(s)+\lambda\sum_{j=0}^n A_j(s-c)D_j\right)ds=f(x)\Leftrightarrow \\
\sum_{i=0}^n y^i D_i-\int_a^b\sum_{i=0}^n q_i(s)\frac{y^i}{i!}\left(f(s)+\lambda\sum_{j=0}^n (s-c)^j D_j\right)ds=0\Leftrightarrow \\
\sum_{i=0}^n y^i\left\{D_i-\lambda\sum_{j=0}^n\left(\int_a^b\frac{q_i(s)}{i!}(s-c)^j\,ds\right)D_j\right\}=\sum_{i=0}^n y^i\left\{\int_a^b\frac{q_i(s)}{i!}f(s)ds\right\}\Leftrightarrow \\
D_i-\lambda\sum_{j=0}^n\left(\int_a^b\frac{q_i(s)}{i!}(s-c)^j\,ds\right)D_j=\int_a^b\frac{q_i(s)}{i!}f(s)ds,\ i=\overline{0,n}.
\end{gathered} \tag{4}$$

If the following notation is introduced in the system of n equations (4):

$$C_{i,j}=\int_a^b\frac{q_i(s)}{i!}(s-c)^j\,ds,\ i,j=\overline{0,n},\quad f_i=\int_a^b\frac{q_i(s)}{i!}f(s)ds,\ i=\overline{0,n}, \tag{5}$$

then we obtain a system of linear algebraic equations with respect to the unknowns $D_i, i=\overline{0,n}$

$$D_i-\lambda\sum_{j=0}^n C_{i,j}D_j=f_i,\ i=\overline{0,n}. \tag{6}$$

The system of equations (6) can be written in matrix form:

$$D_i-\lambda\sum_{j=0}^n C_{i,j}D_j=f_i,\ i=\overline{0,n}\ ,(I-\lambda C)D=f\Leftrightarrow D=(I-\lambda C)^{-1}f. \tag{7}$$

The inverse matrix $(I - \lambda C)^{-1}$ in the program was computed using the Msimsl library in the Fortran language. The matrix entries $C_{i,j}$ and the right-hand-side coefficients of (6) can be written in the form:

$$\begin{cases} C_{i,j} = \int\limits_a^b \frac{q_i(s)}{i!}(s-c)^j\, ds = \int\limits_{-h}^{h} \frac{q_i(c+y)}{i!} y^j dy,\ i,j = \overline{0,n},\ h = \frac{b-a}{2}, y \in [-h,h], \\ f_i = \int\limits_a^b \frac{q_i(s)}{i!} f(s)ds = \int\limits_{-h}^{h} \frac{q_i(c+y)}{i!} f(c+y)dy,\ \ i = \overline{0,n}. \end{cases} \tag{8}$$

In formulas (8), the variable $y \in [-h,h]$ changes sign and has an absolute value smaller than that of the variable x on the interval $[a, b]$, therefore the entries of matrix $C_{i,j}$ have smaller absolute values than when the system of basis functions $\{A_i(y) = y^i\}_{i=0}^n, y \in [-h,h]$ is used instead of the system of functions $\{A_i(x) = x^i\}_{i=0}^n, x \in [a,b]$ [1, p. 137]. This reduces the norm of matrix $\|C\|$ and expands the nonsingularity domain of matrix $I - \lambda C$, that is, it expands the domain in which the inverse matrix exists $(I - \lambda C)^{-1}$.

The power-type basis functions $\{A_i(y) = y^i\}_{i=0}^n$ not only enter as factors in the Taylor expansion (2) of the integral kernel $K(x, s)$ with respect to the variable x, but also ensure the correctness of the SLAE (4).

Solution (3) is a polynomial function of degree n that can be compared with the exact solution at every point of the interval $x \in [a, b]$, unlike in [9], where the solution is sought in tabular form at grid nodes.

In [9, p. 11], integral quadrature formula (9) for computing a definite integral with a twelfth-order error term is presented. This formula is used to compute the matrix entries and the right-hand-side coefficients of system (6) according to formulas (8):

$$\begin{gathered} \langle y_1, y_2 \rangle = \int\limits_a^b y_1(x) y_2(x) dx = 5h \sum_{i=0}^{n_1} y_1(x_i)\, y_2(x_i) + O(h^{12}), \\ n_1 = 10p, h = \frac{b-a}{n_1}, p \in N, \end{gathered} \tag{9}$$

where

$$C_i = \begin{cases} \frac{16067}{299376}, if\ i = 0\ or\ i = n_1, \\ \frac{16067}{149688}, if\ (i \equiv 0 \bmod 10)\ and\ (0 < i < n_1), \\ \frac{26575}{74844}, if\ (i \equiv 1 \bmod 10)\ or\ (i \equiv 9 \bmod 10), \\ \frac{-16175}{99792}, if\ (i \equiv 2 \bmod 10)\ or\ (i \equiv 8 \bmod 10), \\ \frac{5675}{6237}, if\ (i \equiv 3 \bmod 10)\ or\ (i \equiv 7 \bmod 10), \\ \frac{-4825}{5544}, if\ (i \equiv 4 \bmod 10)\ or\ (i \equiv 6 \bmod 10), \\ \frac{17807}{12474}, if\ i \equiv 5 \bmod 10. \end{cases}$$

Thus, algorithm (2)–(9) numerically solves Fredholm integral equation of the second kind (1). The inverse matrix $(I - \lambda C)^{-1}$ in formula (7) was computed by the Msimsl library in the Fortran. Algorithm (2)–(7) will be referred to as a solution of Fredholm integral equation (1) by the degenerate-kernel method.

Theorem 1 (criterion for existence and uniqueness of the solution in algorithm (2)–(7)). For algorithm (2)–(7) to have a unique solution, it is necessary and sufficient that the matrix $I - \lambda C$ be nonsingular.

The proof of Theorem 1 follows from formula (7), which requires the existence of the inverse matrix; this is equivalent to the determinant of the matrix being nonzero. **Theorem 1** is proved.

Here I is the identity matrix of order n.

Theorem 2 (sufficient conditions for the correctness of algorithm (2)–(7)). Let the norm of the vector f in equation (7) be finite. If $q = |\lambda| \|C\| < 1$, then algorithm (2)–(7) is correct, and the following estimate for the norm of the inverse matrix holds

$$\left\| (I - \lambda C)^{-1} \right\| < \frac{1}{1-q} = \frac{1}{1 - |\lambda| \|C\|}.$$

Proof. By the assumption of Theorem 2, $q = |\lambda|\|C\| < 1$. Therefore, the inverse matrix can be represented by the infinite series

$$(I - \lambda C)^{-1} = \sum_{k=0}^{\infty} \lambda^k C^k, \ \left\|(I - \lambda C)^{-1}\right\| = \left\|\sum_{k=0}^{\infty} \lambda^k C^k\right\| \le \sum_{k=0}^{\infty} |\lambda|^k \|C\|^k = \frac{1}{1 - |\lambda|\|C\|} < \infty,$$

$$\|D\| = \left\|(I - \lambda C)^{-1} f\right\| \le \left\|(I - \lambda C)^{-1}\right\| \|f\| \le \frac{\|f\|}{1 - |\lambda|\|C\|} < \infty.$$

Theorem 2 is proved.

Definition 1. The factorial Chebyshev norm of the vector function $f(x) : [a,b] \to C\left([a,b], R^{n+1}\right)$, $f(x) = \{f_0(x), f_1(x), ..., f_n(x)\}$ is defined as the number $\|f\|_{\infty}^{F} = \max\limits_{\substack{i=\overline{0,n} \\ x \in [a,b]}} \dfrac{|f_i(x)|}{i!}$.

Theorem 3. The fulfillment of the condition $\|q\|_{\infty}^{F} < \dfrac{1}{2|\lambda| sh(h)}$ is sufficient for the correctness of the algorithm (2)–(7).

Proof. Suppose that the conditions of **Theorem 2** $q = |\lambda|\|C\| < 1$. Estimate the infinite norm of the matrix C using formula (8):

$$\|C\|_{\infty} = \max_{i=\overline{0,n}} \sum_{j=0}^{n} |C_{i,j}| = \max_{i=\overline{0,n}} \sum_{j=0}^{n} \left| \int_{-h}^{h} \frac{q_i(c+y)}{i!} y^j dy \right| \le$$

$$\le \sum_{j=0}^{n=2k} \max_{\substack{i=\overline{0,n} \\ y \in [-h,h]}} \frac{1}{i!} |q_i(c+y)| \left| \int_{-h}^{h} y^j dy \right| = \sum_{j=0}^{n=2k} \|q\|_{\infty}^{F} \left| \int_{-h}^{h} y^j dy \right| = 2\|q\|_{\infty}^{F} \sum_{j=0}^{n=2k} \left(h + \frac{h^3}{3!} + \frac{h^5}{5!} + ... + \frac{h^{2k+1}}{(2k+1)!} \right).$$

Since $e^h = 1 + h + \dfrac{h^2}{2!} + \dfrac{h^3}{3!} + \dfrac{h^4}{4!} + \dfrac{h^5}{5!} + ...$, $e^{-h} = 1 - h + \dfrac{h^2}{2!} - \dfrac{h^3}{3!} + \dfrac{h^4}{4!} - \dfrac{h^5}{5!} + ...$, that

$$e^h - e^{-h} = 2\left(h + \frac{h^3}{3!} + \frac{h^5}{5!} + ... \right) \Leftrightarrow h + \frac{h^3}{3!} + \frac{h^5}{5!} + ... = \frac{e^h - e^{-h}}{2} = sh(h).$$

Denote the finite sum

$$I_{n=2k} = h + \frac{h^3}{3!} + \frac{h^5}{5!} + ... + \frac{h^{2k+1}}{(2k+1)!}, I_{n=2k} + R_{n=2n} = sh(h), I_{n=2k} < sh(h), R_{n=2n} > 0.$$

$$R_{n=2n} = sh(h) - I_{n=2k} = \frac{h^{2k+3}}{(2k+3)!} + \frac{h^{2k+5}}{(2k+5)!} + \frac{h^{2k+7}}{(2k+7)!} + \frac{h^{2k+9}}{(2k+9)!} + ... =$$

$$= \frac{h^{2k+3}}{(2k+3)!} \left(1 + \frac{(2k+3)!}{(2k+5)!} h^2 + \frac{(2k+3)!}{(2k+7)!} h^4 + \frac{(2k+3)!}{(2k+9)!} h^6 + ... \right) = \frac{h^{2k+3}}{(2k+3)!} \cdot$$

$$\cdot \left(1 + \frac{h^2}{(2k+4)(2k+5)} + \frac{h^4}{(2k+4)(2k+5)(2k+6)(2k+7)} + \right.$$

$$\left. + \frac{h^6}{(2k+4)(2k+5)(2k+6)(2k+7)(2k+8)(2k+9)} + ... \right) \le$$

$$\le \frac{h^{2k+3}}{(2k+3)!} \left(1 + \left(\frac{h}{2k+4} \right)^2 + \left(\frac{h}{2k+4} \right)^4 + \left(\frac{h}{2k+4} \right)^6 + ... \right) = \frac{h^{2k+3}}{(2k+3)!} \frac{1}{1 - \left(\frac{h}{2k+4} \right)^2}.$$

$$sh(h) - I_{n=2k} \le \frac{h^{2k+3}}{(2k+3)!} \frac{1}{1 - \left(\frac{h}{2k+4} \right)^2} \Leftrightarrow I_{n=2k} \ge sh(h) - \frac{h^{2k+3}}{(2k+3)!} \frac{1}{1 - \left(\frac{h}{2k+4} \right)^2}.$$

Since $q = |\lambda|\|C\| < 1 \Leftrightarrow \|C\| < \dfrac{1}{|\lambda|}$, and also $\|C\|_{\infty} \le 2\|q\|_{\infty}^{F} I_{n=2k} < \dfrac{1}{|\lambda|}$, the following estimates hold

$$\|q\|_{\infty}^{F} < \frac{1}{2|\lambda| sh(h)} < \frac{1}{2|\lambda| I_{n=2k}} \le \frac{1}{2|\lambda| \left(sh(h) - \frac{1}{(2k+3)!} \frac{h^{2k+3}}{\left(1 - \left(\frac{h}{2k+4} \right)^2 \right)} \right)}, n = 2k.$$

Theorem 3 is proved.

Remark. Note that on the right-hand side of inequality (10), the two estimates virtually coincide, because if $n = 2k = 10$, $h = \pi/2$ are taken, the additional term is very small:

$$\frac{1}{(2k+3)!}\frac{h^{2k+3}}{\left(1-\left(\frac{h}{2k+4}\right)^2\right)} = \frac{1}{13!}\frac{1.57^{13}}{\left(1-\left(\frac{1.57}{14}\right)^2\right)} \approx 5.73\cdot 10^{-8}.$$

Theorem 4.

1) Let C be a positive matrix, $C_{i,j} > 0, i, j = \overline{0,n}$ and $\lambda > 0$ (or let C be a negative matrix, $C_{i,j} > 0, i, j = \overline{0,n}$ and $\lambda < 0$) with main diagonal entries $1 - |\lambda||C_{i,i}| > |\lambda| \sum_{j=0, j\neq i}^{n} |C_{i,j}|, i = \overline{0,n}$; then algorithm (2)–(7) is correct.

2) The following estimate for the norm of the inverse matrix is valid

$$\frac{1}{r^*} \le \left\| (I - \lambda C)^{-1} \right\|_\infty \le \frac{1}{r_*}, r_* = \min_{i=0,n}\left(1 - \lambda\sum_{i=0}^{n} C_{i,j}\right), r^* = \max_{i=0,n}\left(1 - \lambda\sum_{i=0}^{n} C_{i,j}\right).$$

Proof.

1) By the assumption of **Theorem 4**

$$1 - |\lambda||C_{i,i}| > |\lambda| \sum_{j=0, j\neq i}^{n} |C_{i,j}|, i = \overline{0,n} \Leftrightarrow |\lambda|\sum_{j=0}^{n} C_{i,j} < 1 \Rightarrow \max_{i=0,n} |\lambda| \sum_{j=0}^{n} |C_{i,j}| = |\lambda| \|C\|_\infty < 1.$$

By **Theorem 2**, algorithm (2)–(7) is correct, and the inverse matrix $(I - \lambda C)^{-1}$ exists with a bounded norm.

The diagonal entries of matrix $I - \lambda C$ are positive $1 - |\lambda||C_{i,i}| > |\lambda| \sum_{j=0, j\neq i}^{n} |C_{i,j}| \ge 0$, while the off-diagonal entries are negative, since $-\lambda C_{i,j} < 0 \forall i, j = \overline{0,n}, i \neq j$. Also, by the assumption of **Theorem 4**, the matrix $I - \lambda C$ is strictly diagonally dominant. Therefore, all conditions of the theorem by Yu.S. Volkov and V.L. Miroshnichenko [10] for a monotone-type matrix $I - \lambda C$ are satisfied, and the estimate holds

$$\frac{1}{r^*} \le \left\| (I - \lambda C)^{-1} \right\|_\infty \le \frac{1}{r_*}, r_* = \min_{i=0,n}\left(1 - \lambda\sum_{i=0}^{n} C_{i,j}\right) > 0, r^* = \max_{i=0,n}\left(1 - \lambda\sum_{i=0}^{n} C_{i,j}\right) > 0.$$

Theorem 4 is proved.

Example 1. The problem considered is

$$y(x) - \frac{1}{2}\int_0^1 e^{x-s} y(s) ds = e^x. \tag{11}$$

with the exact solution $y(x) = 2e^x$.

We verify this: $2e^x - \frac{1}{2}\int_0^1 e^{x-s} 2e^s ds = e^x \Leftrightarrow 2e^x - e^x = e^x$.

Apply algorithm (2)–(9) and the sufficient conditions for algorithm correctness (Theorem 3) to example (10).

For $n = 20$, we obtain:

$$\lambda = 1/2,\ K(x,s) = e^{x-s},\ f(x) = e^x, a = 0, b = 1, c = h = 1/2, K_x^{(i)}(c,s) = q_i(s) = K_x^{(i)}(1/2, s) = e^{1/2-s},$$

$$i = \overline{0,n}, s \in [0,1], \|q\|_\infty^F < \frac{1}{2|\lambda| sh(h)} \Leftrightarrow \|q\|_\infty^F = \max_{\substack{s\in[0,1],\\ i=0,n}} \frac{\left|e^{1/2-s}\right|}{i!} = e^{1/2} \approx 1.649 < \frac{1}{2\cdot(1/2)sh(1/2)} \approx 1.919.$$

Table 1

Numerical and exact solution of example (10).
Number of basis functions $n = 20$, number of subintervals in the quadrature formula (9) $n_1 = 10$

x	u^{num}	u^{exact}	$u^{num} - u^{exact}$
0.000000000000000E+000	2.00000000000000	2.00000000000000	8.88178419E–016
0.100000000000000	2.21034183615130	2.21034183615130	4.44089209E–016
0.200000000000000	2.44280551632034	2.44280551632034	–4.4408920E–016
0.300000000000000	2.69971761515201	2.69971761515201	4.44089209E–016
0.400000000000000	2.98364939528254	2.98364939528254	0.0000000000E+000
0.500000000000000	3.29744254140026	3.29744254140026	8.881784197E–016
0.600000000000000	3.64423760078102	3.64423760078102	8.881784197E–016
0.700000000000000	4.02750541494095	4.02750541494095	8.8817841970E–016
0.800000000000000	4.45108185698493	4.45108185698494	–8.881784197E–016
0.900000000000000	4.91920622231390	4.91920622231390	8.8817841970E–016
1.00000000000000	5.43656365691809	5.43656365691809	8.8817841970E–016

The Chebyshev norm [11] of the residual of the problem (the difference between the numerical and exact solutions) at the grid nodes of the quadrature formula is

$$\left\| u^{num} - u^{exact} \right\|_C = \max_{i=0,n_1} \left| u_i^{num} - u_i^{exact} \right| = 8.881784197001252\text{E}-016, x_i = a + h \cdot i, i = \overline{0, n_1}.$$

Using the found solution (3), the residual norm at intermediate grid nodes can be determined; it is equal to:

$$\left\| u^{num} - u^{exact} \right\|_C = \max_{i=\overline{1,n_1}} \left| u_i^{num} - u_i^{exact} \right| = 1.776356839400250\text{E}-015, x_i = a + h \cdot (i - 1/2), i = \overline{1, n_1}.$$

The residual norm values show that the functional solution (3) has double precision and provides 15 correct significant digits in the solution (Table 1).

Example 2. The problem considered is

$$y(x) - \frac{1}{2}\int_0^1 e^{x+s} y(s) ds = e^x. \tag{12}$$

with the exact solution $y(x) = \frac{4}{5 - e^2} e^x$.

We verify this:

$$\frac{4}{5-e^2} e^x - \frac{1}{2}\int_0^1 e^{x+s} \left(\frac{4}{5-e^2} \right) e^s ds = e^x \Leftrightarrow \frac{4}{5-e^2} - \frac{2}{5-e^2}\left(\frac{e^2-1}{2} \right) = \frac{5-e^2}{5-e^2} = 1 = 1.$$

Applying algorithm (2)–(9) to example (12), we obtain

$$\lambda = 1/2,\ K(x,s) = e^{x+s},\ f(x) = e^x, a = 0, b = 1, c = 1/2, K_x^{(i)}(c,s) = q_i(s) = K_x^{(i)}(1/2, s) = e^{1/2+s}.$$

The infinite norm of matrix C, computed by the program with $n = 20$ basis functions, is:

$$\|C\|_\infty = 3.39714811032309,\ |\lambda| \|C\|_\infty = (1/2) 3.39714811032309 = 1.69857405516155 > 1.$$

Therefore, the sufficient conditions in Theorems 2, 3, and 4 are not satisfied, and Theorems 2, 3, and 4 are not applicable to Example 2.

Table 2

Numerical and exact solution of example (11).
Number of basis functions $n = 20$, number of subintervals in the quadrature formula (9) $n_1 = 30$

x	u^{num}	u^{exact}	$u^{num} - u^{exact}$
0.000000000000000E+000	–1.67430141208924	1.67430141208924	2.2204460492E–016
0.100000000000000	–1.85038922873402	–1.85038922873402	0.0000000000E+000
0.200000000000000	–2.04499636271726	–2.04499636271727	1.3322676295E–015
0.300000000000000	–2.26007050764560	–2.26007050764560	8.8817841970E–016
0.400000000000000	–2.49776419785038	–2.49776419785038	4.4408920985E–016
0.500000000000000	–2.76045635167479	–2.76045635167479	4.4408920985E–016
0.600000000000000	–3.05077608048818	–3.05077608048818	4.4408920985E–016
0.700000000000000	–3.37162900171635	–3.37162900171635	8.8817841970E–016
0.800000000000000	–3.72622631923734	–3.72622631923734	4.4408920985E–016
0.900000000000000	–4.11811696218917	–4.11811696218917	0.0000000000E+000
1.00000000000000	–4.55122310384550	–4.55122310384550	8.881784197E–016

The Chebyshev norm [11] of the residual of the problem (the difference between the numerical and exact solutions) at the grid nodes of the quadrature formula is:

$$\left\| u^{num} - u^{exact} \right\|_C = \max_{i=0,n_1} \left| u_i^{num} - u_i^{exact} \right| = 1.332267629550188\text{E}-015, x_i = a + h \cdot i, i = \overline{0, n_1}.$$

Example 3. The problem considered is

$$y(x) - \frac{1}{2}\int_0^\pi \sin(x+s) y(s) ds = \sin x + \cos x. \tag{13}$$

with the exact solution $y(x) = \frac{4}{4 - \pi}(\sin x + \cos x)$.

We verify this:

$$\frac{1}{2}\int_0^{\pi}(\sin x\cos s+\cos x\sin s)\left(\frac{4}{4-\pi}\right)(\sin s+\cos s)\,ds=\frac{4}{4-\pi}(\sin x+\cos x)-\frac{2}{4-\pi}(\sin x+\cos x)\frac{\pi}{2}=$$

$$\frac{4}{4-\pi}(\sin x+\cos x)-\frac{1}{2}\int_0^{\pi}\sin(x+s)\frac{4}{4-\pi}(\sin s+\cos s)\,ds=\frac{4}{4-\pi}(\sin x+\cos x)-$$

$$=\left(\frac{4-\pi}{4-\pi}\right)(\sin x+\cos x)=\sin x+\cos x.$$

Apply algorithm (2)–(9) to Example 3; we obtain

$$\lambda=1/2,\ K(x,s)=\sin(x+s),\ f(x)=\sin x+\cos x, a=0, b=\pi,$$

$$c=\pi/2, K_x^{(i)}(c,s)=q_i(s)=K_x^{(i)}(\pi/2,s)=\sin\left(s+(i+1)\frac{\pi}{2}\right),\ i=\overline{0,n}, s\in[0,\pi].$$

The infinite norm of matrix C, computed by the program with $n = 20$ basis functions in Example 3, is

$$\|C\|_{\infty}=1528.89560494716,\ |\lambda|\|C\|_{\infty}=(1/2)1528.89560494716=764.447802473580>1.$$

Therefore, the sufficient conditions in Theorems 2, 3, and 4 are not satisfied, and Theorems 2, 3, and 4 are not applicable to Example 3.

Table 3

Numerical and exact solution of example (12).
Number of basis functions $n = 20$, number of subintervals in the quadrature formula (9) $n_1 = 30$

x	u^{num}	u^{exact}	$u^{num}-u^{exact}$
0.000000000000000E+000	4.65979236632548	4.65979236632549	–2.66453525E–015
0.314159265358979	5.87168092602949	5.87168092602949	–2.66453525E–015
0.628318530717959	6.50880844628713	6.50880844628714	–3.55271367E–015
0.942477796076938	6.50880844628713	6.50880844628714	–1.77635683E–015
1.25663706143592	5.87168092602949	5.87168092602949	–1.77635683E–015
1.57079632679490	4.65979236632549	4.65979236632549	0.0000000000E+000
1.88495559215388	2.99177086312304	2.99177086312304	–8.881784197E–016
2.19911485751286	1.03089398294480	1.03089398294480	8.8817841970E–016
2.51327412287183	–1.03089398294480	–1.03089398294480	1.11022302E–015
2.82743338823081	–2.99177086312304	–2.99177086312304	0.000000000000E+000
3.14159265358979	–4.65979236632548	–4.65979236632549	1.776356839400E–015

The Chebyshev norm [11] of the residual of the problem (the difference between the numerical and exact solutions) at the grid nodes of the quadrature formula is:

$$\left\|u^{num}-u^{exact}\right\|_C=\max_{i=0,n_1}\left|u_i^{num}-u_i^{exact}\right|=1.776356839400250\text{E}-015, x_i=a+h\cdot i, i=\overline{0,n_1}.$$

Discussion. A modified degenerate-kernel method for solving a Fredholm integral equation of the second kind is proposed for the first time. The idea of the method is to expand the integral kernel with respect to the variable x in a Taylor series at the midpoint of the integration interval. Three theorems are proved that give sufficient conditions for the correctness of algorithm (2)–(7), including an estimate for the norm of the inverse matrix in formula (7). The factorial Chebyshev norm of a vector function is defined. For the first time, sufficient condition (10) is obtained, relating the factorial norm of the system of functions composed of the partial derivatives of the integral kernel to the parameter λ. Algorithm (2)–(7) was tested on three examples in which the integral kernel has an exponential feature or a periodic sign change.

Conclusion. The degenerate-kernel method is of interest in functional analysis and numerical methods. The kernel of the integral equation must be sufficiently smooth with respect to the variable x.

References

1. Bakhvalov N.S., Lapin A.V., Chizhonkov E.V. *Numerical methods in problems and exercises*. Binom. lab. Knowledge. 2010. 240 p. (In Russ.)

2. Burova I.G., Altsybeev G.O. The use of second-order H alsoths to solve integral equations of the second kind. *Computational methods and programming*. 2025;2(26):175–191. (In Russ.) https://doi.org/10.26089/NumMet.v26r213

3. Solovyova, S.A. On the special version of the method of resolving the integrated equations of Fredgolm of the second kind. *Computational methods and programming*. 2018;3(19):230–234. (In Russ.) https://doi.org/10.26089/NumMet.v19r322

4. Solovyova S.A. On one version of the collocation method for the integrated equations of Fredgolm of the second kind. *Computational methods and programming*. 2017;2(18):187–191. (In Russ.) https://doi.org/10.26089/NumMet.v18r216

5. Hermider O.V., Popov V.N. On the method of collocation when constructing a solution to the integral equation of Voltaire's second kind using polynomials of Chebyshev and Lyandra. *Izvestia of the Irkutsk State University. Series: Mathematics*. 2024;50:19–35. (In Russ.) https://doi.org/10.26516/1997-7670.2024.50.19

6. Junghanns P., Roch St., Silbermann B. Collocation methods for systems of cauchy singular integral equations. *Computational Technologies*. 2001;1(6):88–124.

7. Davydov A.A., Khachatryan H.A., Petrosyan A.S. On the solutions of one system of non-linear integrated equations such as a soften throughout the numerical direct. *Differential equations*. 2023;11(59):1500–1514. (In Russ.) https://doi.org/10.31857/S0374064123110055

8. Volosova N.K., Volosov K.A., Volosova A.K., Karlov M.I., Pastuhov D.F., Pastuhov Yu.F. The solution of the integral equations of Fredgolm by replacing the integrated square with the twelfth order of the error in the matrix form. *Bulletin of Perm University. Mathematics. Mechanics. Computer science*. 2023;1(60):5–14. (In Russ.) https://doi.org/10.17072/1993-0550-2023-1-5-14

9. Volosova N.K., Volosov K.A., Volosova A.K., Karlov M.I., Pastuhov D.F., Pastuhov Yu.F. The solution of the integral equations of Fredgolm by replacing the integrated square with the twelfth order of the error in the matrix form. *Bulletin of Perm University. Mathematics. Mechanics. Computer science*. 2022;4(59):9–17. (In Russ.) https://doi.org/10.17072/1993-0550-2022-4-9-17

10. Volkov Yu.S., Miroshnichenko V.L. Assessments of the norms of matrices, opposite to matrices of a monotonous kind and quite non-negative matrices. *Siberian mathematical journal*. 2009;6(50):1248–1254. (In Russ.)

11. Bahvalov N.S., Zhidkov N.P., Kobelkov G.M. *Numerical methods: a textbook for students of physics and mathematics specialties of higher educational institutions*. Binom. lab. Knowledge; 2011. 636 p. (In Russ.)

About the Authors:

Natalya K. Volosova, Post-graduate Student of Bauman Moscow State Technical University (5–1, 2nd Baumanskaya St., Moscow, 105005, Russian Federation), navalosova@yandex.ru

Konstantin A. Volosov, Doctor of Physical and Mathematical Sciences, Professor of the Department of Applied Mathematics of the Russian University of Transport (9–9, Obraztsova St., Moscow, GSP-4, 127994, Russian Federation), ORCID, SPIN-code, konstantinvolosov@yandex.ru

Aleksandra K. Volosova, Candidate of Physical and Mathematical Sciences, Chief Analytical Department "Tramplin" LLC, Russian University of Transport (9–9, Obraztsova St., Moscow, GSP-4, 127994, Russian Federation), ORCID, SPIN-code, alya01@yandex.ru

Mikhail I. Karlov, Candidate of Physical and Mathematical Sciences, Associate Professor of the Department of Mathematics, Moscow Institute of Physics and Technology (9, Institutsky Lane, GSP-4, Dolgoprudny, 141701, Russian Federation), SPIN-code, karlov.mipt@gmail.com

Dmitriy F. Pastukhov, Candidate of Physical and Mathematical Sciences, Associate Professor of Polotsk State University (29, Blokhin St., Novopolotsk, 211440, Republic of Belarus), ORCID, SPIN-code, dmitrij.pastuhov@mail.ru

Yuriy F. Pastukhov, Candidate of Physical and Mathematical Sciences,Associate Professor of Polotsk State University (29, Blokhin St., Novopolotsk, 211440, Republic of Belarus), ORCID, SPIN-code, pulsar1900@mail.ru

Contributions of the authors:

N.K. Volosova: ideas; formulation or evolution of overarching research goals and aims; writing — original draft preparation.

K.A. Volosov: supervision; methodology.

A.K. Volosova: translation; study of the history of the task; literature.

M.I. Karlov: formal analysis.

D.F. Pastukhov: visualization; validation; software.

Yu.F. Pastukhov: testing of existing code components.

Conflict of Interest Statement: **the authors declare no conflict of interest.**

All authors have read and approved the final manuscript.

Об авторах:

Наталья Константиновна Волосова, аспирант Московского государственного технического университета им. Н.Э. Баумана (105005, Российская Федерация, г. Москва, ул. 2-я Бауманская, 5, стр. 1), navalosova@yandex.ru

Константин Александрович Волосов, доктор физико-математических наук, профессор кафедры прикладной математики Российского университета транспорта (127994, ГСП-4, Российская Федерация, г. Москва, ул. Образцова, 9, стр. 9), ORCID, SPIN-код, konstantinvolosov@yandex.ru

Александра Константиновна Волосова, кандидат физико-математических наук, начальник аналитического отдела ООО «Трамплин» Российского университета транспорта (127994, ГСП-4, Российская Федерация, г. Москва, ул. Образцова, 9, стр. 9), ORCID, SPIN-код, alya01@yandex.ru

Михаил Иванович Карлов, кандидат физико-математических наук, доцент кафедры математики Московского физико-технического института (141701, ГСП-4, Российская Федерация, г. Долгопрудный, Институтский переулок, 9), SPIN-код, karlov.mipt@gmail.com

Дмитрий Феликсович Пастухов, кандидат физико-математических наук, доцент кафедры технологий программирования Полоцкого государственного университета (211440, Республика Беларусь, г. Новополоцк, ул. Блохина, 29), ORCID, SPIN-код, dmitrij.pastuhov@mail.ru

Юрий Феликсович Пастухов, кандидат физико-математических наук, доцент кафедры технологий программирования Полоцкого государственного университета (211440, Республика Беларусь, г. Новополоцк, ул. Блохина, 29), ORCID, SPIN-код, pulsar1900@mail.ru

Заявленный вклад соавторов:

Н.К. Волосова: постановка задачи; написание черновика рукописи; формулировка идей исследования, целей и задач.
К.А. Волосов: научное руководство; разработка методологии.
А.К. Волосова: перевод; изучение истории задачи; поиск литературы.
М.И. Карлов: формальный анализ.
Д.Ф. Пастухов: визуализация; валидация; разработка программного обеспечения.
Ю.Ф. Пастухов: тестирование существующих компонентов кода.

Конфликт интересов: **авторы заявляют об отсутствии конфликта интересов.**

Все авторы прочитали и одобрили окончательный вариант рукописи.

Received / Поступила в редакцию 30.08.2025
Reviewed / Поступила после рецензирования 26.10.2025
Accepted / Принята к публикации 12.12.2025

MATHEMATICAL MODELLING
МАТЕМАТИЧЕСКОЕ МОДЕЛИРОВАНИЕ

UDC 519.6:504.05

Original Empirical Research

https://doi.org/10.23947/2587-8999-2026-10-2-17-30

Mathematical Model of Plankton Dynamics Accounting for the Transformation of Nutrient Compounds, Suspended and Dissolved Substances

Inna Yu. Kuznetsova, Yulia V. Belova

Don State Technical University, Rostov-on-Don, Russian Federation

✉ ikuznecova@donstu.ru

Abstract

Introduction. In the context of increasing anthropogenic pressure and imbalance of nutrients, the development of phytoplankton dynamics models becomes particularly relevant. The proposed approach integrates the description of oxygen and carbon dioxide cycles, which is critically important for assessing the risks of cyanobacterial water "blooms" and reservoir deoxygenation.

Materials and Methods. An approach to constructing a comprehensive mathematical model is considered. Unlike existing analogues, this model simultaneously accounts for the dynamics of three functionally distinct phytoplankton groups with their specific preferences for nitrogen and phosphorus sources, as well as the complete silicon cycle, which is critically important for diatoms. The model integrates gas exchange processes, enabling the assessment of plankton dynamics' impact on the oxygen regime of the aquatic environment and acidity, which are key indicators of ecosystem health.

Results. Stationary solutions were obtained for the problem of plankton dynamics, considering the transformation of nutrient compounds, suspended and dissolved substances, including oxygen and carbon dioxide. Depending on external conditions (light, temperature, input nutrient concentrations), several qualitatively different stable stationary states are possible.

Discussion. The obtained results can be used for forecasting the consequences of reservoir eutrophication and water "blooms"; assessing the seasonal succession of plankton communities; developing strategies to reduce anthropogenic load on water bodies; and evaluating the role of marine and freshwater ecosystems in CO_2 absorption and oxygen production.

Conclusions. Understanding the conditions under which the system reaches a particular stationary state (equilibrium) allows us to predict the long-term consequences of anthropogenic impact and develop effective management solutions.

Keywords: plankton dynamics, nutrients, dissolved oxygen, carbon dioxide, stationary solution

Acknowledgements. The authors express their sincere gratitude to Alexander I. Sukhinov, Doctor of Physical and Mathematical Sciences, Professor, Corresponding Member of the Russian Academy of Sciences, for his attentive attitude and assistance in the work, constructive comments, and valuable recommendations that contributed to improving the quality of the study.

Funding. The study was supported by the Russian Science Foundation grant No. 22–71–10102–П, https://rscf.ru/project/22-71-10102/

For Citation. Kuznetsova I.Yu., Belova Yu.V. A Mathematical Model of Plankton Dynamics Accounting for the Transformation of Nutrient Compounds, Suspended and Dissolved Substances. *Computational Mathematics and Information Technologies*. 2026;10(2):17–30. https://doi.org/10.23947/2587-8999-2026-10-2-17-30

Оригинальное эмпирическое исследование

Математическая модель динамики фитопланктона с учетом трансформации биогенных соединений, взвешенных и растворённых веществ

И.Ю. Кузнецова ✉, **Ю.В. Белова**
Донской государственный технический университет, г. Ростов-на-Дону, Российская Федерация
✉ ikuznecova@donstu.ru

Аннотация

Введение. В условиях возрастающей антропогенной нагрузки и нарушения баланса биогенных элементов особую актуальность приобретает разработка моделей динамики фитопланктона. Предлагаемый в настоящей работе подход интегрирует описание циклов кислорода и углекислого газа, что критически важно для оценки рисков «цветения» воды цианобактериями и деоксигенации водоемов.

Материалы и методы. Рассмотрен подход к построению комплексной математической модели, которая в отличие от существующих аналогов одновременно учитывает динамику трех функционально различных групп фитопланктона с их специфическими предпочтениями к источникам азота и фосфора, а также полный цикл кремния, критически важный для диатомей. Модель интегрирует ключевые показатели здоровья экосистемы — кислотность и процессы газообмена, что позволяет оценивать влияние динамики планктона на кислородный режим водной среды.

Результаты исследования. Получены стационарные решения задачи динамики планктона с учетом трансформации биогенных соединений, взвешенных и растворённых веществ, в том числе кислорода и углекислого газа. В зависимости от внешних условий (свет, температура, входные концентрации биогенных веществ) возможны несколько качественно различных устойчивых стационарных состояний.

Обсуждение. Полученные результаты могут быть использованы для прогноза последствий эвтрофикации водоемов, «цветения» вод, оценки сезонной сукцессии планктонных сообществ; разработки стратегий снижения антропогенной нагрузки на водоемы; оценки роли морских и пресноводных экосистем в поглощении CO_2 и продуцировании кислорода.

Заключение. Проанализированы условия, при которых система приходит к тому или иному стационарному состоянию (равновесию), что позволит спрогнозировать долгосрочные последствия антропогенного воздействия и разрабатывать эффективные управляющие решения.

Ключевые слова: динамика планктона, биогенные вещества, растворенный кислород, углекислый газ, стационарное решение

Благодарности. Авторы выражают искреннюю благодарность Александру Ивановичу Сухинову, доктору физико-математических наук, профессору, член-корреспонденту РАН за внимательное отношение и помощь в работе, конструктивные замечания и ценные рекомендации, которые способствовали улучшению качества исследования.

Финансирование. Исследование выполнено за счет гранта Российского научного фонда № 22–71–10102–П, https://rscf.ru/project/22-71-10102/

Для цитирования. Кузнецова И.Ю., Белова Ю.В. Математическая модель динамики планктона с учетом трансформации биогенных соединений, взвешенных и растворённых веществ. *Computational Mathematics and Information Technologies*. 2026;10(2):17–30. https://doi.org/10.23947/2587-8999-2026-10-2-17-30

Introduction. The ecosystem of a water body is a complex organized structure in which different groups of aquatic organisms interact both with organic substances and with environmental factors such as salinity, temperature, and others. The level of dissolved oxygen has a substantial effect on the ecosystem, since oxygen deficiency may lead to mass mortality of living organisms. Growth in industrial production and the discharge of industrial waste and pollutants into water bodies sharply increase the load on aquatic ecosystems. For example, in recent decades the carbon cycle has had a significant impact on aquatic ecosystems, because the level of carbon dioxide uptake by the world ocean has been increasing. This, in turn, affects both the pH of water and the chemical reactions occurring in the water column, which substantially influence the vital activity of living organisms.

Phytoplankton, as the main producer in most aquatic ecosystems, plays a key role in global biogeochemical cycles by producing oxygen and absorbing carbon dioxide. However, under anthropogenic impact, primarily eutrophication, i. e. enrichment of waters with biogenic elements (nitrogen and phosphorus), the natural balance of plankton communities is disturbed. This disturbance is often manifested as massive water blooms, which may be caused by different phytoplankton groups. Blooms of cyanobacteria (blue-green algae) are especially hazardous, since many of them produce toxins dangerous

to aquatic organisms, animals, and humans. In addition, the decomposition of dead plankton biomass leads to deoxygenation of water, resulting in "dead zones", hypoxic and anoxic areas unsuitable for aerobic organisms [1]. A shift in dominant phytoplankton species, for example from diatoms to cyanobacteria, is an indicator of serious changes in ecosystem status.

A key aspect of aquatic ecosystem functioning is the transformation of substances. The input of mineral forms of phosphorus and nitrogen stimulates phytoplankton growth. The death and excretion of organic matter initiate degradation processes that are closely related to the dynamics of dissolved oxygen (O_2) and carbon dioxide (CO_2). The oxygen regime in surface waters is formed mainly by production processes, whereas in near-bottom waters it is determined primarily by the biochemical decomposition of bottom sediments [2]. Dissolved oxygen is not only a source for the respiration of aquatic organisms but also a factor determining the completeness and rate of organic matter mineralization in a water body. A characteristic feature of the oxygen regime of the Sea of Azov is its instability, which is determined by a number of permanent and seasonal factors: absorption of atmospheric oxygen by the surface water layer, uneven inflow of river and Black Sea waters, development and decline of organism activity, circulation processes that control the penetration of oxygen into near-bottom layers, and other processes [3].

In this regard, the relevant task is not merely to forecast the growth of phytoplankton biomass, but to provide integrated modeling of the plankton community structure and the associated biogeochemical cycles. Mathematical modeling becomes an indispensable tool for solving this problem, since it makes it possible to integrate heterogeneous data on physical, chemical, and biological processes and to predict the response of the system to changing external conditions.

Classical models, such as the Monod equation or the Michaelis-Menten model, describe the dependence of phytoplankton growth rate on the concentration of a single limiting substance (nitrogen or phosphorus) [4]. More complex models take into account simultaneous limitation by several resources. To describe phytoplankton adaptation to changing conditions, models of phytoplankton growth have been developed in which the growth rate depends on the internal content of nutrients in the cell, rather than only on their concentration in the surrounding environment (the Droop model) [5].

The competitive exclusion model (Gause's law or principle) predicts that, in a stationary state, only as many species can survive as there are limiting resources [6]. This stimulated the development of models that include additional factors allowing a larger number of species to coexist: spatial heterogeneity, temporal variability of parameters, allelopathy, and the presence of predators (zooplankton). In the context of the present study, models that consider competition among phytoplankton with different strategies for consuming nutrients, for example the ability of cyanobacteria to fix atmospheric nitrogen, are of particular importance.

The works of such researchers as Riley, Steele, and Lorenz laid the foundations for including biogeochemical processes in ecosystem models [7, 8]. Models of the nitrogen cycle incorporating nitrification and denitrification were developed, including WASP (Water Quality Analysis Simulation Program) [9] and ERSEM (European Regional Seas Ecosystem Model) [10]. In the 1990s and 2000s, models of plankton dynamics were integrated with biogeochemical models, which made it possible to describe seasonal variability in species composition and the related changes in elemental cycles.

The dynamics of O_2 and CO_2 are traditionally modeled through the balance of photosynthesis, respiration, and air-water gas exchange [11]. The complexity lies in the need to account for diurnal dynamics, which are often averaged in models intended for long-term forecasts. Recently, increasing attention has been paid to modeling the carbonate system (pH, alkalinity) and its effect on the growth of different phytoplankton species.

Classical models, such as the NPZ (Nutrient-Phytoplankton-Zooplankton) model [12], focus on the interaction among nutrients, phytoplankton, and zooplankton. However, they often treat biogenic elements in a simplified way, for example by representing "nitrogen" or "phosphorus" as a single pool.

More complex models take into account the transformation of different forms of elements. For example, the nitrogen cycle is detailed by considering nitrification (oxidation of ammonium to nitrites and then to nitrates) and denitrification [13]. This is critically important because different phytoplankton species have different preferences for nitrogen sources: diatoms prefer nitrates, many green algae prefer ammonium, and some cyanobacteria are able to fix atmospheric nitrogen (N_2), which gives them a competitive advantage in nitrogen-poor waters.

Similarly, to describe the dynamics of diatoms adequately, the silicon cycle must be taken into account, since their frustule consists of silica (SiO_2). Models that ignore silicon limitation may substantially overestimate forecasts of diatom biomass.

Models that include oxygen and CO_2 dynamics represent the next level of complexity. They make it possible to assess the consequences of eutrophication not only in terms of algal biomass, but also in terms of ecosystem health (oxygen regime) and its role in the carbon cycle. Such models are often based on stoichiometric ratios (Redfield ratios [11]) among carbon, nitrogen, and phosphorus in plankton biomass.

Despite the existence of integrated models, such as the ERSEM family of models, the literature still lacks models that simultaneously account for competition among several specific phytoplankton species with different nutritional strategies, the complete silicon cycle, and gas dynamics within a closed system of equations. The present study aims to fill this gap by constructing an integrated model and conducting a systematic analysis of its stationary states, which is a fundamental task for understanding the resilience of aquatic ecosystems to anthropogenic impact.

Materials and Methods

1. Mathematical model of plankton dynamics. The proposed model of plankton dynamics is based on a system of transport equations for nutrients [11, 13, 14]:

$$\frac{\partial q_i}{\partial t}+\frac{\partial (uq_i)}{\partial x}+\frac{\partial (vq_i)}{\partial y}+\frac{\partial ((w+w_{s,i})q_i)}{\partial z}=\frac{\partial}{\partial x}\left(\mu\frac{\partial q_i}{\partial x}\right)+\frac{\partial}{\partial y}\left(\mu\frac{\partial q_i}{\partial y}\right)+\frac{\partial}{\partial z}\left(\upsilon\frac{\partial q_i}{\partial z}\right)+R_{q_i}+C_{q_i}, \quad (1)$$

where q_i is the concentration of the i-th component, mg/L (the components are listed in Table 1); $\mathbf{V} = \{u,v,w\}$ are the components of the water-flow velocity vector, m/s; $w_{s,i}$ is the gravitational settling velocity of the i-th component if it is suspended; μ, υ are the horizontal and vertical components of the turbulent exchange coefficient, m²/s; R_{q_i} is the source function for nutrients, mg/(L·s); C_{q_i} is the flux of oxygen and carbon dioxide from the atmosphere, mg/(L·s).

The model under consideration accounts for the following factors (components), presented in Table 1 and forming the system of equations (1).

Table 1

Components of the mathematical model (1)

i	Sym.	Name
1.	F_1	concentration of green algae (*Chlorella vulgaris*)
2.	F_2	concentration of blue-green algae (*Aphanizomenon flos-aquae*)
3.	F_3	concentration of diatoms (*Sceletonema costatum*)
4.	PO_4	concentration of phosphates, mineral phosphorus
5.	POP	concentration of suspended organic phosphorus
6.	DOP	concentration of dissolved organic phosphorus
7.	NO_3	concentration of nitrates
8.	NO_2	concentration of nitrites
9.	NH_4	concentration of ammonium
10.	Si	concentration of dissolved inorganic silicon (silicic acid, $Si(OH)_4$)
11.	O_2	concentration of dissolved oxygen
12.	CO_2	concentration of carbon dioxide (gaseous carbon dioxide, dissolved organic carbon, and total inorganic carbon)

In the further consideration of the model, the following assumptions are adopted:

1. Temperature and light regime are specified as external control parameters.

2. Hydrodynamic processes are taken into account. The velocity vector of the aquatic environment is calculated on the basis of a mathematical model of shallow-water hydrodynamics [15].

3. Zooplankton and higher aquatic vegetation are excluded from consideration in order to focus on primary production and decomposition processes.

4. The input of nutrients (PO_4, NO_3, NH_4, Si) from external sources is constant.

5. Nitrification proceeds in two stages: oxidation of NH_4^+ to NO_2^- and oxidation of NO_2^- to NO_3^-.

6. Mineralization, nitrification, and respiration processes depend on temperature according to the Van't Hoff law.

7. The stoichiometric ratios of elements in phytoplankton biomass (C:N:P:Si) are assumed to be constant for each species.

2. Equations for phytoplankton. The chemical-biological reactions for phytoplankton describing the nutrient source function can be written as follows [11, 14]:

$$R_{F_i}=C_{F_i}\left(1-K_{F_iR}\right)q_{F_i}-K_{F_iD}q_{F_i}-K_{F_iE}q_{F_i},\ i=\overline{1,3}, \quad (2)$$

where C_{F_i} is the growth rate of the i-th phytoplankton species; K_{F_iR} is the specific respiration rate of the i-th phytoplankton species; K_{F_iD} is the specific mortality (natural death) rate of the i-th phytoplankton species; K_{F_iE} is the specific phytoplankton excretion rate.

The growth rate of the i-th phytoplankton species is modeled with multiple-resource limitation: for F_1 and F_2, silicon limitation is absent; for F_2, fixation of molecular nitrogen (N_2) may be taken into account, which removes nitrogen limitation at low NH_4 and NO_3 concentrations (this can be represented by introducing an additional term $K_{N_2F_2}$, that depends on O_2 concentration, since fixation is inhibited by oxygen), but N_2 is not considered in the present study; for F_3, silicon limitation is mandatory; for F_3, NH_4 uptake is preferred over NO_3 uptake (suppression effect).

Taking these constraints into account, the following function is obtained to describe the phytoplankton growth rate:

$$C_{F_{1,2}} = K_{NF_{1,2}} f_T(T) f_I(I) f_S(S) \min\{f_P(q_{PO_4}), f_N(q_{NO_3}, q_{NO_2}, q_{NH_4})\},$$
$$C_{F_3} = K_{NF_3} f_T(T) f_I(I) f_S(S) \min\{f_P(q_{PO_4}), f_N(q_{NO_3}, q_{NO_2}, q_{NH_4}), f_{Si}(q_{Si})\}, \quad (3)$$

where K_{NF_i} is the maximum specific phytoplankton growth rate; $f_T(T), f_I(I), f_S(S)$ are functions describing the dependence of the growth rate of a particular phytoplankton species on temperature, illumination, and salinity, respectively; $f_P(q_{PO_4})$, $f_N(q_{NO_3}, q_{NO_2}, q_{NH_4})$, $f_{Si}(q_{Si})$ are functions describing the dependence of the phytoplankton growth rate on the water content of phosphorus, nitrogen compounds, and silicon, respectively.

Liebig's law of the minimum, in the form $\min\{f_P(q_{PO_4}), f_N(q_{NO_3}, q_{NO_2}, q_{NH_4})\}$ and $\min\{f_P(q_{PO_4}), f_N(q_{NO_3}, q_{NO_2}, q_{NH_4}), f_{Si}(q_{Si})\}$ is used to account for the combined limiting effect of several nutrient compounds.

The dependence of phytoplankton growth on temperature and salinity is described by:

$$f_T(T) = \exp\left(-\alpha\{(T - T_{opt})/T_{opt}\}^2\right), f_S(S) = \exp\left(-\beta\{(S - S_{opt})/S_{opt}\}^2\right), \quad (4)$$

where T_{opt} is the temperature, S_{opt} is the salinity optimal for a particular phytoplankton species, and $\alpha > 0$ and $\beta > 0$ are the coefficients determining the width of the phytoplankton tolerance intervals for temperature and salinity, respectively.

The dependence of phytoplankton growth on illumination is described by Steele's model:

$$f_T(T) = (I/I_{opt})\exp(1 - I/I_{opt}), \quad (5)$$

where I_{opt} is the optimal light intensity for photosynthesis.

The phosphorus limitation function is:

$$f_P(q_{PO_4}) = \frac{q_{PO_4}}{q_{PO_4} + K_{PO_4}}, \quad (6)$$

where K_{PO_4} is the phosphate half-saturation constant.

The nitrogen-compound limitation function is:

$$f_N(q_{NO_3}, q_{NO_2}, q_{NH_4}) = f_N^{(1)}(q_{NO_3}, q_{NO_2}, q_{NH_4}) + f_N^{(2)}(q_{NH_4}),$$
$$f_N^{(1)}(q_{NO_3}, q_{NO_2}, q_{NH_4}) = \frac{(q_{NO_3} + q_{NO_2})\exp(-K_{psi} q_{NH_4})}{K_{NO_3} + (q_{NO_3} + q_{NO_2})}, \quad (7)$$
$$f_N^{(2)}(q_{NH_4}) = \frac{q_{NH_4}}{K_{NH_4} + q_{NH_4}},$$

where K_{NO_3} is the nitrate half-saturation constant; K_{NH_4} is the ammonium half-saturation constant; K_{psi} is the ammonium inhibition coefficient.

The silicon limitation function is:

$$f_{Si}(q_{Si}) = \frac{q_{Si}}{q_{Si} + K_{Si}}, \quad (8)$$

where K_{Si} is the silicon half-saturation constant.

3. Equations for the transformation of nutrients

3.1. Phosphorus cycle. Equation for phosphates (PO_4): the chemical-biological reaction describing the source function for phosphates (PO_4) can be written as follows [11, 14]:

$$R_{PO_4} = -\sum_{i=1}^{3} s_P C_{F_i}(1 - K_{F_i R}) q_{F_i} + K_{PN} q_{POP} + K_{DN} q_{DOP}, \quad (9)$$

where s_p is the normalization coefficient corresponding to the stoichiometric ratio, K_{PN} is the *POP* phosphatization coefficient; K_{DN} is the *DOP* phosphatization coefficient. The first term in (9) reflects phosphate uptake by phytoplankton. It should also be noted that mineralization (hydrolysis) of *DOP* to phosphates occurs faster than mineralization of *POP*.

Equation for suspended organic phosphorus (*POP*):

$$R_{POP} = \sum_{i=1}^{3} s_P K_{F_i D} q_{F_i} - K_{PD} q_{POP} - K_{PN} q_{POP}, \quad (10)$$

where K_{PD} is the specific *POP* autolysis rate. The first term in (10) reflects the input of *POP* from dead phytoplankton biomass, while the second and third terms represent loss due to the transition of a part of *POP* to *DOP* during decomposition and mineralization (phosphatization) of *POP*.

Equation for dissolved organic phosphorus (*DOP*):

$$R_{DOP} = \sum_{i=1}^{3} s_P K_{F_i E} q_{F_i} + K_{PD} q_{POP} - K_{DN} q_{DOP}. \quad (11)$$

The first term in (11) reflects the input of *DOP* due to lysis and exosmosis of dead phytoplankton biomass; the second term represents the transition of a part of *POP* to *DOP* during decomposition; and the third term represents mineralization of *DOP* to phosphates.

3.2. Nitrogen cycle. Equation for ammonium (NH_4): the chemical-biological reaction describing the source function for ammonium (NH_4) can be written as follows [11, 14]:

$$R_{NH_4} = -\sum_{i=1}^{3} s_N C_{F_i} \left(1 - K_{F_i R}\right) \frac{f_N^{(2)}\left(q_{NH_4}\right)}{f_N\left(q_{NO_3}, q_{NO_2}, q_{NH_4}\right)} q_{F_i} + \sum_{i=1}^{3} s_N \left(K_{F_i D} + K_{F_i E}\right) q_{F_i} - K_{42} q_{NH_4}, \quad (12)$$

where s_N is the normalization coefficient corresponding to the stoichiometric ratio, K_{42} is the specific rate of ammonium oxidation to nitrites during nitrification (in the general case, it depends on the concentrations of ammonium and oxygen). The first term in (12) reflects ammonium uptake by phytoplankton.

Equation for nitrites (NO_2):

$$R_{NO_2} = -\sum_{i=1}^{3} s_N C_{F_i} \left(1 - K_{F_i R}\right) \frac{f_N^{(1)}\left(q_{NO_3}, q_{NO_2}, q_{NH_4}\right)}{f_N\left(q_{NO_3}, q_{NO_2}, q_{NH_4}\right)} \cdot \frac{q_{NO_2}}{q_{NO_2} + q_{NO_3}} q_{F_i} + K_{42} q_{NH_4} - K_{23} q_{NO_2}, \quad (13)$$

where K_{23} is the specific rate of nitrite oxidation to nitrates during nitrification. The first term in (13) reflects nitrite uptake by phytoplankton (usually insignificant), the second term represents the inflow due to the first stage of nitrification (oxidation of ammonium to nitrites), and the third term represents the outflow due to the second stage of nitrification (oxidation of nitrites to nitrates).

Equation for nitrates (NO_3):

$$R_{NO_3} = -\sum_{i=1}^{3} s_N C_{F_i} \left(1 - K_{F_i R}\right) \frac{f_N^{(1)}\left(q_{NO_3}, q_{NO_2}, q_{NH_4}\right)}{f_N\left(q_{NO_3}, q_{NO_2}, q_{NH_4}\right)} \cdot \frac{q_{NO_3}}{q_{NO_2} + q_{NO_3}} q_{F_i} + K_{23} q_{NO_2}. \quad (14)$$

The first term in (14) reflects nitrate uptake by phytoplankton, while the second term represents the inflow due to the second stage of nitrification (oxidation of nitrites to nitrates).

3.3. Silicon cycle. The chemical-biological reaction describing the source function for dissolved silicon (*Si*) can be written as follows [11, 14]:

$$R_{Si} = -s_{Si} C_{F_3} \left(1 - K_{F_3 R}\right) q_{F_3} + s_{si} K_{F_3 D} q_{F_3}, \quad (15)$$

where s_{si} is the normalization coefficient corresponding to the stoichiometric ratio. The first term in (15) represents silicon uptake by diatoms, and the second term represents the inflow due to dissolution of biogenic silicon from the frustules of dead diatoms.

4. Equations for dissolved gases

4.1. Dissolved oxygen

$$R_{O_2} = s_O \sum_{i=1}^{3} s_P C_{F_i} \left(K_{F_i R} - 1\right) q_{F_i} + s_O \left(K_{PN} q_{POP} + K_{DN} q_{DOP}\right) + \gamma_{O_2}^{(1)} K_{42} q_{NH_4} - \gamma_{O_2}^{(2)} K_{23} q_{NO_2} + C_{O_2}, \quad (16)$$

where s_O is the normalization coefficient corresponding to the stoichiometric ratio, $\gamma_{O_2}^{(1)}$ is the oxygen consumption coefficient for the first stage of nitrification (oxidation of ammonium to nitrites), $\gamma_{O_2}^{(2)}$ is the oxygen consumption coefficient for the second stage of nitrification (oxidation of nitrites to nitrates), and C_{O_2} is gas exchange with the atmosphere. The first term in (16) reflects O_2 production during photosynthesis and O_2 consumption for phytoplankton respiration; the second and third terms reflect the participation of O_2 in phosphatization; and the fourth and fifth terms reflect the participation of O_2 in nitrification. To describe oxygen gas exchange between the atmosphere and the ocean, we use [16]:

$$C_{O_2} = k_{O_2} \left(\frac{Sc}{660}\right)^{-0,5} \left(C_{O_2 eq} - q_{O_2}\right), \quad (17)$$

where k_{O_2} is the relative gas-exchange rate, which can be calculated as a function of wind speed, $k_{O_2}(u) = 0.365u^2 + 0.4u$ [16], where u is wind speed; *Sc* is the Schmidt number, which reflects the ratio between kinematic viscosity and the turbulent exchange coefficient; for oxygen at 20 °C, *Sc* = 660; and $C_{O_2 eq}$ is the equilibrium oxygen concentration, calculated as a function of temperature and salinity according to UNESCO standards (1986) [17]; at 20 °C it is 31 mL/L.

4.2. Carbon dioxide

$$R_{CO_2} = s_C \sum_{i=1}^{3} C_{F_i} \left(K_{F_i R} - 1 \right) q_{F_i} + C_{CO_2}, \tag{18}$$

where s_C is the normalization coefficient corresponding to the stoichiometric ratio, C_{CO_2} is gas exchange with the atmosphere. The first term in (18) reflects CO_2 consumption during photosynthesis and CO_2 release during phytoplankton respiration.

To describe carbon dioxide gas exchange between the atmosphere and the ocean, we use the following formula [18]:

$$C_{CO_2} = k_{CO_2} \left(C_{CO_2 eq} - q_{CO_2} \right), \tag{19}$$

where k_{CO_2} is the exchange coefficient calculated from near-surface wind speed using empirical formulas according to [19], and $C_{CO_2 eq}$ is the equilibrium carbon dioxide concentration calculated by Henry's law: $C = kP$, where P is the partial pressure of carbon dioxide and k is Henry's constant, which depends on the gas and the liquid.

5. Specification of initial and boundary conditions. For system (1), we prescribe the vector field of water-flow velocities calculated on the basis of a mathematical model of shallow-water hydrodynamics [15, 20], the salinity field S and temperature field T, as well as the initial values of the concentration functions q_i, where the index i corresponds to the components presented in Table 1:

$$q_i (x, y, z, 0) = q_t^0 (x, y, z), \ (x, y, z) \in \bar{G}, \ t = 0, \tag{20}$$

$$\mathbf{V}(x,y,z,0) = \mathbf{V}_0(x,y,z),\ T(x,y,z,0) = T_0(x,y,z),\ S(x,y,z,0) = S_0(x,y,z).$$

We consider the mathematical model (1)–(19) in the computational domain G, which is a closed basin bounded by the undisturbed water surface Σ_0, the bottom $\Sigma_H = \Sigma_H (x, y)$ and the cylindrical (lateral) surface σ over the time interval $0 < t \le T$. $\Sigma = \Sigma_0 \cup \Sigma_H \cup \sigma$ is the piecewise smooth boundary of the domain G. Let $\mathbf{n}$ be the outward normal vector to the surface Σ, and $u_{\mathbf{n}}$ be the component of the water-flow velocity vector normal to Σ.

For the concentrations of all substances except O_2 and CO_2, we assume that there is no substance input through the upper boundary of the computational domain:

$$\frac{\partial q_i}{\partial z} = 0, \ i = \overline{1,10}. \tag{21}$$

For dissolved oxygen and carbon dioxide, gas exchange with the atmosphere is calculated according to formulas (17) and (19):

$$\frac{\partial q_{11}}{\partial z} = C_{O_2} (q_{11}), \ \frac{\partial q_{12}}{\partial z} = C_{CO_2} (q_{12}). \tag{22}$$

On the lateral boundary σ, the following conditions are specified for the concentrations of all substances presented in Table 1:

$$q_i = 0, \text{ если } u_{\mathbf{n}} < 0; \ \frac{\partial q_i}{\partial \mathbf{n}} = 0, \text{ если } u_{\mathbf{n}} \ge 0. \tag{23}$$

At the bottom Σ_H the following conditions are specified for the concentrations of all substances presented in Table 1:

$$\frac{\partial q_i}{\partial z} = \varepsilon_i q_i, \tag{24}$$

where ε_i is the absorption coefficient of the i-th component by bottom sediments.

The proposed model (1)–(24) can be used to simulate the movement and accumulation of dissolved oxygen and carbon dioxide in the water column and to study their effect on the ecosystem of a water body.

Model parameter selection. To refine the parameters of the phytoplankton-dynamics model accounting for the transformation of nutrient compounds, suspended and dissolved substances, including oxygen and carbon dioxide, we find stationary solutions of the model (1)–(24). For the computational experiment, a program was written in the *R* programming language. It implements the solution of the system of ordinary differential equations (ODEs) (2), (9)–(16), (18) by the fourth-order Runge-Kutta method, constructs plots of the resulting stationary solutions for the concentrations of phytoplankton, nutrient compounds, suspended and dissolved substances, and checks the stability of the obtained stationary solutions. Numerical experiments were performed under the assumption that phytoplankton development depends on a single limiting substance.

The input values of the parameters of the phytoplankton-dynamics model accounting for the transformation of nutrient compounds, suspended and dissolved substances, including oxygen and carbon dioxide, as well as the initial concentrations of phytoplankton, nutrient compounds, suspended and dissolved substances, are presented in Table 2. Limitation by temperature, salinity (4), and illumination (5) was not taken into account: $T = T_{opt}$, $I = I_{opt}$, $S = S_{opt}$.

Table 2

Values of phytoplankton-dynamics model parameters and initial concentrations of the studied substances

Sym.	Name	Value	Unit
Model parameters			
Green alga (*Chlorella vulgaris*)			
K_{NF_1}	maximum specific growth rate	2.8000	1/day
K_{F_1R}	specific respiration rate	0.1500	1/day
K_{F_1D}	specific mortality rate	0.0500	1/day
K_{F_1E}	specific excretion rate	0.1500	1/day
K_{PO_4}	phosphate half-saturation constant	0.2400	
K_{NO_3}	nitrate half-saturation constant	0.3000	
K_{NH_4}	ammonium half-saturation constant	0.2000	
Blue-green alga (*Aphanizomenon flos-aquae*)			
K_{NF_2}	maximum specific growth rate	2.8000	1/day
K_{F_2R}	specific respiration rate	0.1500	1/day
K_{F_2D}	specific mortality rate	0.0500	1/day
K_{F_2E}	specific excretion rate	0.1500	1/day
K_{PO_4}	phosphate half-saturation constant	0.2400	
K_{NO_3}	nitrate half-saturation constant	0.3000	
K_{NH_4}	ammonium half-saturation constant	0.2000	
Diatom (*Sceletonema costatum*)			
K_{NF_3}	maximum specific growth rate	2.8000	1/day
K_{F_3R}	specific respiration rate	0.1500	1/day
K_{F_3D}	specific mortality rate	0.0500	1/day
K_{F_3E}	specific excretion rate	0.15	1/day
K_{PO_4}	phosphate half-saturation constant	0.2400	
K_{NO_3}	nitrate half-saturation constant	0.3000	
K_{NH_4}	ammonium half-saturation constant	0.2000	
K_{Si}	silicon half-saturation constant	3.0000	
Phosphorus cycle			
K_{PD}	specific *POP* autolysis rate	0.0150	1/day
K_{PN}	*POP* phosphatization coefficient	0.0200	1/day
K_{DN}	*DOP* phosphatization coefficient	0.1000	1/day
s_P	normalization coefficient	0.0100	
Nitrogen cycle			
K_{42}	specific rate of ammonium oxidation to nitrites	0.9000	1/day
K_{23}	specific rate of nitrite oxidation to nitrates	2.5000	1/day
K_{psi}	ammonium inhibition coefficient	1.4600	1/day
s_N	normalization coefficient	0.0160	
Silicon cycle			
S_{Si}	normalization coefficient	0.0230	
Dissolved oxygen			
s_O	normalization coefficient	0.0500	
$\gamma_{O_2}^{(1)}$	oxygen consumption coefficient for the first stage of nitrification	0.0500	1/day
$\gamma_{O_2}^{(2)}$	oxygen consumption coefficient for the second stage of nitrification	0.0015	1/day
C_{O_2eq}	equilibrium oxygen concentration[1]	9,1000	mg/L

[1] For simplicity, the equilibrium oxygen concentration was calculated based on an empirical temperature dependence formula: $C_{CO_2eq}(T) = 14.6 - 0.42 \cdot T + 0.008 \cdot T^2$, $T = T_{opt} = 25$ °C.

End of Table 2

Sym.	Name	Value	Unit
Model parameters			
Carbon dioxide			
s_C	normalization coefficient	0.0020	1/day
C_{CO_2eq}	equilibrium carbon dioxide concentration	1.5000	mg/L
Initial concentrations			
q_1	initial concentration of green algae	2.5000	mg/L
q_2	initial concentration of blue-green algae	2.6000	mg/L
q_3	initial concentration of diatoms	0.9100	mg/L
q_{PO_4}	initial concentration of phosphates	0.0050	mg/L
q_{POP}	initial concentration of suspended organic phosphorus	0.0700	mg/L
q_{DOP}	initial concentration of dissolved organic phosphorus	0.0700	mg/L
q_{NO_3}	initial concentration of nitrates	0.3040	mg/L
q_{NO_2}	initial concentration of nitrites	0.0178	mg/L

Fig. 1 presents the simulation results for the stationary regime of the ODE system under the assumption that phytoplankton development is limited by phosphorus, nitrogen, and silicon. The limitation functions are calculated on the basis of (6)–(8).

The computational experiments show that, for the initial concentrations and equation parameters specified in Table 2, stationary regimes arise for the ODE system (2), (10)–(17), (19), which describes the case of a spatially uniform distribution of substances.

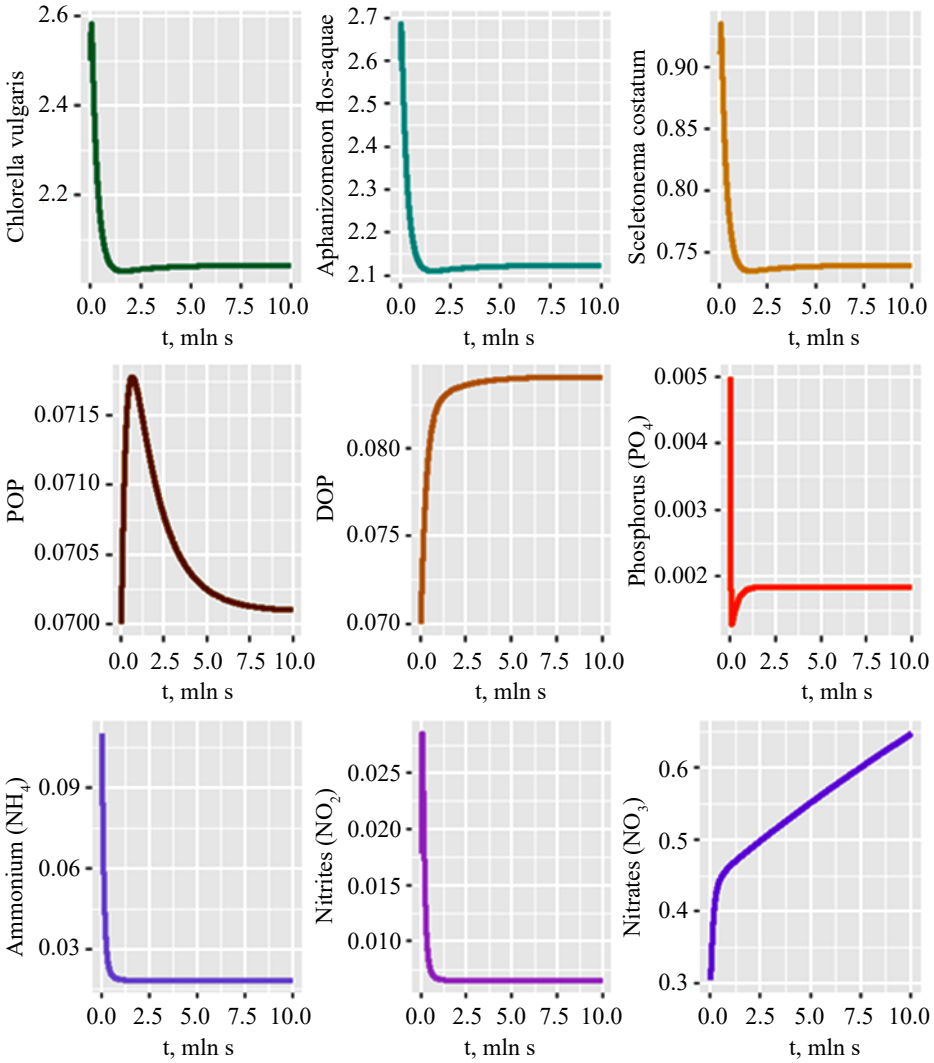

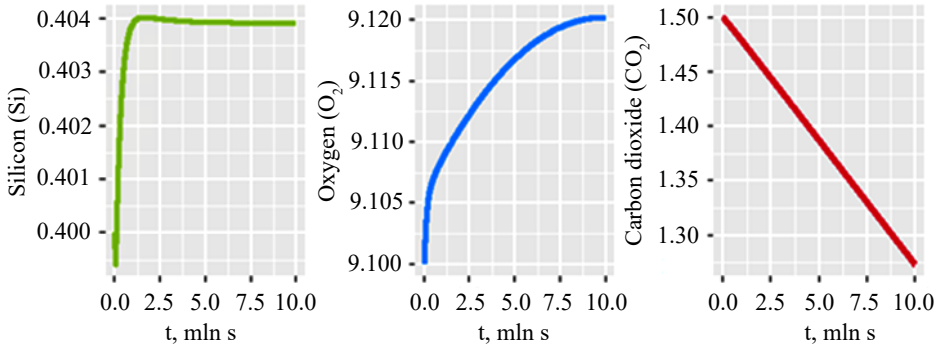

Fig. 1. Stationary regimes of the phytoplankton-dynamics model

Over time, the dynamics become smooth and oscillations decrease until a stationary state is reached. For nitrates in Fig. 1, an increase in concentration is observed, but it does not exceed 10^{-6} mg/L. The decrease in carbon dioxide concentration in Fig. 1 also does not exceed 10^{-5} mg/L. These results illustrate the stable distribution of algae and oxygen in the water body achieved by the model.

Silicon deficiency scenario. On the basis of the refined model parameters, several scenarios of phytoplankton dynamics accounting for the transformation of nutrient compounds, suspended and dissolved substances, including oxygen and carbon dioxide, are considered. As the first scenario, we consider the case of a low silicon concentration. The model parameters and initial concentrations were specified according to Table 2, except for the silicon concentration, which was set to $q_{Si} = 0.01$ mg/L. The simulation results are presented in Fig. 2. As shown by the obtained results, silicon deficiency substantially affected the concentration of diatoms, which by the end of the simulation period did not exceed $2 \cdot 10^{-9}$ mg/L. At the same time, the concentrations of green and blue-green algae were higher than in Fig. 1 (with the initial silicon concentration $q_{Si} = 0.4$ mg/L).

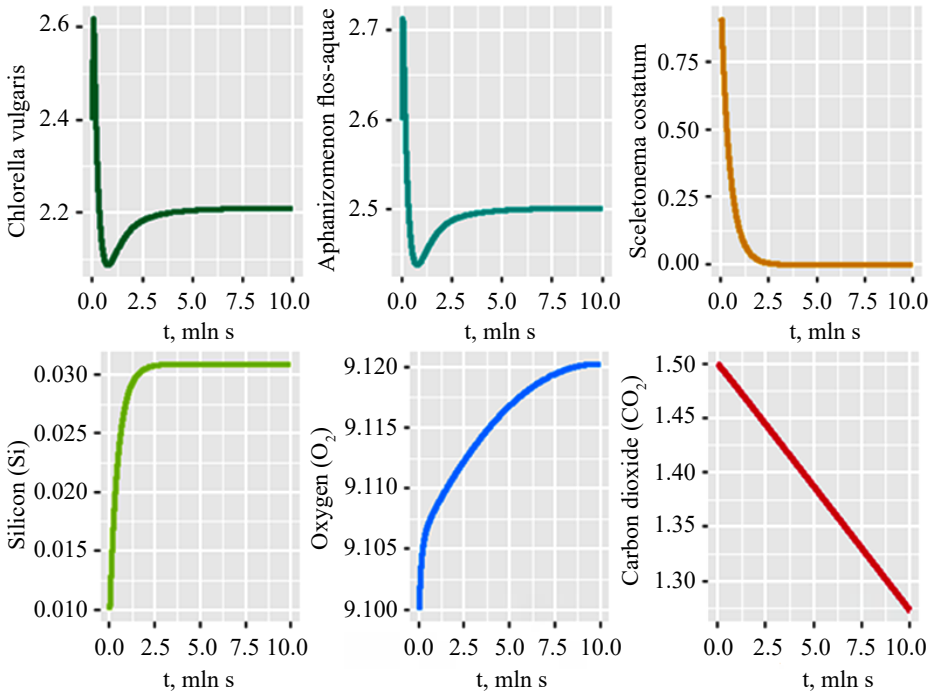

Fig. 2. Stationary regimes of the phytoplankton-dynamics model under silicon deficiency

Nitrogen deficiency scenario. As the second scenario, we consider the case of nitrogen deficiency. The model parameters and initial concentrations were specified according to Table 2, except for the concentrations of nitrates, nitrites, and ammonium, which were set to $q_{NO_2} = 0{,}001$ mg/L, $q_{NO_3} = 0{,}001$ mg/L, $q_{NH_4} = 0{,}01$ mg/L.

The simulation results are presented in Fig. 3. The deficiency of nitrogen compounds substantially reduced the biomass of all three phytoplankton species (to $7.7 \cdot 10^{-5}$ mg/L, $8 \cdot 10^{-5}$ mg/L, and $2.8 \cdot 10^{-5}$ mg/L for green, blue-green, and diatom algae, respectively) and also affected the concentrations of other nutrient and dissolved substances.

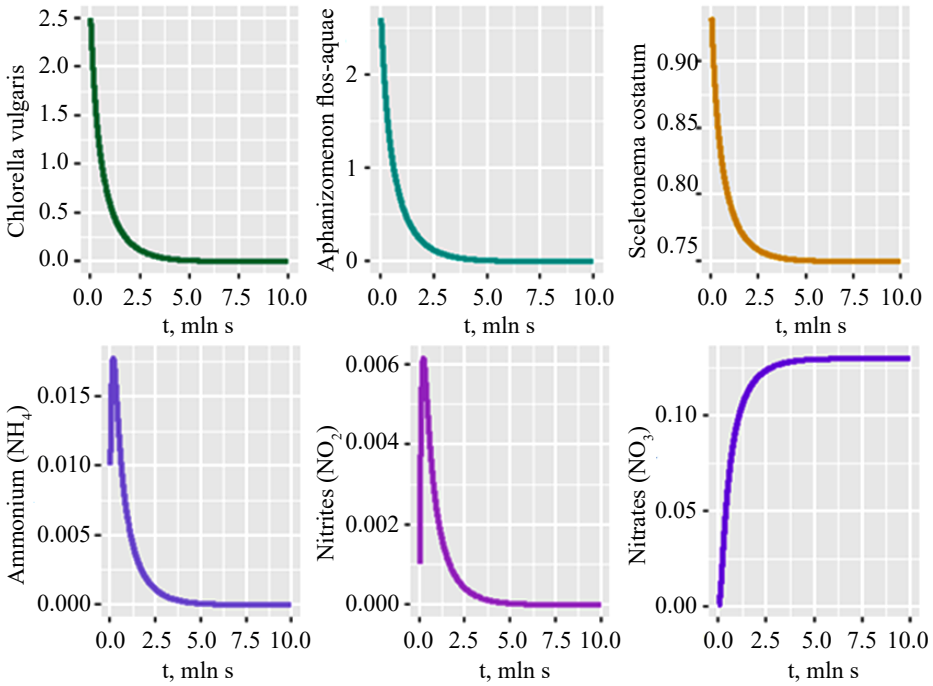

Fig. 3. Stationary regimes of the phytoplankton-dynamics model under nitrogen deficiency

Phosphorus deficiency scenario. As the third scenario, we consider the case of phosphorus deficiency. The model parameters and initial concentrations were specified according to Table 2, except for the concentrations of phosphates and suspended and dissolved organic phosphorus: $q_{PO_4} = 0.0005$ mg/L, $q_{POP} = 0.007$ mg/L, $q_{DOP} = 0.007$ mg/L.

The simulation results are presented in Fig. 4. The deficiency of phosphorus compounds reduced the biomass of all three phytoplankton species, although not as strongly as nitrogen deficiency.

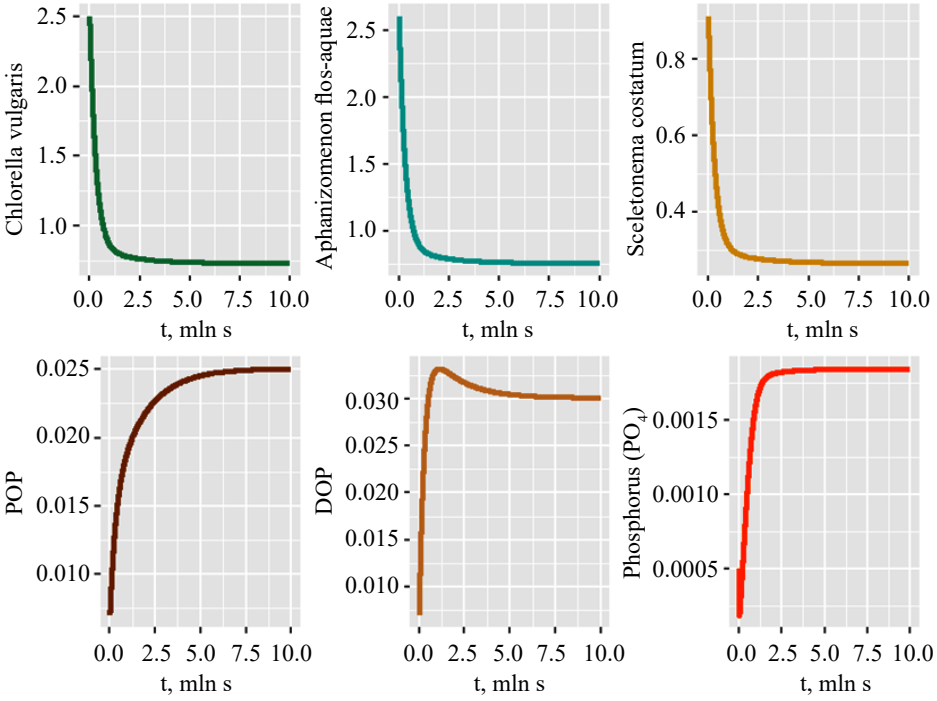

Fig. 4. Stationary regimes of the phytoplankton-dynamics model under phosphorus deficiency

Nutrient abundance scenario. As the fourth scenario, we consider the case of abundant compounds of all nutrients. The model parameters were specified according to Table 2. The initial concentrations of substances were as follows: $q_1 = 2.5$ mg/L; $q_2 = 2.6$ mg/L; $q_3 = 0.91$ mg/L; $q_{PO_4} = 0.05$ mg/L; $q_{POP} = 0.7$ mg/L; $q_{DOP} = 0.7$ mg/L; $q_{NO_3} = 0.09$ mg/L; $q_{NO_2} = 0.17$ mg/L; $q_{NH_4} = 0.8$ mg/L; $q_{Si} = 2$ mg/L; $q_{O_2} = 9.1$ mg/L; $q_{CO_2} = 2.5$ mg/L.

The simulation results are presented in Fig. 5. As expected, an abundance of nutrients leads to accelerated growth of all three phytoplankton species. The final concentrations of substances are as follows: q_1 = 15.14 mg/L; q_2 = 15.75 mg/L; q_3 = 5.51 mg/L; q_{PO_4} = 0.0018 mg/L; q_{POP} = 0.52 mg/L; q_{DOP} = 0.624 mg/L; q_{NO_3} = 4.786 mg/L; q_{NO_2} = 0.052 mg/L; q_{NH_4} = 0.145 mg/L; q_{Si} = 1.89 mg/L; q_{O_2} = 9.44 mg/L; q_{CO_2} = 0.819 mg/L.

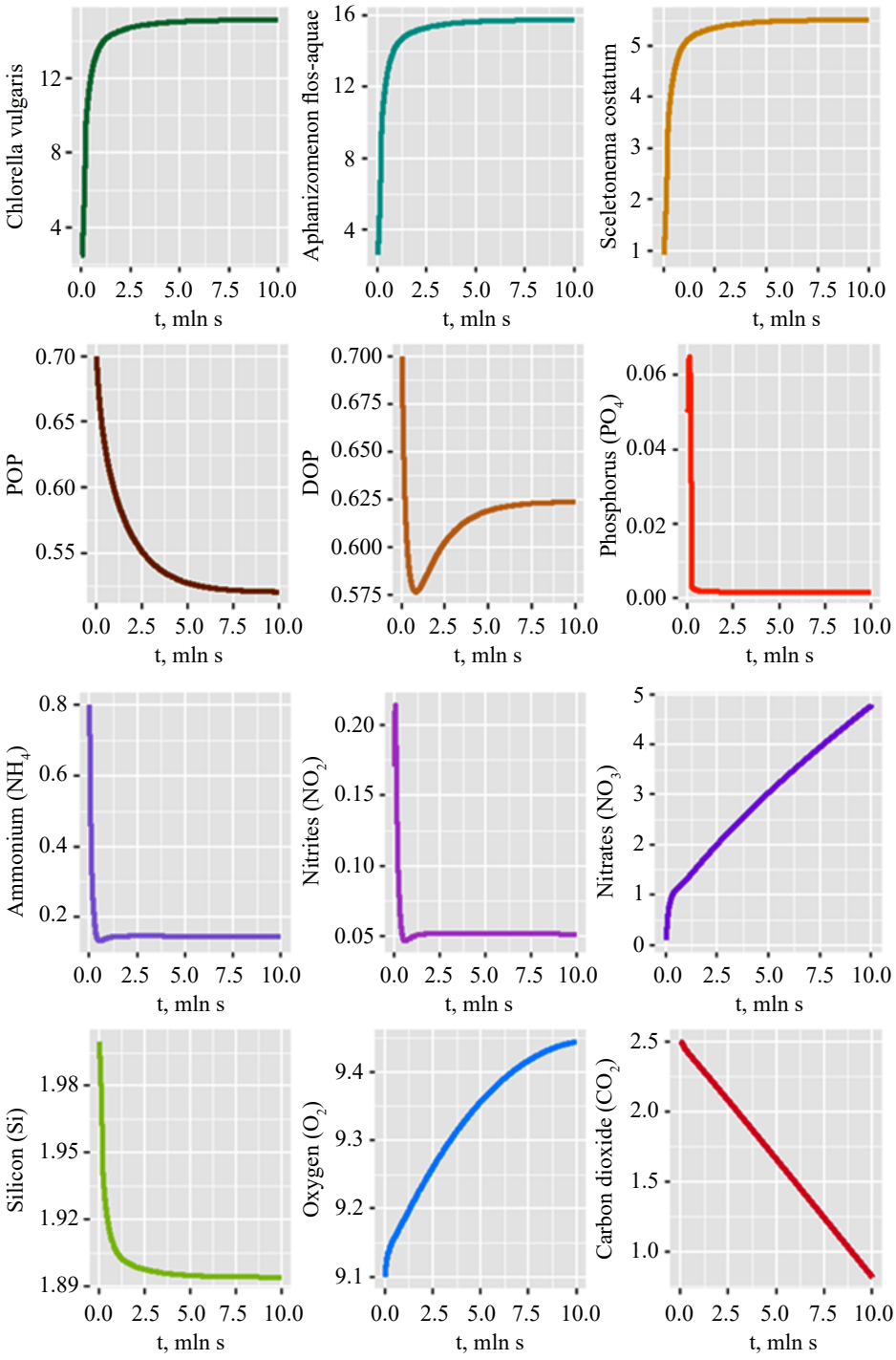

Fig. 5. Stationary regimes of the plankton-dynamics model under nutrient abundance

Discussion. In the course of the study, an integrated mathematical model of plankton dynamics was considered with allowance for the transformation of nutrient compounds, suspended and dissolved substances, including oxygen and carbon dioxide. The model is characterized by a high level of detail in the description of biogeochemical cycles, which makes it possible to describe processes in real aquatic ecosystems more adequately.

The main result of the study is a qualitative investigation of stationary solutions of this model. Various scenarios of nutrient concentrations were considered. The obtained solutions are consistent with data from field experiments.

It was established that the key factors determining the structure of the plankton community at equilibrium are the ratios of biogenic elements. The rate of gas exchange with the atmosphere and O_2-dependent nitrification processes are critical feedbacks that can stabilize or destabilize the system.

Conclusion. The results of the study make it possible to forecast the consequences of anthropogenic impact on water bodies. For example, the model predicts that a set of measures may be required to shift the system to a more favorable state, such as diatom dominance. Such measures may include reducing the input of phosphorus compounds, managing silicon runoff, and intensifying water mixing to improve the oxygen regime.

Further research should focus on increasing the model complexity by including zooplankton, detailing light-transmission processes, accounting for spatial heterogeneity, and validating the model against field data.

References

1. Debol'skaya E.I., Yakushev E.V., Sukhinov A.I. Formation of Fish Kills and Anaerobic Conditions in the Sea of Azov. *Water Resources*. 2005;32(2):151–162. https://doi.org/10.1007/s11268-005-0020-5

2. Chistyakov A.E., Nikitina A.V., Ougolnitsky G.A., Puchkin M.V., Semenov I.S., Sukhinov A.I., Usov A.B. A Differential Game Model of Preventing Fish Kills in Shallow Waterbodies. *Game Theory and Applications*. 2015;17:37–48.

3. Belova Yu.V., Chistyakov A.E. Modeling the Dynamics of Harmful Phytoplankton Species Concentration in Taganrog Bay of the Azov Sea. *Safety of Technogenic and Natural Systems*. 2025;9(4):284–293. https://doi.org/10.23947/2541-9129-2025-9-4-284-293

4. Di Toro, D.M. Applicability of cellular equilibrium and monod theory to phytoplankton growth kinetics. *Ecological Modelling.* 1980;8:201–218. https://doi.org/10.1016/0304-3800(80)90038-1

5. Abakumov A.I., Pak S.Ya. Modeling the Photosynthesis Process and Assessing The Dynamics of Phytoplankton Biomass based on the Droop Model. *Mathematical Biology and Bioinformatics*. 2021;16(2):380–393. (In Russ.) https://doi.org/10.17537/2021.16.380

6. Bratus A.S., Novozhilov A.S., Platonov A.P. *Dynamic Systems and Models of Biology*. Moscow: Fizmatlit; 2010. 400 p. (In Russ.)

7. Hutchinson G.E. Marginalia – Eutrophication. *American Scientist*. 1973;61:269–279.

8. Pannard A., Souchu P., Chauvin C., Delabuis M., Gascuel-Odoux C., Jeppesen E. Why are There so Many Definitions of Eutrophication? *Ecological Monographs*. 2024;94:1616. https://doi.org/10.1002/ecm.1616

9. Dumlu E., Şebnem E. Application of the WASP Model for Assessment of Aeration Impact on Water Quality of Porsuk River, Turkey. *Scientific Research Communications*. 2022;2(2). https://doi.org/10.52460/src.2022.008

10. Trancoso A.R., Braunschweig F., Chambel Leitão P., Obermann M., Neves R. An Advanced Modelling Tool for Simulating Complex River Systems. *Science of The Total Environment*. 2009;407(8):3004–3016. https://doi.org/10.1016/j.scitotenv.2009.01.015

11. Yakushev E., Mikhailovsky G. Mathematical modeling of the influence of marine biota on the carbon dioxide ocean-atmosphere exchange in high latitudes. *Air-Water Gas Transfer, selected papers from the Third International Symposium*. 1995:37–48.

12. Franks P.J.S. NPZ Models of Plankton Dynamics: Their Construction, Coupling to Physics, and Application. *Journal of Oceanography*. 2002;58(2):379–387. https://doi.org/10.1023/A:1015874028196

13. Sukhinov A.I., Belova Yu.V. The mathematical model of transformation of phosphorus, nitrogen and silicon forms in the moving turbulent water environment in problems of dynamics of planktonic populations. *Engineering journal of Don*. 2015;37(3):50. (In Russ.)

14. Belova Yu.V., Atayan A.M., Chistyakov A.E., Strazhko A.V. Study on stationary solutions to the problem of phytoplankton dynamics considering transformation of phosphorus, nitrogen and silicon compounds. *Vestnik of Don State Technical University*. 2019;19(1):4–12. https://doi.org/10.23947/1992-5980-2019-19-1-4-12

15. Sukhinov A.I., Chistyakov A.E., Kuznetsova I.Yu., Atayan A.M., Nikitina A.V. Regularized difference scheme for solving hydrodynamic problems. *Mathematical Models and Computer Simulations*. 2022;14:745–754. https://doi.org/10.1134/S2070048222050155

16. Sukhinov A.I., Belova Yu.V., Kuznetsova I.Yu., Atayan A.M., Chistyakov A.E. Mathematical models and methods of forecasting biological kinetics processes considering the oxygen regime. *Bulletin of the South Ural State University. Ser. Mathematical Modelling, Programming & Computer Software*. 2025;18(2):52–65. https://doi.org/10.14529/mmp250205

17. UNESCO Progress on oceanographic tables and standards 1983–1986: work and recommendations of the UNESCO/SCOR/ ICES/IAPSO Joint Panel. *UNESCO Technical Papers in Marine Science*. 1986;50:9.

18. Lyahin Yu.I. Estimation of CO2 exchange rate between sea water and atmospheric air. *Okeanologiya*. 1975;15(3):458–464.

19. Vasala V., Maksyutov S. Simulation and assimilation of global ocean pCO2 and air-sea CO2 fluxes using ship observations of surface ocean pCO_2 in a simplified biogeochemical offline model. *Tellus B*. 2010;62(5):821–840. https://doi.org/10.1111/j.1600-0889.2010.00495.x

20. Sukhinov A.I., Chistyakov A.E., Belova Yu.V., Kuznetsova I.Yu. Analytical and numerical study of the problem of the plankton population dynamics in the presence of microplastics. *Mathematical Models and Computer Simulations*. 2024;16(5):717–729. https://doi.org/10.1134/S2070048224700352

About the Authors:

Inna Yu. Kuznetsova, Senior Lecturer, Department of Mathematics and Computer Science, Don State Technical University (1, Gagarin Sq., Rostov-on-Don, 344003, Russian Federation), ORCID, SPIN-code, ResearcherID, ScopusID, ikuznecova@donstu.ru

Yulia V. Belova, Candidate of Physico-Mathematical Sciences, Associate Professor of the Department of Mathematics and Computer Science at the Don State Technical University (1, Gagarin Sq., Rostov-on-Don, 344003, Russian Federation), ORCID, SPIN-код, ScopusID, yvbelova@yandex.ru

Contributions of the authors:

I.Yu. Kuznetsova: ideas; conducting a research and investigation process, specifically performing the computational experiments; preparation, creation of the published work, specifically visualization; making graphic materials.

Yu.V. Belova: formulation of overarching research goals and aims; preparation, creation of the published work, specifically critical review; conclusions correction; text revision.

Conflict of Interest Statement: **the authors declare no conflict of interest.**

All authors have read and approved the final manuscript.

Об авторах:

Инна Юрьевна Кузнецова, старший преподаватель кафедры математики и информатики Донского государственного технического университета (344003, Российская Федерация, г. Ростов-на-Дону, пл. Гагарина, 1), ORCID, SPIN-код, ResearcherID, ScopusID, ikuznecova@donstu.ru

Юлия Валериевна Белова, кандидат физико-математических наук, доцент кафедры математики и информатики Донского государственного технического университета (344003, Российская Федерация, г. Ростов-на-Дону, пл. Гагарина, 1), ORCID, SPIN-код, ScopusID, yvbelova@yandex.ru

Заявленный вклад авторов:

И.Ю. Кузнецова: формулирование основной концепции исследования; осуществление научно-исследовательского процесса, включая проведение вычислительных экспериментов; создание и подготовка рукописи: визуализация результатов исследования и полученных данных; оформление графических материалов.

Ю.В. Белова: формулирование целей и задач исследования; создание и подготовка рукописи: критический анализ черновика рукописи; корректировка выводов; доработка текста.

Конфликт интересов: ***авторы заявляют об отсутствии конфликта интересов.***

Все авторы прочитали и одобрили окончательный вариант рукописи.

Received / Поступила в редакцию 25.03.2026
Reviewed / Поступила после рецензирования 28.04.2026
Accepted / Принята к публикации 27.05.2026

MATHEMATICAL MODELLING
МАТЕМАТИЧЕСКОЕ МОДЕЛИРОВАНИЕ

UDC 532.517:551.46

Original Empirical Research

https://doi.org/10.23947/2587-8999-2026-10-2-31-45

Numerical Study of Wave-Induced Hydrodynamic Loads on a Ship Hull in Shallow Water Conditions

Alexander I. Sukhinov[1], Sofia V. Protsenko[1,2] ✉, Natalya D. Panasenko[1], Elena A. Protsenko[2]

[1] Don State Technical University, Rostov-on-Don, Russian Federation

[2] Taganrog Institute named after A.P. Chekhov (branch of Rostov State University of Economics), Taganrog, Russian Federation

✉ rab55555@rambler.ru

Abstract

Introduction. The hydrodynamic impact of waves on a ship hull in shallow water represents one of the key challenges in modern marine hydrodynamics. Limited water depth leads to amplification of wave action, a shift of resonance frequencies, and an increase in motion amplitudes, which significantly intensifies the loads acting on the hull.

Materials and Methods. Numerical simulations were performed using the ANSYS Aqwa software package within the framework of linear potential flow theory. A hybrid approach was implemented, combining frequency-domain analysis for determining Response Amplitude Operators (RAO) and subsequent time-domain simulations of irregular waves based on the JONSWAP spectrum. Various water depths, wave parameters (significant wave height and peak period), and wave incidence angles were considered.

Results. It was found that a decrease in water depth results in an increase in vertical motion amplitudes of up to 40% and a shift of resonance frequencies toward longer waves. Maximum hydrodynamic loads occur under beam wave conditions, whereas for following wave directions, pitch motion plays a significant role in redistributing loads along the hull. Quantitative estimates of pressure distribution and integral forces acting on the hull were obtained, and critical combinations of wave parameters and water depth were identified.

Discussion. It is shown that the formation of extreme loads is governed not only by wave height but also by spectral characteristics, primarily the coincidence of the peak wave period with the natural frequencies of ship motions. The significant role of shallow-water effects in amplifying the hydrodynamic response and altering the structure of the wave field near the hull is demonstrated.

Conclusion. The results expand current understanding of ship hydrodynamics in shallow water and can be applied in ship design, selection of operational regimes, and development of decision-support systems to ensure navigation safety under complex environmental conditions.

Keywords: hydrodynamic loads, shallow water, wave-structure interaction, RAO, JONSWAP spectrum, numerical simulation, ANSYS Aqwa

Funding. The study was supported by the Russian Science Foundation grant No. 22–11–00295–П, https://rscf.ru/en/project/22-11-00295-П/

For Citation. Sukhinov A.I., Protsenko S.V., Panasenko N.D., Protsenko E.A. Numerical Study of Wave-Induced Hydrodynamic Loads on a Ship Hull in Shallow Water Conditions. *Computational Mathematics and Information Technologies*. 2026;10(2):31–45. https://doi.org/10.23947/2587-8999-2026-10-2-31-45

Оригинальное эмпирическое исследование

Численное исследование гидродинамических нагрузок на корпус судна при волнении в мелководных условиях

А.И. Сухинов[1], С.В. Проценко[1,2] ✉, Н.Д. Панасенко[1], Е.А. Проценко[2]

[1] Донской государственный технический университет, г. Ростов-на-Дону, Российская Федерация

[2] Таганрогский институт имени А.П. Чехова (филиал) РГЭУ (РИНХ), г. Таганрог, Российская Федерация

✉ rab55555@rambler.ru

Аннотация

Введение. Гидродинамическое воздействие волн на корпус судна в условиях мелководья представляет собой одну из ключевых проблем современной морской гидродинамики, поскольку ограниченная глубина приводит к усилению волнового воздействия, смещению резонансных частот и росту амплитуд колебаний, что существенно увеличивает силовые нагрузки на корпус.

Материалы и методы. Численное моделирование выполнено с использованием программного комплекса *ANSYS Aqwa* в рамках линейной потенциальной теории течений. Реализован комбинированный подход, включающий расчёты в частотной области с определением операторов амплитудно-частотных характеристик (*RAO*) и последующее моделирование во временной области для нерегулярного волнения на основе спектра *JONSWAP*. Рассмотрены различные глубины воды, параметры волн (значительная высота, пиковый период) и углы волнения.

Результаты исследования. Установлено, что уменьшение глубины приводит к увеличению амплитуды вертикальных перемещений корпуса до 40 % и смещению резонансных частот в область длинных волн. Показано, что максимальные гидродинамические нагрузки реализуются при волнении с траверза, тогда как при кормовых углах существенную роль играет килевая качка, определяющая перераспределение нагрузок по длине корпуса. Получены количественные оценки давления и интегральных сил, действующих на корпус, а также выявлены критические сочетания параметров волн и глубины.

Обсуждение. Показано, что формирование экстремальных нагрузок определяется не только высотой волн, но и их спектральными характеристиками, в первую очередь совпадением пикового периода с собственными частотами колебаний судна. Установлена существенная роль мелководного эффекта в усилении гидродинамического отклика и изменении структуры волнового поля вблизи корпуса.

Заключение. Полученные результаты расширяют представления о гидродинамике судов в мелководных условиях и могут быть использованы при проектировании судов, выборе эксплуатационных режимов и разработке систем поддержки принятия решений для обеспечения безопасности судоходства.

Ключевые слова: гидродинамические нагрузки, мелководье, волновое воздействие, *RAO*, спектр *JONSWAP*, численное моделирование, *ANSYS Aqwa*

Финансирование. Исследование выполнено за счет гранта Российского научного фонда № 22–11–00295–П, https://rscf.ru/en/project/22-11-00295-П/

Для цитирования. Сухинов А.И., Проценко С.В., Панасенко Н.Д., Проценко Е.А. Численное исследование гидродинамических нагрузок на корпус судна при волнении в мелководных условиях. *Computational Mathematics and Information Technologies*. 2026;10(2):31–45. https://doi.org/10.23947/2587-8999-2026-10-2-31-45

Introduction. The hydrodynamic action of waves on a ship hull is one of the key factors determining operational reliability, structural durability, and navigation safety [1, 2]. In shallow-water areas, the nature of wave-ship interaction differs substantially from deep-water conditions: limited depth transforms the wave spectrum, changes the kinematic structure of the flow, and enhances nonlinear effects associated with wave deformation and energy redistribution [3–5]. As a result, the resonance frequencies of hull motions shift toward longer waves, and motion amplitudes increase, which is accompanied by higher hydrodynamic loads.

These processes are particularly relevant for water bodies such as the Sea of Azov and its coastal zones, including Taganrog Bay, where shallow depths, intense wind forcing, and limited fetch produce specific wave-generation conditions [6, 7]. Such areas are characterized by short-period but steep waves, as well as significant water-level fluctuations that increase the variability of hydrodynamic loads. Under these conditions, traditional engineering estimates based on simplified relationships are insufficient for an adequate description of actual ship behavior.

Modern studies of ship hydrodynamics increasingly rely on numerical methods that make it possible to account for complex hull geometry and a wide range of wave actions. Potential flow theory, implemented in specialized software packages such as ANSYS Aqwa, is widely used for diffraction and radiation analyses and for calculating Response

Amplitude Operators (RAO) [8–10]. Recent studies show that such approaches provide satisfactory accuracy when compared with experimental data, especially in the field of linear hydrodynamics and moderate wave action [11–13].

At the same time, a considerable part of the existing research focuses either on individual characteristics of ship motion or on the assessment of navigation-accident risks, whereas a comprehensive investigation of wave-induced force action on the hull, taking into account the shallow-water effect, wave parameters, and wave direction, remains insufficiently developed [14–16]. In particular, the combined influence of water depth, wave height and period, and wave propagation angle on the distribution of hydrodynamic pressure and resultant forces along the hull has not been studied sufficiently. In addition, few works directly link frequency-domain analysis (RAO) with time-domain simulation of irregular waves to obtain realistic load estimates.

This paper proposes a numerical approach to studying wave-induced hydrodynamic loads on a ship hull in shallow water, based on a combination of frequency-domain and time-domain analyses. At the first stage, RAOs are calculated for six degrees of freedom, which makes it possible to determine the dynamic sensitivity of the ship to wave action over a wide frequency range [12, 13]. At the second stage, time-domain simulation is performed using a spectral description of waves, providing statistically significant characteristics of motions and loads [4, 17].

The scientific novelty of the study lies in the integrated consideration of water depth, wave parameters, and wave incidence angle in assessing hydrodynamic loads, as well as in the integration of frequency-domain and time-domain approaches for estimating wave-induced force action under shallow-water conditions. Unlike most existing studies, the main emphasis is placed not only on the kinematics of ship motions but also on quantitative assessment of the loads acting on the hull and their temporal variability.

The practical significance of the results is associated with their possible use in ship design, selection of operating modes, and development of recommendations for ensuring navigation safety under complex hydrometeorological conditions. The proposed approach may also serve as a basis for further studies aimed at accounting for nonlinear effects and interaction with seabed morphodynamics in shallow-water areas.

Materials and Methods

Problem statement. The problem considered is the numerical simulation of wave-induced hydrodynamic action on a ship hull under limited-depth conditions. The main objective is to quantitatively assess hull-motion amplitudes and the distribution of hydrodynamic loads for different parameters of external wave forcing [18, 19].

Ship motion is described within six degrees of freedom:

$$\mathbf{x}(t) = \{\xi_1, \xi_2, \xi_3, \xi_4, \xi_5, \xi_6\},$$

where ξ_1, ξ_2, ξ_3 are translational or linear displacements of the ship center of mass (surge, sway, and heave), and ξ_4, ξ_5, ξ_6 are angular displacements or rotations of the ship about the axes (roll, pitch, and yaw) [11–13].

Wave action is specified either as a superposition of harmonic components or as a spectral description of irregular waves. It is necessary to determine Response Amplitude Operators (RAO), time histories of hull motions, hydrodynamic forces and moments, and integral loads acting on the hull [20, 21].

Hydrodynamic model. The simulation is based on linear potential flow theory, which assumes that the fluid is incompressible and inviscid and that the flow is irrotational [1, 2, 22].

The velocity field is described by the velocity potential $\phi(\mathbf{x},t)$ satisfying Laplace's equation:

$$\nabla^2\phi = 0.$$

The potential is represented as a superposition:

$$\phi = \phi I + \phi D + \sum_{j=1}^{6} \dot{\xi}_j \phi_{Rj},$$

where ϕI is the incident-wave potential; ϕD is the diffracted potential; ϕ_{Rj} are the radiation potentials corresponding to ship motions; $\dot{\xi}_j = \dfrac{d\xi_j}{dt}$ is the velocity of the corresponding translational or angular motion [2, 22].

The boundary conditions on the free surface (linearized condition) are defined as follows:

$$\frac{\partial^2\phi}{\partial t^2} + g\frac{\partial\phi}{\partial z} = 0 \text{ при } z = 0,$$

on the ship hull (impermeability):

$$\frac{\partial\phi}{\partial n} = \mathbf{V}\cdot\mathbf{n},$$

on the bottom (limited depth):

$$\frac{\partial \phi}{\partial z} = 0 \text{ при } z = -h.$$

The boundary conditions reflect the physical nature of the problem: the free-surface condition describes wave motion under gravity, the hull condition represents impermeability, and the bottom condition specifies the absence of vertical flow, corresponding to the limited depth of the water area.

Equations of ship motion. Ship dynamics is described by a system of equations in the frequency domain:

$$\left[-\omega^2(\mathbf{M} + \mathbf{A}(\omega)) + i\omega\mathbf{B}(\omega) + \mathbf{C}\right]\xi(\omega) = \mathbf{F}(\omega),$$

where **M** is the mass matrix; **A**(ω) is the added-mass matrix; **B**(ω) is the damping matrix; **C** is the hydrostatic stiffness matrix; and **F**(ω) is the vector of wave forces [11–13, 23].

The Response Amplitude Operator is defined as

$$RAO_j(\omega) = \frac{\xi_j(\omega)}{\eta(\omega)},$$

where η is the wave amplitude.

The frequency-domain equation of ship motion reflects the balance between inertial, damping, and restoring forces that determine the ship response to wave action.

Methodology for numerical simulation of the dynamic ship response to wave action. A spectral representation is used to simulate irregular waves:

$$\eta(t) = \sum_{n=1}^{N} \sqrt{2S(\omega_n)\Delta\omega}\cos(\omega_n t + \varphi_n),$$

where $S(\omega_n)$ is the wave energy spectral density; ϕ_n are random phases [4, 17].
Ship motion is determined through convolution with the RAO:

$$\xi_j(t) = \int_0^{\infty} RAO_j(\omega)\eta(\omega)e^{i\omega t}d\omega.$$

Irregular waves are simulated as a superposition of harmonic components with different frequencies and random phases based on a specified energy spectrum. Ship motion in the time domain is determined by transforming the RAO, which makes it possible to account for the frequency-dependent response of the system to wave action [20, 21]. The scheme for generating the dynamic response is shown in Fig. 1.

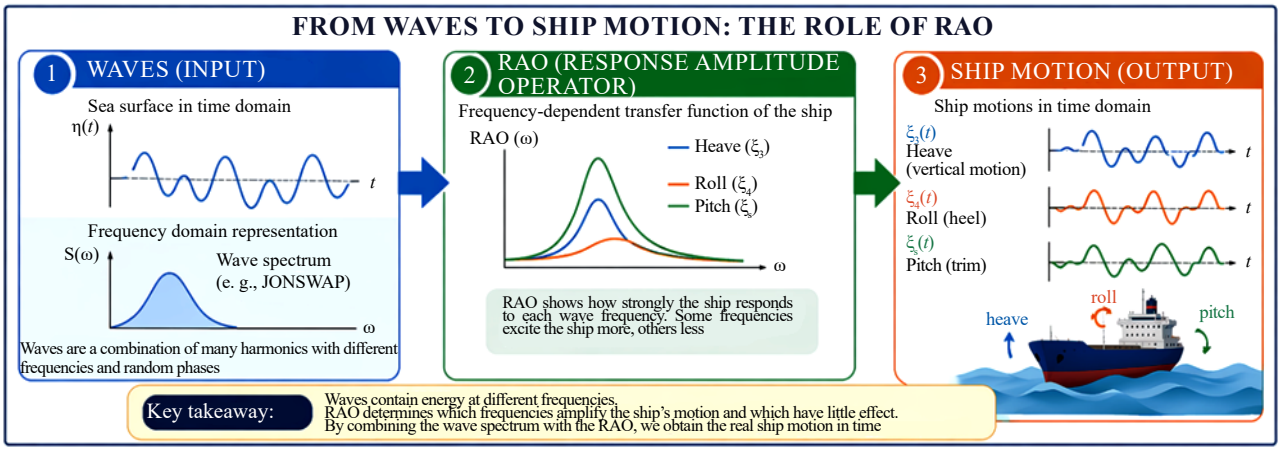

Fig. 1. Scheme for generating the dynamic ship response to wave action (waves → RAO → ship motion)

As shown in Fig. 1, the dynamic response of the ship is formed through a sequential transformation of wave action into the frequency response of the system (RAO), followed by transition to time histories of motions. This formulation directly links the spectral characteristics of waves with hull-motion kinematics and subsequent loads.

Spectral wave model. The JONSWAP spectrum is used to describe irregular waves:

$$S(\omega) = \alpha g^2 \omega^{-5} exp\left(-\frac{5}{4}\left(\frac{\omega_p}{\omega}\right)^4\right)\gamma^{exp\left[-\frac{(\omega-\omega_p)^2}{2\sigma^2\omega_p^2}\right]},$$

where $S(\omega)$ is the wave spectrum, showing how wave energy is distributed over frequencies; $\omega_p = \frac{2\pi}{T_p}$, γ is the peak enhancement factor; σ = 0.07 or 0.09 [4, 17].

The JONSWAP spectrum is used to describe irregular waves as an energy distribution over frequencies with a pronounced peak corresponding to the dominant wave period. This model adequately describes developing wind waves in fetch-limited water areas.

Calculation of hydrodynamic loads. The pressure on the hull is determined from the unsteady Bernoulli equation:

$$p = -\rho\frac{\partial\phi}{\partial t} - \rho g z.$$

Integral force:

$$F(t) = \int_S p\mathbf{n}dS,$$

moment:

$$\mathbf{M}(t) = \int_s \mathbf{r} \times (p\mathbf{n})dS.$$

Hydrodynamic loads on the ship hull are determined from the pressure distribution calculated using the unsteady Bernoulli equation [1, 2, 24]. Integration of pressure over the hull surface makes it possible to determine the resultant forces and moments caused by the nonuniform pressure distribution.

Numerical implementation. The numerical implementation was performed using the ANSYS Aqwa software package, designed for solving wave diffraction and radiation problems within linear potential flow theory [10, 15]. Calculation of the ship hydrodynamic characteristics is based on the panel method, in which the underwater hull surface is approximated by a finite number of elements, and the solution is reduced to determining the velocity-potential distribution on the fluid-solid boundary [22, 25].

The use of this approach is justified by its widespread application in marine hydrodynamics and its proven effectiveness in calculating Response Amplitude Operators (RAO), added masses, damping coefficients, and wave loads [11–13, 25]. In contrast to full CFD models, the panel method substantially reduces computational cost while maintaining adequate accuracy in the range of small and moderate wave amplitudes, which corresponds to the adopted problem formulation [8, 9].

The underwater hull was discretized using approximately 1500–2000 panels, in accordance with recommendations for ships of the class considered [25]. The selected mesh density provides sufficient accuracy in approximating the hull geometry, including the bow and stern regions, where the largest pressure gradients are observed.

The quality of the panel model was controlled using hydrostatic characteristics: displacement, center of buoyancy, and metacentric height. Deviations of the calculated values from the design values did not exceed 1%, confirming the correctness of the geometric approximation and the suitability of the model for subsequent hydrodynamic calculations.

Frequency-domain calculations were performed in the range of $0.1 \le \omega \le 2.0$ rad/s, which corresponds to wave periods of approximately 3–60 s and fully covers the wave spectral range characteristic of shallow-water areas [17, 20]. The frequency range was discretized with a step of $\Delta\omega = 0.05 – 0.10$ rad/s with additional refinement near resonance frequencies. This approach ensures correct reproduction of RAO peaks and avoids distortions in the transition to the time domain [11–13]. Calculations were performed for wave incidence angles $\beta = 0°$, 30°, 45°, 60°, 90°, 120°, 135°, 150°, 180°, which covers all characteristic directions of wave action, from head to following waves. This is fundamentally important because the ship response depends substantially on the wave incidence angle [12, 14].

Based on the obtained frequency characteristics, time-domain simulation was performed for irregular waves. The wave field was generated using the JONSWAPspectrum, which describes the distribution of wave energy over frequencies under fetch-limited conditions [4, 17]. The calculation duration was $T_{sim} = 1800$ s, which ensured statistically stable time series of motions and loads. The initial transient interval of 200–300s was excluded from the analysis. The integration time step was $\Delta t = 0{,}1 – 0{,}2$ s, which ensured adequate resolution of high-frequency wave components and stability of the numerical scheme [20, 21]. The time-step choice was dictated by the need for accurate reproduction of peak values of motions and loads, prevention of numerical oscillations, and convergence of statistical characteristics. Test calculations showed that the selected Δt range provides a balance between accuracy and computational efficiency.

Based on the results of time-domain simulation, statistical analysis of the time series was performed, including determination of:

– maximum and minimum displacement values;

– extreme values of forces and moments;

– root-mean-square deviations;

– the probability of reaching critical regimes [20, 21].

Special attention was paid to estimating extreme hydrodynamic loads, since they determine the potential hazard of ship operation under shallow-water and storm-wave conditions.

It should be noted that the model used is based on linear potential flow theory and does not account for several effects that may be significant under extreme conditions, in particular:

– nonlinear wave transformation in shallow water;

– viscous effects and turbulence;

– interaction with variable bottom geometry [8, 9, 26].

Nevertheless, for comparative analysis and assessment of the influence of the main factors (depth, wave parameters, and wave incidence angle), the selected approach is well justified and widely used in engineering practice [10, 25].

Geometry and main characteristics of the ship. A river-sea transport ship intended for operation in shallow-water areas and coastal zones, including the Sea of Azov and Taganrog Bay, was considered as the computational object. The choice of this ship type is determined by its characteristic geometric and hydrodynamic features, as well as by its correspondence to the limited-depth conditions considered in this study.

The ship belongs to the class of displacement monohull vessels with a developed underwater hull and pronounced bow and stern extremities. The hull lines are characterized by moderate fullness and a smooth variation of shape along the length, which provides a typical distribution of hydrodynamic loads under wave action.

The main geometric characteristics of the ship were adopted as follows:

– length between perpendiculars L = 105 m;

– beam B = 16 m;

– draft T = 4.2 m;

– displacement $\Delta \approx 4200$ t;

– block coefficient CB ≈ 0.75.

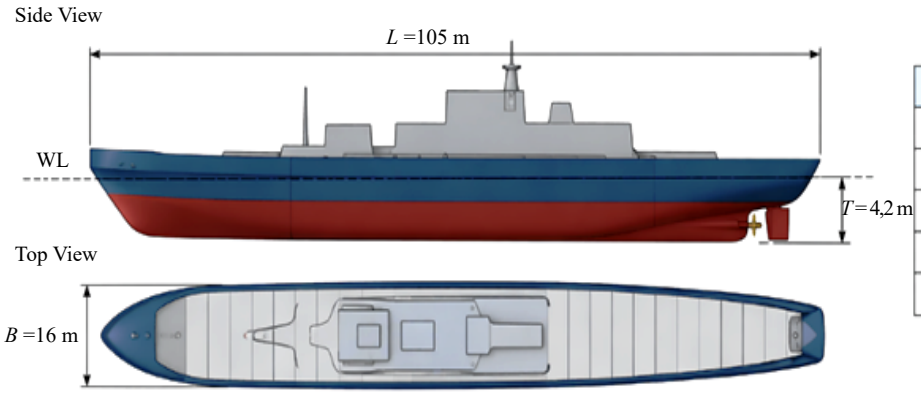

Main particulars	Value
Length between perpendiculars, L	105 m
Beam, B	16 m
Draft, T	4.2 m
Displacement, Δ	≈ 4200 t
Block coefficient, C_B	≈ 0.75

Fig. 2. Geometry and main characteristics of the computational ship

The considered ship is a generalized geometric model of a river-sea transport vessel (Fig. 2).

The ratio of water depth to ship draft in the computational scenarios is h/T = 1.3–2.1, which corresponds to limited-depth conditions and ensures the manifestation of a pronounced shallow-water effect. The underwater hull was approximated using panel discretization with approximately 1500–2000 elements. This level of detail provides an adequate representation of the hull geometry, including regions with the largest pressure gradients (bow and stern extremities), and is consistent with recommendations for numerical modeling of ships of this class.

The selected geometry is typical of river-sea transport ships and is widely used in numerical modeling of hydrodynamic processes in shallow-water areas, which allows the results obtained to be regarded as representative for this type of vessel [4, 5, 27].

Validation of the numerical model. To assess the reliability of the results, the numerical model was validated by comparing the obtained Response Amplitude Operators (RAO) with published numerical and experimental results.

Reference data were taken from studies devoted to the analysis of the dynamic response of ships in regular and irregular waves, obtained using both panel methods and experimental investigations of ship models in basins [11–13, 20].

The comparison was performed for the following characteristics:

– Response Amplitude Operators for vertical motions (heave);

– resonance-response frequencies;

– RAO amplitude levels in the peak region.

It was found that the RAO values obtained in this study show qualitative and quantitative agreement with literature data. In particular, the range of resonance frequencies (0.9–1.2 rad/s) and the pattern of change in response amplitudes with decreasing depth correspond to previously published results [11–13].

Deviations of RAO amplitudes in the resonance-peak region do not exceed 10–15%, which corresponds to the typical level of discrepancy between different numerical methods (panel methods, strip theory) and experimental data.

In addition, integral hydrodynamic loads were compared with numerical studies that used time-domain methods to model the ship response to irregular waves [20, 21]. The obtained dependences of maximum loads on depth and wave parameters demonstrate similar trends, including:

– an increase in loads with decreasing depth;

– a shift of the region of maximum values toward longer waves;

– amplification of the response under beam waves.

Thus, the comparison confirms the correctness of the numerical model used and its applicability to the analysis of hydrodynamic loads on a ship hull in shallow water.

Results. Numerical experiments were performed for a series of computational scenarios covering the range of depths typical of navigation channels and adjacent waters of Taganrog Bay under normal water levels, wind set-down, and storm-surge conditions. The calculations considered depths h = 5.5, 7, 8, and 9 m, significant wave heights Hs = 0.5–3.5 m, peak periods T_p = 3.5–6 s, and wave incidence angles β from 0° to 180°.

The calculations were carried out in two stages. At the first stage, frequency-domain analysis was performed with determination of Response Amplitude Operators (RAO) for six degrees of freedom [11–13]. At the second stage, the results of the frequency-domain analysis were used to simulate irregular waves in the time domain and to obtain time histories of vertical motions, angular deviations, and integral hydrodynamic loads [20, 21].

The main attention was paid to vertical hull motions, pitch and roll, and the vertical and transverse components of wave forces, because these quantities largely determine the intensity of wave action on the hull under limited-depth conditions.

Results of the frequency-domain analysis

Response Amplitude Operators for vertical motions. The obtained RAOs for vertical motions showed a pronounced dependence on water depth and wave direction. For all calculated depths, one dominant peak is observed in the range of 0.95–1.15 rad/s, corresponding to the main region of the hull resonance response in heave.

The most substantial changes were identified when the depth decreased from 9.0 m to 5.5 m. In this case, the maximum heave RAO increased from 1.07 to 1.49 m/m, that is, by approximately 39%. At the same time, the peak frequency shifted from 1.14 to 0.96 rad/s, corresponding to an increase in the characteristic response period from 5.5 to 6.5 s. This tendency is in good agreement with the physics of the shallow-water effect: decreasing depth changes the added masses and hydrostatic restoring, which increases the natural periods of the system [3–5, 19].

Table 1

Heave RAO parameters under beam waves (β = 90°)

Water depth h, m	RAOmax (heave), mm	Peak frequency ω_p, rad/s	Period T, s
9.0	1.07	1.14	5.51
8.0	1.14	1.09	5.76
7.0	1.23	1.03	6.10
5.5	1.49	0.96	6.54

It should be noted that the increase in response with decreasing depth has a nonlinear accelerating character: the transition from 9.0 to 8.0 m produces a relatively moderate change, whereas in the range of 7.0–5.5 m the amplitude increase becomes noticeably sharper. This indicates that the system approaches regimes in which shallow-water influence becomes dominant.

Fig. 3 presents the Response Amplitude Operators for vertical ship motions at different water depths. It can be seen that decreasing depth increases the response amplitude and shifts the resonance frequency toward longer waves, reflecting the influence of the shallow-water effect on system dynamics.

Influence of wave incidence angle. The wave incidence angle affects different degrees of freedom in different ways. For vertical motions, the maximum RAO values are observed under beam waves and in the range of oblique waves of 60°–120°. For pitch, by contrast, the strongest response is typical of head and following waves, when wave action effectively excites the longitudinal mode of motion.

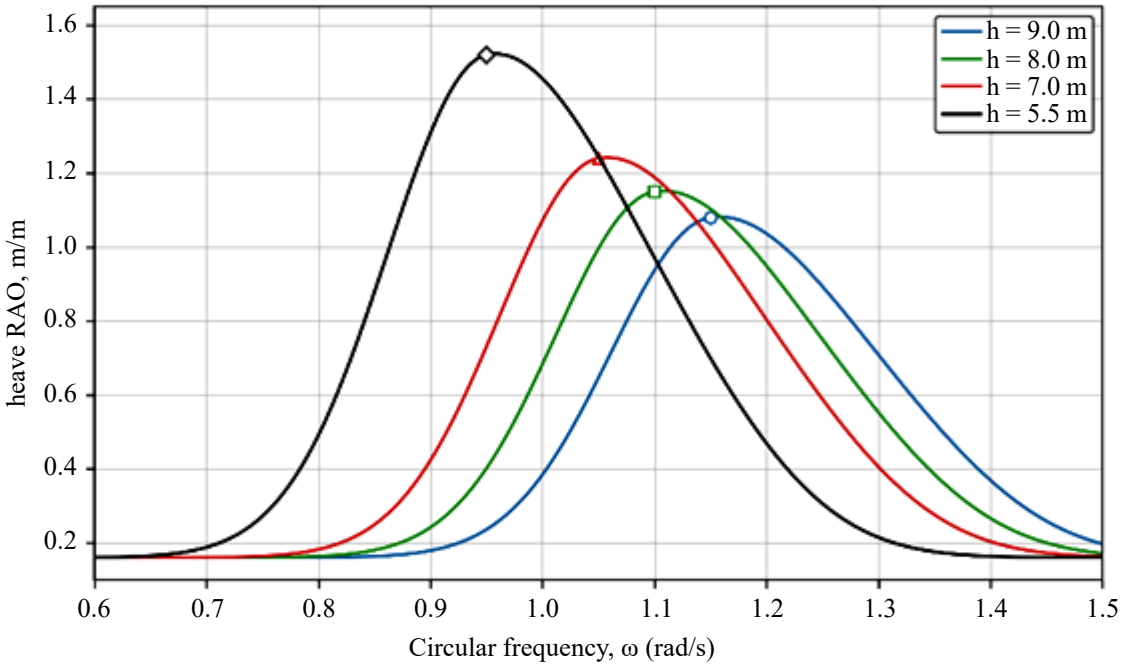

Fig. 3. Response Amplitude Operators of ship vertical motions (heave) under beam waves (β = 90°) for different water depths

Table 2

Maximum RAO values at h = 7 m

Wave incidence angle β, °	RAOmax (heave), mm	RAOmax (pitch), deg/m	RAOmax (roll), deg/m
0	0.56	1.14	0.07
30	0.79	1.06	0.43
45	0.93	0.94	0.98
60	1.11	0.68	1.46
90	1.23	0.29	1.88
120	1.05	0.76	1.39
135	0.87	0.98	0.91
150	0.66	1.07	0.48
180	0.51	1.16	0.05

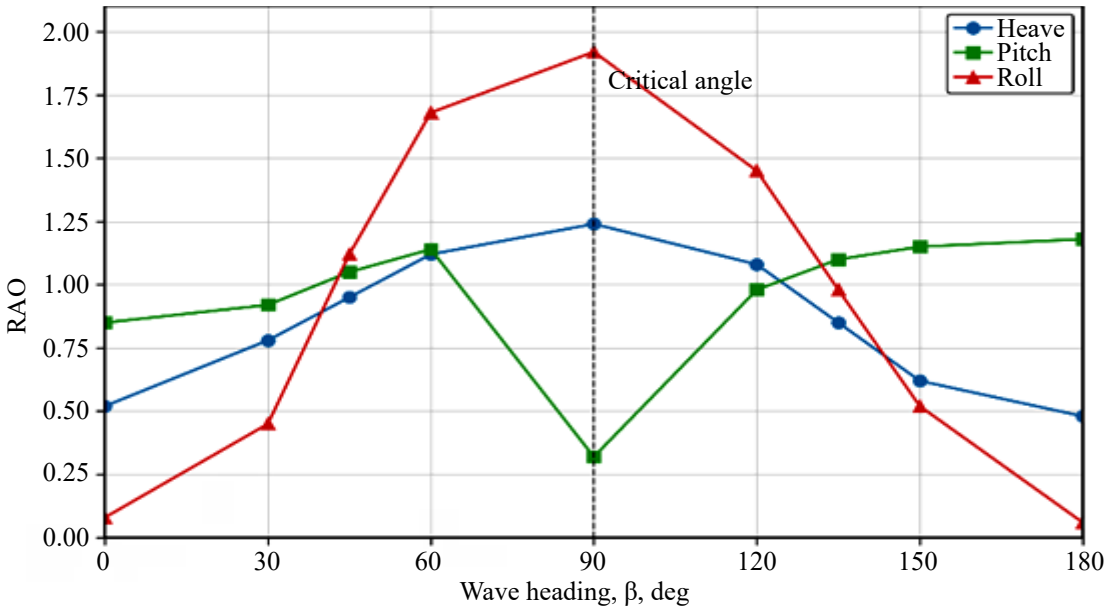

Fig. 4. Influence of wave incidence angle on the Response Amplitude Operators of ship response in heave, pitch, and roll

As illustrated in Fig. 4, the wave incidence angle has a decisive influence on the ship dynamic response. Maximum values of vertical motions (heave) and roll occur under beam-wave conditions (β = 90°), which corresponds to the most unfavorable excitation regime. At the same time, pitch reaches its maximum at following-wave angles (β = 150–180°). The results confirm the pronounced anisotropy of the dynamic response and the need to account for wave direction when assessing hydrodynamic loads [12, 14].

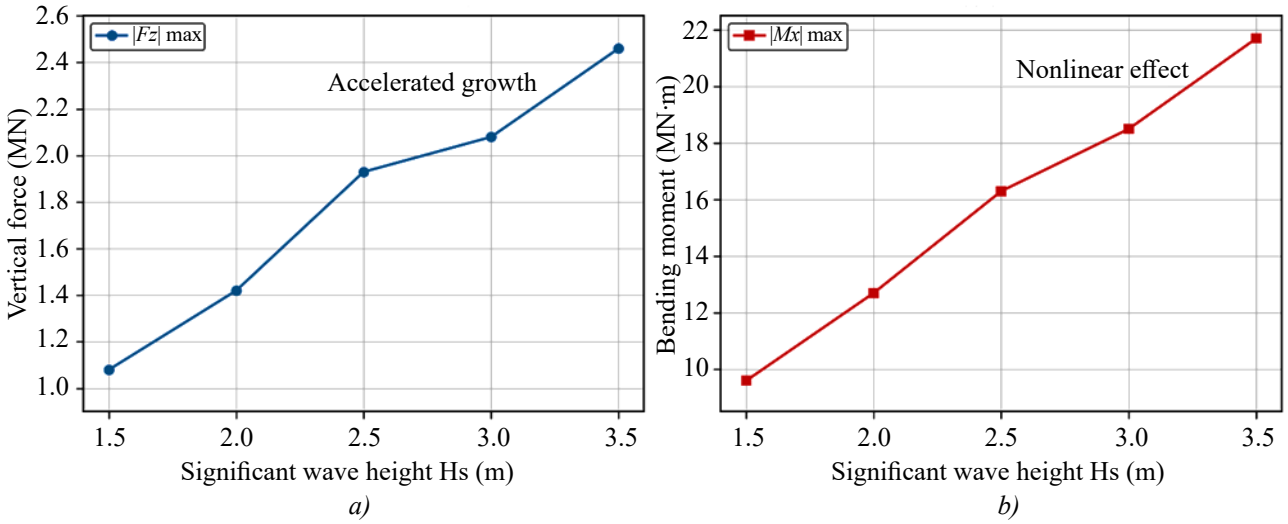

Fig. 5. Dependence of hydrodynamic loads on significant wave height:
a — vertical force; *b* — bending moment

As shown in Fig. 5, an increase in significant wave height leads to an increase in hydrodynamic loads. The dependence is nonlinear: in the range of high waves, both the vertical force and the bending moment increase at an accelerated rate, which is associated with amplification of the ship dynamic response and redistribution of pressure over the hull [8–10].

Thus, the most pronounced vertical hull response is formed at β = 90°, whereas for pitch the hazardous regimes are those close to β = 0° and β = 180°. This distinction is fundamentally important when interpreting integral loads: the maximum of one degree of freedom does not necessarily correspond to the maximum resultant force action on a particular hull extremity.

Hydrodynamic forces and moments in the frequency domain. Calculation of exciting wave forces showed that in shallow water not only hull motions but also the amplitudes of integral loads increase [19–21]. The most noticeable growth is observed for the vertical force F_z and the rolling moment M_x. When the depth decreases to 5.5 m, the maximum vertical force near the resonance frequency increases by approximately 27% compared with a depth of 9 m, while the transverse moment increases by 31%.

For beam waves, the increase in Fz is mainly associated with amplification of the heave response and redistribution of hydrodynamic pressure over the underwater hull. For oblique following waves, longitudinal oscillations and trim begin to make a substantial contribution, leading to load asymmetry between the bow and stern extremities.

Results of time-domain simulation. In the time domain, irregular wave actions generated according to the JONSWAP spectrum were analyzed [4, 17]. For each scenario, time series with a duration of 1800 s were calculated, with the first 300 s excluded as a transient interval.

For the severe-storm scenario (Hs = 3 m, T_p = 5.5 s) at a depth of 7 m, the maximum absolute vertical hull displacements were obtained under beam-wave conditions. The extreme negative values, corresponding to the deepest hull immersion, reached 2.6–2.8 m relative to the mean position.

A slight negative shift in the mean value $\overline{\zeta}_{heave}$ in all scenarios reflects weak asymmetry of the time signal, characteristic of a finite realization length and spectral excitation near the resonance region. Physically, the most important quantities are not the mean values themselves but the extreme negative values that determine the worst hull-immersion regimes.

Since wave-induced force action on the hull is not limited to vertical motions alone, a combined analysis of heave and pitch was performed. To estimate the additional draft variation at the extremities, the following relationship was used

$$\Delta T_{pitch}(t) \approx \frac{Lpp}{2}\theta_{pitch}(t),$$

where θ_{pitch} is expressed in radians [2, 11].

Table 3

Statistical characteristics of vertical motions at h = 7 m, Hs = 3.0 m, T_p = 5.5 s

β, °	Mean, m	RMS, m	Max, m	Min, m
0	–0.09	0.49	1.14	–1.36
45	–0.06	0.81	1.92	–2.14
90	–0.04	1.08	2.54	–2.77
135	–0.07	0.90	2.08	–2.29
180	–0.10	0.57	1.31	–1.58

The calculations showed that under beam waves the vertical response is maximal, but the contribution of pitch is comparatively small. Conversely, under oblique following and following waves, vertical motions are smaller; however, the increase in trim leads to a substantial local increase in load on the bow or stern extremity.

Table 4

Maximum estimates of bow draft variation at h = 7 m, Hs = 3 m, T_p = 5.5 s

β, °	Min heave, m	Max pitch, deg	Pitch contribution, m	Total draft variation, m
0	–1.36	2.6	2.45	–3.81
45	–2.14	2.1	1.98	–4.12
90	–2.77	0.8	0.76	–3.53
135	–2.29	2.3	2.17	–4.46
180	–1.58	2.9	2.74	–4.32

The table shows that the largest local increase in draft at the extremities occurs not at β = 90°, but at β from 135° to 180°, when a moderately high heave response is combined with considerable trim. This circumstance is of fundamental importance for assessing actual hull loads and analyzing hazardous operating regimes.

Hydrodynamic loads on the ship hull. In all scenarios, the vertical component of the wave force $F_z(t)$ showed the highest sensitivity to depth and peak wave period. In the frequency range close to the main heave resonance frequency, the amplitude of F_z increased sharply. For the scenario h = 7 m, Hs = 2.5 m, T_p = 5.5 s, and β = 90°, the maximum vertical force over a 1500 s time interval was approximately 1.9–2.1 MN. At a depth of 5.5 m under the same wave parameters, the maximum increased to 2.5–2.7 MN.

For beam and oblique beam waves, the maximum values of the transverse force Fy and rolling moment Mx were formed in the same frequency range, close to the roll-response peak. When the depth decreased from 9 m to 5.5 m, the root-mean-square value of Mx increased by approximately 25%, and the extreme values by 30–35%. This indicates amplification not only of the general hull motions but also of local loads acting on side structures.

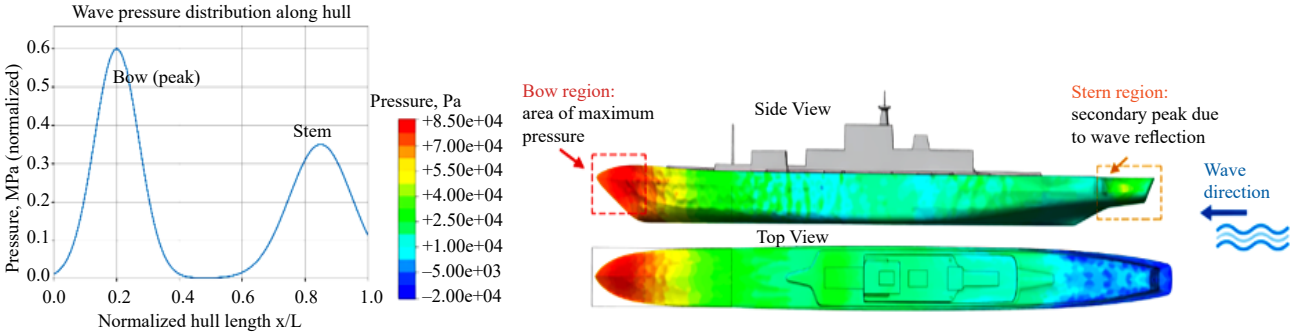

Fig. 6. Distribution of wave pressure along the ship hull

Fig. 6 presents the distribution of wave pressure along the ship hull. It was found that the maximum pressure values are localized in the bow region, where the most intensive interaction between the hull and the incoming wave occurs. Additional local maxima are observed in the stern region, which is associated with reflection and redistribution of wave energy. The results indicate a nonuniform load distribution, leading to significant bending moments and increased loading of hull structural elements. Thus, the most hazardous zones in terms of force action are the bow and, to a lesser extent, the stern parts of the ship.

Analysis of the hydrodynamic pressure distribution over the hull showed that under head-wave conditions the pressure is distributed more uniformly along the hull length, whereas under oblique and following waves pronounced local load-concentration zones arise in the bow and midship regions. In shallow water, these regions shift closer to the waterline, which is associated with changes in the shape of the wave field around the hull and amplification of reflected components.

Influence of wave parameters. At a fixed depth h = 7 m and peak period T_p = 5.5 s, an increase in significant wave height from 1.5 to 3.5 m led to an almost linear increase in the root-mean-square values of forces; however, the extreme values grew faster than linearly. This is explained by the fact that, when approaching resonance conditions, higher waves more strongly excite the region of maximum response.

Table 5

Influence of Hs on extreme loads at h = 7 m, T_p = 5.5 s, β = 90°

Hs, m	Max heave, m	F_z max, MN	Bending moment, MN·m
1.5	1.42	1.08	9.6
2.0	1.88	1.42	12.7
2.5	2.29	1.93	16.3
3.0	2.77	2.08	18.5
3.5	3.19	2.46	21.7

Table 5 presents the maximum values of vertical hull motions and integral hydrodynamic loads as functions of significant wave height. The data show that increasing *Hs* leads to a monotonic increase in both motions and force characteristics, with the most intensive increase observed for bending moments.

The largest loads were observed at T_p = 5.5–6 s, which corresponds to the resonance-response region [2, 12, 13] identified in the frequency-domain analysis. When the period decreased to 4.5 s, the extreme loads decreased by 30–40%, even with the same significant wave height.

Table 6

Influence of Tp on vertical loads at h = 7 m, *Hs* = 2.5 m, β = 90°

T_p, s	ω_p, rad/s	Max heave, m	F_z max, MN
4.5	1.40	1.56	1.22
5.0	1.26	1.94	1.58
5.5	1.14	2.26	1.93
6.0	1.05	2.43	2.01

Table 6 gives the calculated maximum vertical motions and hydrodynamic loads as functions of the peak wave period. It can be seen that increasing the period leads to an increase in response amplitude, with maximum values reached in the range of 5.5–6 s, corresponding to resonant interaction between waves and the ship.

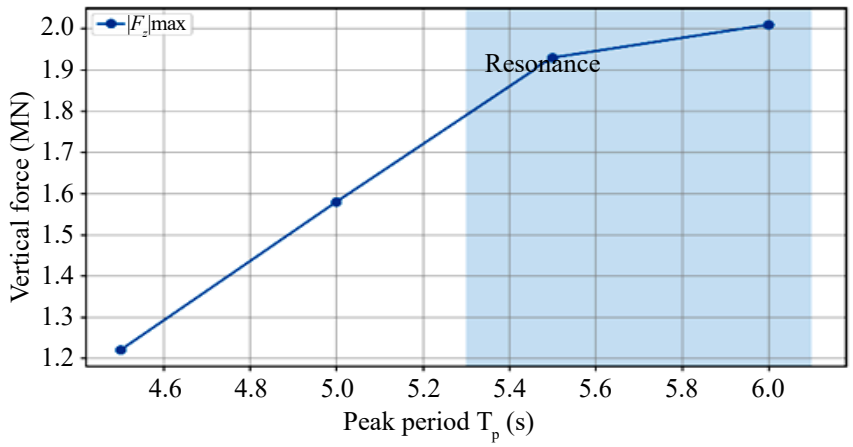

Fig. 7. Dependence of hydrodynamic loads on peak wave period (resonant amplification of the response)

Fig. 7 presents the dependence of hydrodynamic loads on the peak wave period. It was found that, as the period increases, the vertical force rises and reaches a maximum in the range T_p = 5.5–6 s. This effect is caused by the coincidence of the external forcing frequency with the natural frequencies of ship motions, resulting in resonant amplification of the response. In the resonance region, even moderate waves can generate significant hydrodynamic loads, which substantially increases operational risk. The results confirm that the most hazardous waves are not simply high waves, but waves with periods close to the natural periods of vertical and angular hull response.

In addition, the effect of changes in hull draft was investigated. Three characteristic loading states were considered: T = 3.2, 3.6, and 4 m. Increasing the draft increased the added masses, changed the hydrostatic characteristics of the system, and simultaneously reduced the static under-keel clearance. The calculations showed that, under identical wave conditions, increasing the draft from 3.2 to 4.0 m leads to an increase in the extreme vertical force by approximately 12–15% and simultaneously increases the system sensitivity to long-period waves. In practical terms, this means that the most heavily loaded ships not only have a smaller depth margin but also experience more intensive dynamic wave action.

The obtained patterns are in good agreement with current concepts of ship hydrodynamics in shallow water [3–5, 19–21]. First, the shift of RAO peaks toward lower frequencies with decreasing depth was confirmed. Second, the characteristic dominance of beam waves for vertical and transverse responses was reproduced, as was the increased contribution of pitch under head and following waves. Third, the time-domain analysis showed that extreme loads are formed within a narrow range of combinations of depth and wave period close to resonance.

In terms of absolute RAO values and integral forces, the obtained estimates fall within a realistic range for ships of this class and do not contradict published calculation results for objects of similar dimensions. At the same time, it should be noted that direct comparison in absolute values is always limited by differences in hull lines, displacement, and problem formulation.

Discussion. The results show that, within the considered parameter range, the shallow-water effect acts not as a secondary correction but as a determining factor in the formation of the ship dynamic and force response. When the depth decreases from 9 to 5.5 m, the maximum vertical-motion RAO increases from 1.07 to 1.49 m/m, that is, by approximately 39%, and the resonance peak shifts from 1.14 to 0.96 rad/s. This indicates an increase in the characteristic natural periods of the ship-fluid system and agrees with the physical interpretation of increasing added masses and changing hydrodynamic restoring under limited-depth conditions. At the same time, the increase in response amplitudes is accompanied by growth in integral loads: for the vertical force and rolling moment near the resonance region, increases of approximately 27% and 31%, respectively, were obtained when moving to the smallest of the depths considered.

A fundamentally important result is the established ambiguity in the relationship between motion maxima and operationally hazardous load maxima. Beam waves ($\beta = 90°$) do indeed produce the largest heave response and maximum roll values; however, this does not mean that this regime is always the most unfavorable in terms of local hull loading. The combined analysis of heave and pitch showed that the largest local increase in draft at the extremities occurs under oblique following and following waves (β from 135° to 180°), when a moderately high vertical response is combined with significant trim. Therefore, when assessing hazardous operating regimes, it is not sufficient to analyze individual degrees of freedom separately; a joint account of the spatial redistribution of loads along the hull is required.

The role of wave spectral characteristics should be emphasized separately. The calculations showed that extreme loads are determined not only by significant wave height but also by the degree of closeness of the peak period to the resonance region of the system. The highest vertical-motion and wave-force values were obtained at T_p = 5.5–6 s, i. e., in the range corresponding to the maximum frequency response. At the same time, an increase in *Hs* leads to an almost linear increase in root-mean-square characteristics, whereas extreme force and moment values grow faster than linearly, indicating an increased contribution of resonant episodes to the time history of the load. An additional increase in ship draft also increases the hazard: when the draft grows from 3.2 to 4.0 m, the extreme vertical force increases by approximately 12–15%, and the system sensitivity to long-period waves increases.

At the same time, interpretation of the obtained dependences must account for the limits of applicability of the model used. The calculations were performed within linear potential flow theory and the panel method; therefore, the results correctly describe the comparative influence of depth, period, height, and wave direction in the range of small and moderate amplitudes. However, the study did not account for nonlinear wave transformation and breaking, viscous and turbulent effects, or the influence of complex bathymetry and possible interaction with seabed morphodynamics. Therefore, when moving to extreme storm conditions or to local structural-analysis problems, the obtained estimates should be regarded as a reliable engineering basis requiring further refinement using nonlinear and hybrid models.

Conclusion. A numerical study of the hydrodynamic response of a river-sea ship under limited-depth conditions was performed using a combined approach that integrates RAO frequency-domain analysis and time-domain simulation of irregular waves. This approach made it possible to link the parameters of external wave action with hull-motion amplitudes, pressure distribution, and integral hydrodynamic loads.

It was found that decreasing the depth from 9 to 5.5 m leads to a systematic shift of the resonance region toward longer waves and to a substantial increase in the ship dynamic response. For vertical motions, the maximum RAO increases by approximately 39%, while integral loads near resonance frequencies also increase significantly: by approximately 27% for the vertical force and approximately 31% for the rolling moment. Thus, it is shown that shallow water has a direct influence not only on motion kinematics but also on the level of wave-induced force action on the hull.

It is shown that wave direction determines not only the magnitude but also the structure of the response. Under beam waves, the maximum heave and roll values occur, whereas under oblique following and following waves the contribution of pitch increases, leading to redistribution of loads along the hull length and to the formation of the most unfavorable local regimes at the bow and stern extremities. Consequently, when assessing the operational safety of a ship in shallow-water areas, it is necessary to consider not only the absolute level of motions but also their combination, which determines local draft variations and load concentration.

It was also found that extreme hydrodynamic loads are determined by the combined action of depth, significant wave height, peak period, and ship draft. The most hazardous regimes correspond to combinations of shallow depths and wave periods close to the natural resonance region of the system; with increasing draft, the intensity of the force response additionally increases and the depth margin decreases. This makes it possible to regard the results obtained as a physically justified basis for assessing hazardous navigation regimes, selecting operational limitations, and developing recommendations for navigation safety in shallow-water areas, including the Sea of Azov and Taganrog Bay.

The practical value of the study lies in the fact that the obtained dependences can be used in preliminary ship design, assessment of allowable operating conditions, and development of engineering criteria for navigation safety. Further development of the study is associated with the inclusion of nonlinear shallow-water effects, viscous-turbulent mechanisms, refined bathymetry, and hybrid potential-viscous models, which will make it possible to move from an engineering estimate to a more complete description of extreme regimes of wave action on the hull.

References

1. Jiao J., Sun S., Ren H. Predictions of wave induced ship motions and loads by large-scale model measurement at sea and numerical analysis. *Brodogradnja*. 2016;67(2):81–100. https://doi.org/10.21278/brod67206

2. Jiao J., Chen C., Ren H. A comprehensive study on ship motion and load responses in short-crested irregular waves. *International Journal of Naval Architecture and Ocean Engineering*. 2019;11:830–847. https://doi.org/10.1016/j.ijnaoe.2018.07.003

3. Kim D., Tezdogan T., Incecik A. Hydrodynamic analysis of ship manoeuvrability in shallow water using high-fidelity URANS computations. *Applied Ocean Research*. 2022;123:103176. https://doi.org/10.1016/j.apor.2022.103176

4. Taimuri G., Matusiak J., Mikkola T., Kujala P., Hirdaris S. A 6-DoF maneuvering model for the rapid estimation of hydro-dynamic actions in deep and shallow waters. *Ocean Engineering*. 2020;218:108103. https://doi.org/10.1016/j.oceaneng.2020.108103

5. Feng L., Wang L., Zhang Y. Numerical Study of the Shallow-Water Effect on the Hydrodynamic Loads and Wake of a Ship in Oblique Flow. *Journal of Ocean University of China*. 2025;24(1):63–74. https://doi.org/10.1007/s11802-025-5854-7

6. Yaitskaya N. The Wave Climate of the Sea of Azov. Water. 2022;14(4):555. https://doi.org/10.3390/w14040555

7. Korshenko E., Panasenkova I., Fomin V. The Sea of Azov's Hydrodynamic Response to Different Atmospheric Forcing Resolutions. *Water*. 2024;16(23):3493. https://doi.org/10.3390/w16233493

8. Mai V.T., Mai T.L., Yoon H.K. Numerical Investigation of Motion Response of the Tanker at Varying Vertical Center of Gravities. *Journal of Ocean Engineering and Technology*. 2024;38(1):1–9. https://doi.org/10.26748/KSOE.2023.037

9. Seo M.G., Ha Y.J., Nam B.W., Kim Y. Experimental and Numerical Analysis of Wave Drift Force on KVLCC2 Moving in Oblique Waves. *Journal of Marine Science and Engineering*. 2021;9(2):136. https://doi.org/10.3390/jmse9020136

10. Karola A., Matusiak J., Mikkola T., Hirdaris S. Wave Loads and Ship Motions Evaluated by Linear Strip and Panel Methods. In: *Proceedings of the ASME 2022 41st International Conference on Ocean, Offshore and Arctic Engineering*. 2022;5A. https://doi.org/10.1115/OMAE2022-79702

11. Parunov J., Guedes Soares C., Hirdaris S., Iijima K., Wang X., Brizzolara S., Qiu W., Mikulić A., Wang S., Abdelwahab H.S. Benchmark study of global linear wave loads on a container ship with forward speed. *Marine Structures*. 2022;84:103162. https://doi.org/10.1016/j.marstruc.2022.103162

12. Xu H., Neng P., Yang F. Motion response analysis of mining vessel based on ANSYS/AQWA. *Journal of Physics: Conference Series*. 2019;1300(1):012010. https://doi.org/10.1088/1742-6596/1300/1/012010

13. Ibinabo I., Tamunodukobipi D.T. Determination of the Response Amplitude Operator(s) of an FPSO. *Engineering*. 2019;11(9):541–556. https://doi.org/10.4236/eng.2019.119038

14. Jiao J., Zhang H., Chen Y., Sun S. Difference in ship motion and wave load in long and short crested irregular waves. *Chinese Journal of Ship Research*. 2023;18(1):107–115. https://doi.org/10.19693/j.issn.1673-3185.02679

15. Xiong L., Lu H., Yang J., Zhao W. Motion responses of a moored barge in shallow water. *Ocean Engineering*. 2015;97:207–217. https://doi.org/10.1016/j.oceaneng.2015.01.018

16. Dong G., Yan S., Ma X., Wang B., Li L. Experimental investigation on the hydrodynamic response of a moored ship to low-frequency harbor oscillations. *Ocean Engineering*. 2022;266:112261. https://doi.org/10.1016/j.oceaneng.2022.112261

17. Hasselmann K., Barnett T.P., Bouws E., Carlson H., Cartwright D.E., Enke K., Ewing J.A., Gienapp H., Hasselmann D.E., Kruseman P., Meerburg A., Müller P., Olbers D.J., Richter K., Sell W., Walden H. Measurements of wind-wave growth and swell decay during the Joint North Sea Wave Project (JONSWAP). *Ergänzungsheft zur Deutschen Hydrographischen Zeitschrift, Reihe A*. 1973;8(12):1–95.

18. Ohyama T., Tsuchida M. Expanded mild-slope equations for the analysis of wave-induced ship motion in a harbor. *Coastal Engineering*. 1997;30(1–2):77–103. https://doi.org/10.1016/S0378-3839(96)00037-3

19. Wermbter M., Perić R., Serr J., Abdel-Maksoud M. An approach to estimate vertical center of gravity, draught and RAO from ship motions based on prolate spheroidal wave functions and time-series filtering. *Ocean Engineering*. 2025;330:122659. https://doi.org/10.1016/j.oceaneng.2025.122659

20. Begovic E., Bertorello C., Çakıcı F., Kahramanoğlu E., Rinauro B. Vertical motions prediction in irregular waves using a time domain approach for hard chine displacement hull. *Journal of Marine Science and Engineering*. 2020;8(5):337. https://doi.org/10.3390/JMSE8050337

21. Duan F., Ma N., Gu X., Zhou Y., Wang S. A fast time domain method for predicting of motion and excessive acceleration of a shallow draft ship in beam waves. *Ocean Engineering*. 2022;262:112096. https://doi.org/10.1016/j.oceaneng.2022.112096

22. Sutulo S., Rodrigues J.M., Guedes Soares C. Hydrodynamic characteristics of ship sections in shallow water with complex bottom geometry. *Ocean Engineering*. 2010;37(10):947–958. https://doi.org/10.1016/j.oceaneng.2010.03.008

23. Duan F., Ma N., Wang S., Zhou Y. Potential and viscous hybrid calculation method for ship motion prediction considering the change of ship motion attitude. *Ocean Engineering*. 2024;311:118824. https://doi.org/10.1016/j.oceaneng.2024.118824

24. Hasselmann D., Bösenberg J. Field measurements of wave-induced pressure over wind-sea and swell. *Journal of Fluid Mechanics*. 1991;230:391–428. https://doi.org/10.1017/S0022112091000848

25. Newman J.N. *Marine Hydrodynamics*. Cambridge, MA: MIT Press; 1977.

26. Jiao J., Ren H., Chen C. Model testing for ship hydroelasticity: A review and future trends. *Journal of Shanghai Jiaotong University (Science)*. 2017;22(6):641–650. https://doi.org/10.1007/s12204-017-1886-5

27. Molland A.F., Turnock S.R., Hudson D.A. *Ship Resistance and Propulsion*. 2nd ed. Cambridge: Cambridge University Press; 2011.

About the Authors:

Alexander I. Sukhinov, Corresponding Member of the Russian Academy of Sciences, Doctor of Physical and Mathematical Sciences, Professor, Director of the Research Institute of Mathematical Modeling and Forecasting of Complex Systems, Don State Technical University (1, Gagarin Sq., Rostov-on-Don, 344003, Russian Federation), ORCID, SPIN-code, ScopusID, ResearcherID, MathSciNet, sukhinov@gmail.com

Sofia V. Protsenko, Candidate of Physical and Mathematical Sciences, Associate Professor of the Department of Mathematics, Research Fellow, A.P. Chekhov Taganrog Institute (branch) Rostov State University of Economics (48, Initiative St., Taganrog, 347936, Russian Federation), ORCID, SPIN-code, rab5555@rambler.ru

Natalya D. Panasenko, Senior Lecturer of the Department of Computer Systems and Information Security, Don State Technical University (1, Gagarin Sq., Rostov-on-Don, 344003, Russian Federation), ORCID, SPIN-code, ScopusID, ResearcherID, natalija93_93@ mail.ru

Elena A. Protsenko, Candidate of Physical and Mathematical Sciences, Associate Professor of the Department of Mathematics, Leading Research Fellow, A.P. Chekhov Taganrog Institute (branch) Rostov State University of Economics (48, Initiative St., Taganrog, 347936, Russian Federation), ORCID, SPIN-code, eapros@rambler.ru

Contributions of the authors:

A.I. Sukhinov: general scientific guidance; problem statement; formulation of research ideas, goals and objectives, development of methodology.

S.V. Protsenko: conducting experiments, formulating achieved results and describing their significance.

N.D. Panasenko: validation; testing of existing components.

E.A. Protsenko: data curation; annotation activities.

Conflict of Interest Statement: **the authors declare no conflict of interest.**

All authors have read and approved the final manuscript.

Об авторах:

Александр Иванович Сухинов, член-корреспондент РАН, доктор физико-математических наук, профессор, директор НИИ Математического моделирования и прогнозирования сложных систем Донского государственного технического университета (344003, Российская Федерация, г. Ростов-на-Дону, пл. Гагарина, 1), ORCID, SPIN-код, ScopusID, ResearcherID, MathSciNet, sukhinov@gmail.com

Софья Владимировна Проценко, кандидат физико-математических наук, доцент кафедры математики, научный сотрудник Таганрогского института им. А.П. Чехова (филиал) Ростовского государственного экономического университета (347936, Российская Федерация, г. Таганрог, ул. Инициативная, 48), ORCID, SPIN-код, rab5555@rambler.ru

Наталья Дмитриевна Панасенко, старший преподаватель кафедры «Вычислительные системы и информационная безопасность» Донской государственный технический университет (344003, Российская Федерация, г. Ростов-на-Дону, пл. Гагарина, 1), ORCID, SPIN-код, ScopusID, ResearcherID, natalija93_93@mail.ru

Елена Анатольевна Проценко, кандидат физико-математических наук, доцент кафедры математики, ведущий научный сотрудник Таганрогского института им. А.П. Чехова (филиал) Ростовского государственного экономического университета (347936, Российская Федерация, г. Таганрог, ул. Инициативная, 48), ORCID, SPIN-код, eapros@rambler.ru

Заявленный вклад авторов:

А.И. Сухинов: общее научное руководство; постановка задачи; формулировка идей исследования, целей и задач, разработка методологии.

С.В. Проценко: проведение экспериментов, формулировка достигнутых результатов и описание их значимости.

Н.Д. Панасенко: валидация; тестирование существующих компонентов.

Е.А. Проценко: курирование данных; деятельность по аннотированию.

Конфликт интересов: ***авторы заявляют об отсутствии конфликта интересов.***

Все авторы прочитали и одобрили окончательный вариант рукописи.

Received / Поступила в редакцию 27.02.2026
Reviewed / Поступила после рецензирования 25.03.2026
Accepted / Принята к публикации 02.04.2026

INFORMATION TECHNOLOGIES
ИНФОРМАЦИОННЫЕ ТЕХНОЛОГИИ

UDC 004.82: 004.92

Original Empirical Research

https://doi.org/10.23947/2587-8999-2026-10-2-46-56

Efficient Visualization of Knowledge Graphs Based on Next-Generation Language Models

Oksana I. Zakharova[1], **Konstantin N. Ivanov**[1], **Sergey P. Levashkin**[1] ✉,
Mikhail V. Yakobovskiy[2]

[1] Povolzhskiy State University of Telecommunications and Informatics (PSUTI), Samara, Russian Federation
[2] Keldysh Institute of Applied Mathematics of the Russian Academy of Sciences (IPM RAS), Moscow, Russian Federation
✉ ai_lab@psuti.ru

Abstract

Introduction. This paper examines a methodology for the automated extraction and graphical representation of knowledge from unstructured texts using modern language models. Such methods are becoming increasingly relevant because of the growing need to structure information and identify semantic relations that are difficult to capture manually.

Materials and Methods. The proposed approach combines locally deployed language models with specialized relation-extraction tools. Local deployment enables data to be processed in a secure environment without reliance on external services. The methodology includes text preprocessing, entity and relation extraction, structuring, and visualization of the resulting knowledge graphs.

Results. Experimental testing on a corpus of Russian-language scientific articles demonstrated that the approach is applicable both to technical descriptions and to texts containing more abstract concepts. The developed web interface supports interactive visualization and comparative analysis of graphs constructed by different models, thereby improving the interpretability of the results. The approach is robust to textual noise and is applicable to scientific, technical, and regulatory tasks.

Discussion. The results show that the proposed methodology is not limited to a single algorithm and permits the combination of direct extraction, specialized models, multi-stage pipelines, and OWL ontologies. The quality of the resulting graphs depends substantially on the structure of the source text, preprocessing accuracy, and the selected post-processing procedures; interactive visualization facilitates comparison of outputs generated by different models and supports the interpretation of semantic relations.

Conclusions. The proposed approach can be applied to the analysis of scientific, technical, and regulatory texts in a secure local environment. It is a natural continuation of the authors' previous research on semantic-associative data analysis and synthesis and the associative-ontological approach. Further development should focus on ensemble schemes, logical validation, semantic inference, and integration with formal ontologies, thereby extending its applicability to information retrieval, research support, and complex-system modelling.

Keywords: knowledge graphs, information extraction, large language models, ontologies, natural language processing, semantic analysis, Python

Funding. The study was supported by the Russian Science Foundation, grant No. 23–61–10032.

For Citation. Zakharova O.I., Ivanov K.N., Levashkin S.P., Yakobovskiy M.V. Efficient Visualization of Knowledge Graphs Based on Next-Generation Language Models. *Computational Mathematics and Information Technologies*. 2026;10(2):46–56. https://doi.org/10.23947/2587-8999-2026-10-2-46-56

Оригинальное эмпирическое исследование

Эффективная визуализация графов знаний на базе языковых моделей нового поколения

О.И. Захарова[1], К.Н. Иванов[1], С.П. Левашкин[1] ✉, М.В. Якобовский[2]

[1] Поволжский государственный университет телекоммуникаций и информатики, г. Самара, Российская Федерация

[2] Институт прикладной математики имени М. В. Келдыша РАН (ИПМ РАН), г. Москва, Российская Федерация

✉ ai_lab@psuti.ru

Аннотация

Введение. Рассматривается методология автоматизированного извлечения и графического представления знаний из неструктурированных текстов с использованием современных языковых моделей. Подобные методы становятся всё более востребованными в связи с необходимостью структурирования информации и выявления смысловых связей, которые трудно фиксировать вручную.

Материалы и методы. Методология включает этапы предварительной обработки текста, извлечения сущностей и связей, структурирования и визуализации полученных графов. Предложенный подход основан на комбинировании локально развернутых языковых моделей и специализированных инструментов извлечения отношений. Использование локальных решений обеспечивает обработку данных в защищённой среде без обращения к внешним сервисам.

Результаты исследования. Разработанный веб-интерфейс обеспечивает интерактивную визуализацию и сравнительный анализ графов, построенных разными моделями, что повышает интерпретируемость результатов. Подход демонстрирует устойчивость к шуму в текстах и применим для решения задач в научной, технической и нормативно-правовой сферах. Экспериментальная апробация на корпусе русскоязычных научных статей показала, что предложенный подход применим как к техническим описаниям, так и к текстам с более абстрактными концепциями.

Обсуждение. Полученные результаты показывают, что предложенная методология не сводится к одному алгоритму и допускает комбинирование прямого извлечения, специализированных моделей, многоступенчатых схем и *OWL*-онтологий. Качество итоговых графов существенно зависит от структуры исходного текста, точности предварительной обработки и выбранных процедур постобработки; при этом интерактивная визуализация облегчает сопоставление результатов разных моделей и интерпретацию семантических связей.

Заключение. Предложенный подход может применяться для анализа научных, технических и нормативно-правовых текстов в защищённой локальной среде. Он является естественным продолжением предыдущих исследований авторов, связанных с семантико-ассоциативным анализом, синтезом данных и ассоциативно-онтологическим подходом. Его дальнейшее развитие целесообразно связывать с ансамблевыми схемами, логической валидацией, семантическим выводом и интеграцией с формальными онтологиями, что расширяет возможности информационного поиска, поддержки научных исследований и моделирования сложных систем.

Ключевые слова: графы знаний, извлечение информации, большие языковые модели, онтологии, обработка естественного языка, семантический анализ, Python

Финансирование. Работа выполнена при финансовой поддержке РНФ (грант № 23–61–10032).

Для цитирования. Захарова О.И., Иванов К.Н., Левашкин С.П., Якобовский М.В. Эффективная визуализация графов знаний на базе языковых моделей нового поколения. *Computational Mathematics and Information Technologies*. 2026;10(2):46–56. https://doi.org/10.23947/2587-8999-2026-10-2-46-56

Introduction. The contemporary information environment is characterized by exponential growth in the volume of unstructured data, a substantial proportion of which is presented in textual form. Scientific publications, reports, regulatory documents, and news materials contain valuable knowledge; however, its manual extraction and structuring are becoming increasingly complex and labor-intensive. Traditional natural language processing methods often exhibit limited adaptability when transferred to new subject domains and insufficient accuracy when handling complex semantic constructions, which motivates the search for new approaches to automated knowledge extraction.

Advances in and adoption of large language models open up new opportunities for processing textual information by enabling more effective identification of contextual dependencies and the formation of structured representations. Such models are increasingly viewed as tools for extracting semantic relations and concepts from unstructured data.

This study evaluates a methodological approach to the automated extraction and representation of knowledge from Russian-language texts. The key stages of the methodology are analyzed: text preprocessing, entity and relation extraction, formalized description, and visualization as graph structures. Different methods and tools may be used at each

stage, making the approach flexible and allowing several implementation variants. To assess its applicability, locally deployed language models with tens of billions of parameters were used; these models can operate under limited computational resources.

Entity and relation extraction methods were implemented using different software tools, and their outputs were integrated into a unified processing pipeline. Experimental testing on real-world documents demonstrated the applicability of the proposed methodology and identified prospects for its further development, including model ensembles and the integration of outputs generated by different approaches.

The scientific novelty of the study lies in the development of a methodological approach that integrates modern information-extraction tools and adapts them to the analysis of Russian-language texts. The practical significance lies in the potential application of the proposed approach to the analysis of scientific publications, information retrieval, and research support, where unstructured data must be transformed into clear and interpretable representations.

Materials and Methods. Knowledge graphs provide a powerful mechanism for representing information in a structured form. They consist of nodes representing entities and edges describing relations between these entities [1]. Entities may be abstract concepts or concrete objects, while relations capture complex interdependencies among them. The advantages of graph representation include readability, intuitive interpretation, the ability to represent complex knowledge structures, and the integration of heterogeneous data from multiple sources [2]. Formalized knowledge models, such as ontologies, play a key role in graph construction by describing a subject domain in terms of classes and properties, thereby ensuring semantic consistency and data unification.

Modern large language models have demonstrated outstanding capabilities in natural-language understanding and generation [3]. Training on massive text corpora enables them to capture subtle semantic nuances and complex syntactic structures. In information extraction, such models are used both to generate structured data directly, for example as semantic triples, and to perform auxiliary tasks such as text classification and named-entity recognition. Particular attention is paid to adapting these models to Russian-language texts, which requires consideration of the language's morphological, syntactic, and semantic characteristics.

For programmatic graph construction and manipulation, specialized software libraries offering extensive functionality for graph structures are widely used [4–11]. Interactive graph visualization is essential for analyzing and interpreting extracted knowledge. Specialized network-diagram libraries combined with web-visualization technologies make it possible to create dynamic, interactive graphs that can be integrated into web applications [5]. Auxiliary user-interface components complement this functionality by providing convenient filtering and navigation across graph elements.

The proposed approach comprises several key components shown in Fig. 1. It should be emphasized that graph-based knowledge representation can be used not only for visualization but also for intelligent data processing. The authors' previous studies demonstrated that representing texts as directed graphs and subsequently processing them with graph neural networks can achieve high accuracy in semantic text classification and clustering [6]. This confirms the practical value of graph models for natural language analysis and further supports their use in the proposed methodology.

Rather than relying on a single fixed algorithm, the proposed methodology permits alternative implementations at each stage — from entity extraction to graph visualization — which may be combined according to the characteristics of the text and the objectives of the analysis.

A distinctive feature of the proposed approach is the use of ontologies formalized using the OWL (Web Ontology Language) standard. OWL is a specialized ontology-description language developed by the W3C and widely used to model complex subject domains and semantic relationships between entities.

OWL can be used not only to define classes, properties, and relations between objects but also to formulate logical constraints and inheritance rules and to specify concept hierarchies and their interrelations at a formal level [7].

OWL provides a high degree of knowledge formalization, which is crucial for the automated analysis and processing of large volumes of unstructured information. By supporting different property types (object properties, data properties, and annotation properties) and allowing axioms to be specified, OWL enables flexible and extensible ontological models that can be readily integrated with tools for semantic search, logical inference, and knowledge-graph visualization. Thus, OWL serves as a formal knowledge-description language, although it is not the only tool available within the methodology. The approach permits the integration of both formal and associative methods, thereby broadening the possibilities for knowledge structuring and interpretation.

Within the proposed methodology, OWL ontologies are used to explicitly describe the subject domain and define key entities, their attributes, and permissible relation types. This makes it possible not only to structure knowledge extracted from text but also to automatically validate the resulting graphs for logical consistency and completeness. Moreover, OWL supports advanced semantic-reasoning mechanisms, enabling implicit relations between entities to be identified, complex queries to be executed against the knowledge graph, and new knowledge to be derived from existing facts [8].

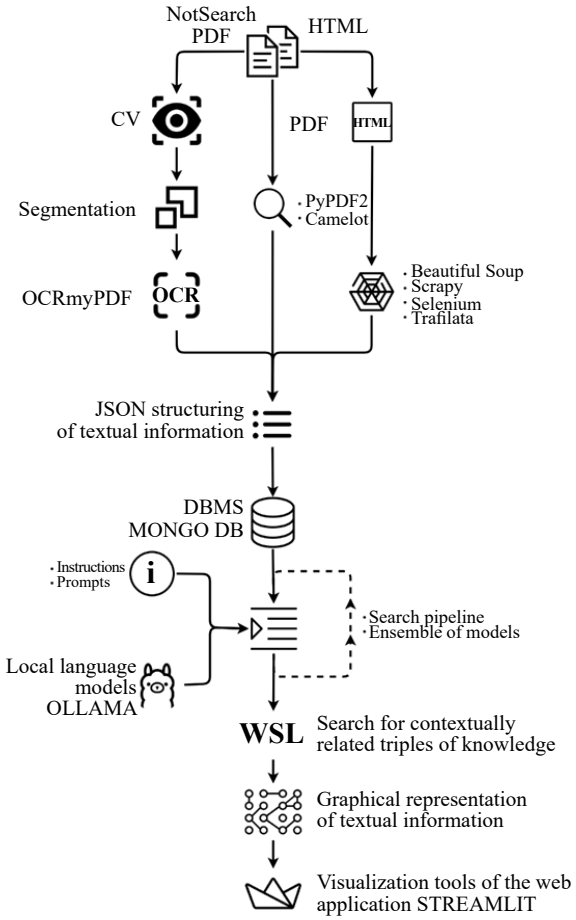

Fig. 1. Flowchart of the developed methodology for automated knowledge extraction and graphical representation from unstructured texts using LLMs

In addition to formal methods, the associative-ontological approach [9] has made a significant contribution to the field by demonstrating the potential of interpretable knowledge representation and automatic ontology generation from unstructured data. Its use in information monitoring and analysis systems confirms the relevance of integrating different ontological methods to improve the quality and completeness of extracted knowledge.

During the experimental study, the developed approach was comprehensively evaluated using three scientific texts differing in subject matter and complexity. The experimental corpus included texts on methodological issues in natural-systems research, highway surveying and design, and uncertainties in observational data.

The results obtained for the text on methodological issues in natural-systems research are of particular interest. The graphs generated from this text clearly illustrate the complex relationships among different aspects of research methodology. Each model interpreted these relationships differently, revealing different levels of abstraction in the knowledge representation. Analysis of graphs generated from the text on highway surveying and design showed that the approach was highly effective for technical documentation. The models successfully extracted and structured information on various aspects of design, including geological conditions, technical requirements, and environmental considerations.

When processing the text on uncertainties in observational data, the approach demonstrated an ability to handle abstract concepts and their interrelations. The generated graphs reflect a complex structure of interdependencies between different types of uncertainty and methods for their assessment. An important finding was that the quality of extracted knowledge depends substantially on the structure of the source text. Texts with a clear logical organization and explicitly stated relations between concepts produced higher-quality graphs. This finding indicates the need for text preprocessing to improve knowledge-extraction results.

Practical testing confirmed the effectiveness of the approach for real-world scientific-text analysis tasks. The developed web interface provides convenient access to the analysis results and supports interactive exploration of the resulting graphs. The availability of multiple visualization modes was particularly valuable, as it allows graphs to be examined at different levels of detail.

Figure 2 presents a scheme of methods for extracting graphs from texts using large language models. The process begins with unstructured text, which may be processed by different methods depending on requirements for accuracy, completeness, or interpretability. These methods represent alternative implementations of a unified methodological framework and may be applied individually or in combination.

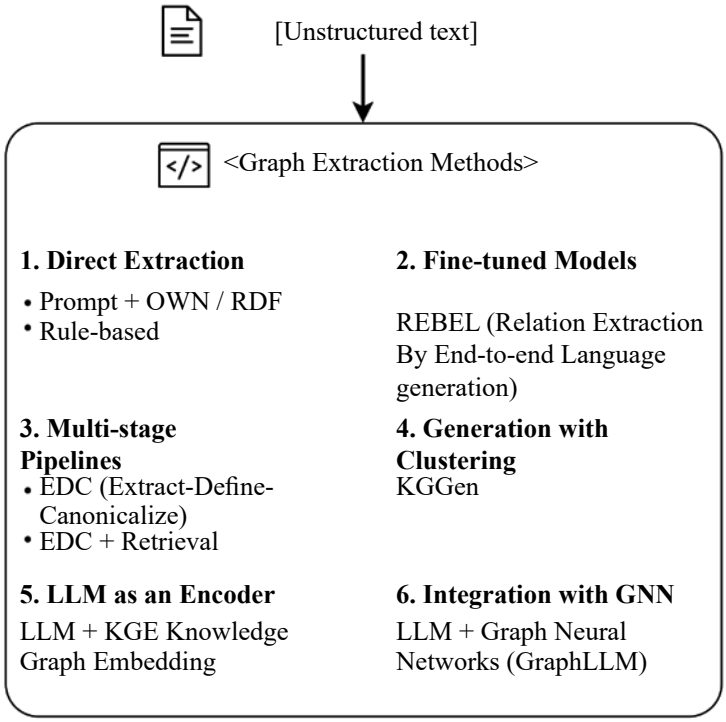

Fig. 2. Methods for extracting graphs from texts using LLMs

Direct extraction uses prompts specifying OWL/RDF output and rule-based approaches. This method supports ontology standards but requires carefully formulated prompts and performs poorly without sufficient context. Pretrained models such as REBEL use a sequence-to-sequence (seq2seq) architecture to extract relational triples from text. These models achieve high accuracy and do not require manually defined rules, although their outputs may be difficult to interpret. Multi-stage pipelines such as EDC (Extract-Define-Canonicalize) comprise three stages: extraction of basic triples, category definition, and canonicalization [10]. This approach is more flexible and scalable but requires multi-stage processing and may introduce errors during schema generation.

Clustering-based generation methods, such as KGGGen, cluster similar entities and relations to reduce noise in extracted graphs. This method is particularly useful for large text corpora but requires sophisticated post-processing. When an LLM is used as an encoder, it is integrated with Knowledge Graph Embeddings (KGE) to generate entity and relation representations. These representations are used for link prediction, entity alignment, and knowledge-graph completion. Integration with GNNs combines LLMs with Graph Neural Networks (GNNs) for graph construction, graph-based learning, and logical inference [11]. This approach provides flexibility and supports the development of reasoning agents, but it requires substantial infrastructure and computational resources.

Formally, the knowledge-extraction task can be represented as constructing the mapping

$$f : (T, \pi) \to G,$$

where T is the source text containing unstructured information; π is a set of instructions (*prompt*), defining the rules for text interpretation, the output representation format, and constraints on the output data; f is the mapping implemented by the language model that transforms the textual representation into a structured form; G is the resulting knowledge graph

$$G = (V, E),$$

where V is the set of graph vertices corresponding to entities in the subject domain; E is the set of graph edges representing relations between entities.

The edge set is defined as

$$E \subseteq V \times R \times V,$$

where R is the set of permissible semantic relations between entities; $r \in R$ is a specific relation type between two entities; $V \times R \times V$ is the space of possible triples of the form "entity — relation — entity".

The use of LLMs makes it possible to estimate the probability that a given text fragment corresponds to the triple:

$$(v_i,r,v_j),$$

where $v_i \in V$ is the source entity; $v_j \in V$ is the target entity; $r \in R$ is the relation between the entities.

The probability of generating a triple can be represented as

$$P((v_i, r, v_j) \mid T, \pi) \propto \prod_{t=1}^{m} P(x_t \mid x_{<t}, T, \pi),$$

where $P((v_i, r, v_j) \mid T, \pi)$ is the probability that the language model extracts the triple (v_i,r,v_j) from text T using instructions π; x_t is a token generated by the model at step t; $x_{<t}$ is the sequence of all tokens generated before step t; m is the total number of tokens describing the extracted triple; $P((v_i, r, v_j) \mid T, \pi)$ is the conditional probability of generating the current token given the previously generated sequence, the source text, and the specified instructions; $\prod_{t=1}^{m}$ is the product of the sequential token-generation probabilities, reflecting the autoregressive operation of the language model; $\propto$ is the proportionality sign, indicating that the probability of the triple is related to the probability of generating the corresponding token sequence.

Thus, the instructions π act as a mechanism for controlling the probability distribution of the generative model by constraining the output space to an RDF/OWL format, JSON structure, or table. This makes it possible to transform the probabilistic textual representation produced by the language model into a space of structured semantic relations.

At the implementation level, the methodology involves:

explicit specification of the expected triple format;

use of examples (few-shot prompting) to stabilize model performance;

post-processing of the resulting structures to correct errors and merge semantically similar entities.

Taken together, these measures transform text generation into a knowledge-graph construction task. Combining different LLM-based graph-extraction methods makes it possible to achieve greater accuracy and flexibility in information processing. Each method has distinct advantages that complement the others, providing a comprehensive approach to knowledge extraction.

Results. The experimental part of the study was designed to assess the applicability of the methodology as a whole and evaluate different implementation variants. In particular, direct extraction methods, specialized models, and multi-stage pipelines were compared. This comparison revealed the advantages and limitations of each approach within the general knowledge-graph construction framework.

Fig. 3 shows a fragment of a knowledge graph generated using the proposed approach. The visualization presents key entities and the relationships between them identified during automated information extraction. Particular attention is paid to text interpretation based on predefined rules formulated in the ontology. To improve the accuracy of knowledge extraction and the relevance of relations in large data volumes, the specific information to be identified in the text and the types of relations to be detected between entities are additionally specified. This approach supports deeper and more meaningful analysis, enabling not only standard relations to be identified but also domain-specific relations relevant to the subject area under consideration.

Thus, integrating OWL ontologies into knowledge-extraction and visualization processes provides not only a formal description of the subject domain but also automation of the analysis, validation, and extension of knowledge graphs. This improves the accuracy, completeness, and interpretability of the results and facilitates integration with external data sources and other semantic systems.

Fig. 4 demonstrates the simultaneous display of several knowledge graphs in the developed web interface. On the left is a fragment of an ontological graph showing the structure of the subject domain and relationships between entities such as government authorities, regulatory documents, rating systems, and individual participants. On the right is an object-property graph showing relation types (e. g., respondsTo, preparesRegulation, and hasRatingSystem) used to describe links between entities in the ontology. This arrangement enables users to analyze both the substantive knowledge structure and the relation types simultaneously, substantially facilitating interpretation of complex domain relationships.

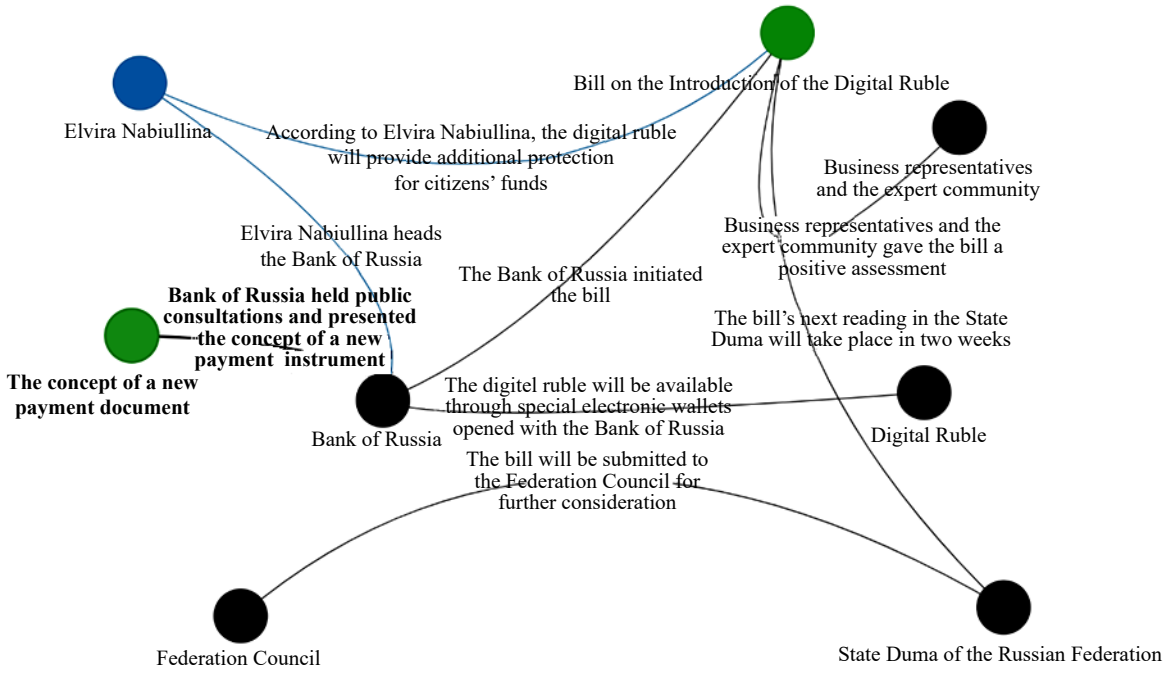

Fig. 3. Graph-based representation of text using the rule-based method

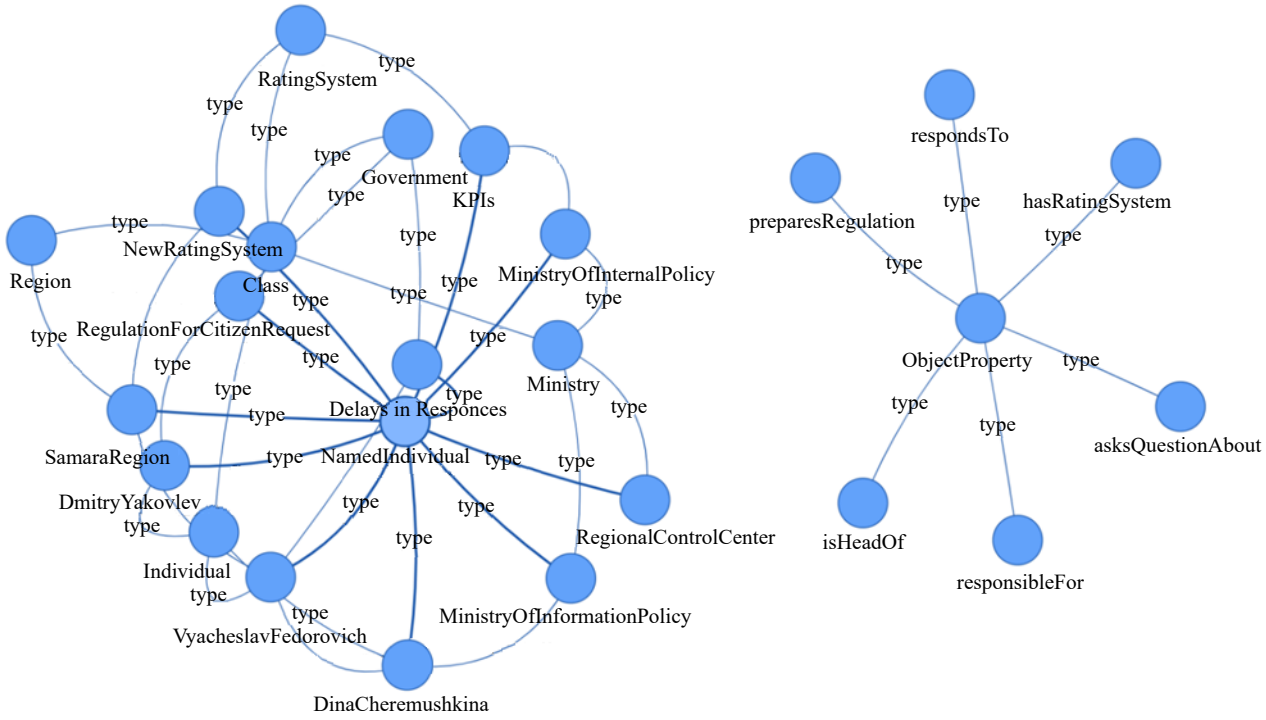

Fig. 4. Graph-based representation of text using the OWL method

Displaying several graphs in parallel improves the clarity of analysis, facilitates the identification of hidden patterns, and provides a deeper understanding of the structure and logic of the represented data [3].

Fig. 5 shows a fragment of a knowledge graph illustrating the hierarchy and constituent parts of objects in the railway-construction domain.

The visualization shows "part of" and "subclass of" relations connecting entities such as "railway," "roadbed," "soil," "foundation," "ice," "snow," and others. The graph clearly demonstrates how complex objects consist of individual components and how hierarchical relations between classes and subclasses are formed. For example, a "railway" includes a "roadbed," which in turn consists of "foundation soil" and other elements. Subclasses such as "ice" and "snow," related to "soil" and "snow cover," respectively, are also shown.

The visualization further facilitates understanding of the structure of complex engineering objects, helps identify key components and their interrelationships, and can be used to construct ontologies and conduct subsequent subject-domain analysis.

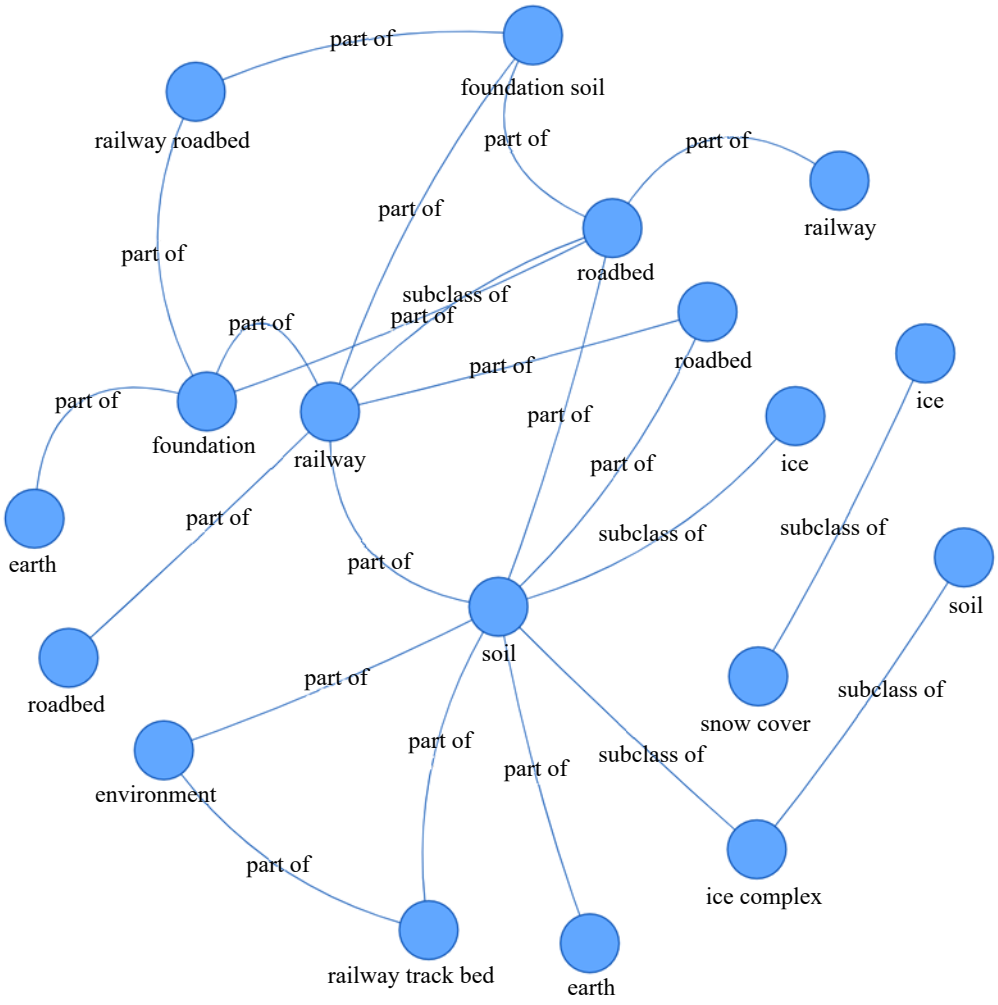

Fig. 5. Graph-based representation of text generated by the mREBEL-Large model

The study results indicate potential for further improvement of the approach. In particular, knowledge-extraction quality can be enhanced by improving text preprocessing, expanding the set of models, introducing post-processing and validation mechanisms, and developing specialized models for particular text types. Recent research in natural language processing has shown substantial progress in knowledge extraction using transformer architectures [10].

The results demonstrate the high effectiveness of the proposed approach and its potential for a wide range of scientific-text analysis tasks. An important finding was the relationship between source-text structure and the quality of the extracted knowledge. Texts with a clear logical organization and explicit markers of relations between concepts produced higher-quality graphs. This observation has practical implications for preparing texts intended for analysis using the proposed approach.

Of particular interest are the results of analyzing the approach's robustness to different types of textual distortion. The experiments showed that the approach remains operational in the presence of typographical errors, formatting irregularities, and even partial loss of context. This makes it applicable to texts of varying quality and format. Recent advances in natural language processing have demonstrated substantial progress in knowledge extraction using transformer architectures, confirming the relevance of the selected research direction.

A comparative analysis of results obtained using different models revealed notable patterns in knowledge extraction. Phi-4 was highly effective for scientific texts, particularly in handling technical terminology and complex cause-and-effect relationships. Its architecture, optimized for scientific literature, enabled accurate identification of key concepts and their interrelations. Gemma-3 performed particularly well on long texts and in preserving contextual information. Its ability to

retain large amounts of text in context enabled the construction of more coherent and complete graphs, especially for texts containing numerous interrelated concepts.

The mREBEL Large model [12] was the most effective at extracting specific facts and statements. Its specialization in relation extraction enabled graphs with highly detailed connections between concepts, which is particularly valuable for texts with a clearly articulated argumentative structure. An ensemble approach combining the strengths of different models yielded a more complete and accurate representation of the analyzed texts.

Discussion. The study showed that next-generation language models combined with formalized text-processing procedures can extract and structure knowledge as graphs. The developed methodology proved applicable both to highly abstract texts and to technical documentation requiring explicit representation of specific conditions and requirements.

An important feature is that the approach relies not on a single algorithm but on a sequence of stages within which different extraction, formalization, and visualization methods may be combined. This makes the methodology adaptable to different text types and enables comparison of outputs generated by different models and tools.

The results confirm the potential of integrating language models into the automated analysis of scientific publications and other types of textual data. At the same time, the quality of the resulting graphs depends substantially on the structure of the source texts, preprocessing quality, and methods used to combine outputs from different models. Individual stages of the methodology therefore require careful adjustment when the approach is transferred to new subject domains.

Conclusion. This study proposed and tested a software and methodological framework for automated knowledge extraction and graphical representation from unstructured Russian-language texts. It integrates modern language models, specialized relation-extraction tools, OWL ontologies, and interactive web-visualization tools.

The practical significance of the results lies in the ability to transform textual information into a clear graph structure suitable for expert analysis, comparison of outputs, and further formalization of domain relations. Local model deployment enables data to be processed in a secure environment without accessing external services.

The use of formal ontologies improves the consistency of knowledge representation and establishes a basis for logical validation and semantic inference. The proposed solution can therefore be regarded as a step toward more robust tools for analyzing scientific, technical, and regulatory texts.

Future research will focus on developing ensemble schemes, expanding the set of models, improving logical-validation procedures, and more rigorously assessing the quality of extracted entities and relations. Together, these directions create opportunities for applying knowledge graphs to information retrieval, research support, and complex-system modelling.

References

1. Fayans A.M. Building an ontology of fundamental concepts based on a transdisciplinary approach. *Ontology of Design*. 2022;12(4):454–469. (In Russ.) https://doi.org/10.18287/2223-9537-2022-12-4-454-469

2. Volkova I.A., Shamaeva E.D. An excursion into knowledge graphs. *International Journal of Open Information Technologies*. 2023;11(3):75–83. (In Russ.)

3. Spesivtsev A.V. Fuzzy-probabilistic approach to formalizing and using expert knowledge to evaluate complex objects states. *Journal of Instrument Engineering*. 2020;63(11):985–994. (In Russ.)

4. Mityakov S.N., Mityakov E.S. Processes machine learning in the tasks of researching innovative processes. *Journal of Applied Research*. 2020;4(1):6–13. (In Russ.)

5. Girin R.V., Orlov S.P. Object-oriented decomposition of artificial neural network's program logic. *Ontology of designing*. 2018;8(1):110–123. (In Russ.)

6. Zakharova O.I., Kuleshov S.V. Development of a graph neural network for processing text data. *Artificial Intelligence and Decision Making*. 2024;(4):67–78. (In Russ.) https://doi.org/10.14357/20718594240406

7. Napolskikh D.L. Approach to developing a cluster ontology. *Ontology of designing*. 2024;14(3):355–365. (In Russ.) https://doi.org/10.18287/2223-9537-2024-14-3-355-365

8. Zhilyaev A.A. Ontologies as a tool for creating open multi-agent resource management systems. *Ontology of designing*. 2019;9(2):261–281. (In Russ.)

9. Kuleshov S.V., Zaitseva A.A., Levashkin S.P. Processing of unstructured information obtained from the Internet using an associative-ontological approach. In: *Problems of Telecommunications Engineering and Technologies PTTT-2020: XXII International Scientific and Technical Conference; IV Scientific Forum Telecommunications: Theory and Technologies TTT-2020, Samara, November 17–20, 2020*. Samara: PGUTI; 2020. P. 7–11. (In Russ.)

10. Tsvetkov V.Ya., Kurdyukov N.S. Informational ontological modeling. *Russian Technological Journal*. 2025;13(2):18–26. (In Russ.) https://doi.org/10.32362/2500-316X-2025-13-2-18-26

11. Mamedova N.A., Afanasev M.A., Nefedov Yu.V., Urintsov A.I. Ontology of Engineering and Computational Architecture of Multimodal Transport and Logistics Center. *Automatic Documentation and Mathematical Linguistics*. 2025;59(2):109–123. https://doi.org/10.3103/S0005105525700554

12. Huguet Cabot P.-L., Tedeschi S., Ngonga Ngomo A.-C., Navigli R. RED: a Filtered and Multilingual Relation Extraction Dataset. In: *Proceedings of the 61st Annual Meeting of the Association for Computational Linguistics (ACL 2023)*. 2023. arXiv:2306.09802. https://doi.org/10.18653/v1/2023.acl-long.237

About the Authors:

Oksana I. Zakharova, Ph.D. (Eng.), Associate Professor, Deputy of Head of the Scientific Research Laboratory of Artificial Intelligence, Povolzhskiy State University of Telecommunications and Informatics (23, Lva Tolstogo St., Samara, 443090, Russian Federation), ORCID, SPIN-code, o.zaharova@psuti.ru

Konstantin N. Ivanov, 3rd-year Ph.D. student, Department of Information Systems and Technologies, Povolzhskiy State University of Telecommunications and Informatics (23, Lva Tolstogo St., Samara, 443090, Russian Federation), ORCID, SPIN-code, k.ivanov@psuti.ru

Sergey P. Levashkin, Ph.D. (Phys.-Math.), Associate Professor, Head of the Artificial Intelligence Research Laboratory, Povolzhskiy State University of Telecommunications and Informatics (23, Lva Tolstogo St., Samara, 443090, Russian Federation), ORCID, SPIN-code, ai_lab@psuti.ru

Mikhail V. Yakobovskiy, Corresponding Member of the Russian Academy of Sciences, Doctor of Physical and Mathematical Sciences, Director, Keldysh Institute of Applied Mathematics of the Russian Academy of Sciences (IPM RAS), (4, Miusskaya Sq., Moscow, 125047, Russian Federation), ORCID, SPIN-code, lira@imamod.ru

Contributions of the authors:

O.I. Zakharova: literature review, obtaining calculation formulas and conducting a numerical experiment, formulating the achieved results and describing their significance, formatting the article material.

K.N. Ivanov: development of methodology, application of mathematical and computational methods for the analysis of research data, visualization of research results and obtained data, coding.

S.P. Levashkin: scientific supervision of the research, setting the problem, formulating research ideas its goals and objectives, and preparing the article material.

M.V. Yakobovskiy: review and editing of the manuscript.

Conflict of Interest Statement: **the authors declare no conflict of interest.**

All authors have read and approved the final manuscript.

Об авторах:

Оксана Игоревна Захарова, кандидат технических наук, доцент кафедры информационных систем и технологий, заместитель заведующего научно-исследовательской лабораторией искусственного интеллекта Поволжского государственного университета телекоммуникаций и информатики (Российская Федерация, 443090, г. Самара, ул. Льва Толстого, 23), ORCID, SPIN-код, o.zaharova@psuti.ru

Константин Николаевич Иванов, аспирант кафедры информационных систем и технологий Поволжского государственного университета телекоммуникаций и информатики, (Российская Федерация, 443090, г. Самара, ул. Льва Толстого, 23), ORCID, SPIN-код, k.ivanov@psuti.ru

Сергей Павлович Левашкин, кандидат физико-математических наук, заведующий научно-исследовательской лабораторией искусственного интеллекта Поволжского государственного университета телекоммуникаций и информатики (Российская Федерация, 443090, г. Самара, ул. Льва Толстого, 23), ORCID, SPIN-код, ai_lab@psuti.ru

Михаил Владимирович Якобовский, член-корреспондент Российской академии наук, доктор физико-математических наук, директор Института прикладной математики имени М. В. Келдыша РАН (Российская Федерация, 125047, г. Москва, Миусская пл., д. 4), ORCID, SPIN-код, lira@imamod.ru

Заявленный вклад авторов:

О.И. Захарова: обзор литературы, получение расчетных формул и проведение численного эксперимента, формулировка достигнутых результатов и описание их значимости, оформление материала статьи.

К.Н. Иванов: разработка методологии, применение математических и вычислительных методов для анализа данных исследования, визуализация результатов исследования и полученных данных, написание программного кода.

С.П. Левашкин: научное руководство исследованием, постановка задачи, формулировка идей исследования его целей и задач, оформление материала статьи.

М.В. Якобовский: рецензирование и редактирование рукописи.

Конфликт интересов: ***авторы заявляют об отсутствии конфликта интересов.***

Все авторы прочитали и одобрили окончательный вариант рукописи.

Received / Поступила в редакцию 08.04.2026
Reviewed / Поступила после рецензирования 12.05.2026
Accepted / Принята к публикации 17.06.2026